WORKSHOP ON

GEOLOGICAL APPLICATIONS of THERMAL INFRARED REMOTE SENSING TECHNIQUES

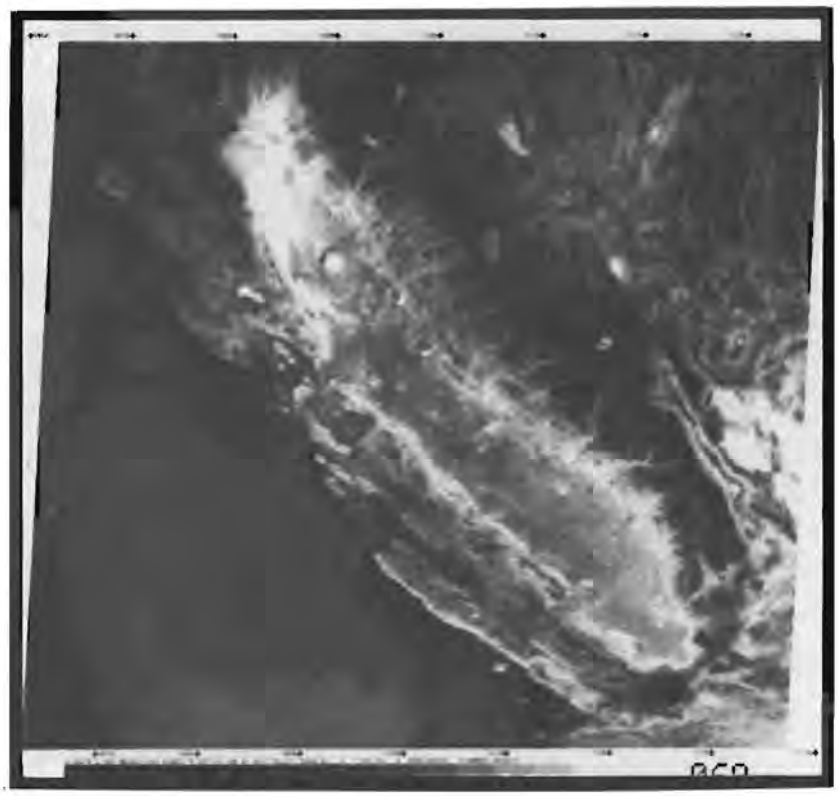

LPI Technical Report Number 81-06
LUNAR AND PLANETARY INSTITUTE 3303 NASA ROAD 1 HOUSTON, TEXAS 77058

WORKSHOP ON

GEOLOGICAL APPLICATIONS of THERMAL INFRARED REMOTE SENSING TECHNIQUES

Editor:
Mark Settle

A Lunar and Planetary Institute Workshop
February 11-13, 1980

Lunar and Planetary Institute 3303 NASA Road 1 Houston, Texas 77058

LPI Technical Report 81-06

Compiled in 1981 by the
LUNAR AND PLANETARY INSTITUTE

The Institute is operated by Universities Space Research Association under Contract NASW-3389 with the National Aeronautics and Space Administration.

This report may be cited as:
Settle, M. (1980) *Geological Applications of Thermal Infrared Remote Sensing Techniques. LPI Tech. Rpt. 81-06. Lunar and Planetary Institute, Houston. 138 pp.*

Papers in this report may be cited as:
Geological Applications of Thermal Infrared Remote Sensing Techniques (M. Settle, Ed.) p. xx–yy. LPI Tech Rpt. 81-06. Lunar and Planetary Institute, Houston.

This report is distributed by:

LIBRARY/INFORMATION CENTER
Lunar and Planetary Institute
3303 NASA Road 1
Houston, TX 77058
Mail order requestors will be invoiced for the cost of postage and handling.

Cover: *Nighttime thermal infrared Heat Capacity Mapping Mission image of the Pacific Ocean, central California, and western Nevada, obtained July 17, 1978. Cooler elements appear as the darkest objects, and the warmer elements as the lightest objects. The scale is about 1:4,000,000. (Images courtesy of the National Space Science Data Center.)*

Contents

Introduction

Background

The Non-Renewable Resources Program within NASA's Office of Space and Terrestrial Applications periodically sponsors specialized workshops to discuss the development of remote sensing techniques which are potentially applicable to geological investigations. These workshops are designed to assess the capabilities of specific remote sensing methods, and to identify future R & D activities which would significantly advance the current state-of-the-art. Attendance at these meetings is typically quite broad, involving individuals with backgrounds in scientific research, geological applications, and sensor engineering. The number of participants is generally restricted to 20–30 individuals so that informal exchange of views and opinions is possible. The impetus for a workshop on thermal infrared methods was provided by the results of several recent research projects and a projected loss of measurement capabilities within the thermal infrared over the next few years.

Evaluation of multispectral remote sensing measurements in the thermal infrared has been in progress during 1979 using airborne scanner data previously obtained over the East Tintic Mountains in Utah. Analysis of this data by researchers at NASA's Jet Propulsion Laboratory (JPL) has shown that variations in the emissivity of naturally occurring rock units can be detected in remote sensing measurements, and that these variations can be used to differentiate rock units on the basis of their free silica content (see abstract by A. Kahle, this volume). Analysis of data collected by the Heat Capacity Mapping Mission (HCMM) satellite has also been underway during 1979 and 1980. The HCMM satellite was designed to obtain broadband measurements of spectral reflectance and thermal emittance from the Earth's surface at altitudes of 620 km. The HCMM orbit was configured in such a way that diurnal measurements of thermal radiance could be obtained during a single 24 hour period, thus permitting evaluation of the apparent thermal inertia of surficial materials. The results of the HCMM project have indicated that areal variations in surface thermal inertia are potentially useful for discriminating different types of geological materials and for analyzing geological structure. In addition to geologic mapping, remote surveys of ground temperature and thermal inertia are

also potentially applicable to studies of hydrology and soil moisture, detection of effluents and pollutants in large bodies of water, and synoptic scale studies of boundary layer meteorology (see article by J. Taranik, this volume).

NASA has also developed thermal infrared sensor systems for observations of other planetary surfaces. A scanning infrared radiometer was flown on Apollo 17, the last mission to the moon. Lunar surface temperatures are quite variable and typically range from 80K (night time) to 400K daytime. Consequently, the Apollo scanning radiometer was designed to operate over a broad spectral region extending from 1.2 to 70 microns. More recently, the Viking orbiter spacecraft which were sent to Mars carried infrared thermal mappers designed to acquire data in the mid and far infrared, specifically within wavelength bands positioned at 6.1–8.3, 8.3–9.8, 9.8–12.5, 14.6–15.4, and 17.7–24.0 microns. Analysis of extraterrestrial thermal infrared data has proven useful for characterizing the physical properties of surficial materials and for detecting boundaries between different geological units.

The 24-channel aircraft scanner employed in the recent JPL experiments has been dismantled due to recurring engineering problems. In addition, operation of the HCMM satellite was terminated in October, 1980 following the completion of its experimental mission. As a consequence of these actions, NASA will possess relatively limited measurement capabilities in the thermal infrared during the coming years—both in terms of narrowband (≤ 0.5 micron) multispectral measurements at aerial altitudes and broadband (≥ 1.0 micron) measurements at orbital altitudes.

Orbital measurement capabilities in the immediate future will be determined by thermal scanners on board existing meteorological satellites. These instruments characteristically obtain broadband measurements in the thermal infrared with relatively poor spatial resolution (>1 km). Existing aircraft scanners can be used to obtain thermal infrared imagery with much better ground resolution. However, these instruments possess limited spectral resolution as discussed above. The next orbital sensor system which will acquire high resolution thermal infrared measurements over land areas is the Thematic Mapper scheduled for launch onbroad Landsat D in 1982. The Thematic Mapper is

designed to obtain measurements of emitted thermal radiation in the 10.4–12.5 micron wavelength region with a nominal ground resolution (instantaneous field of view) of 120 × 120m.

As the proceeding discussion illustrates, we are currently at a critical juncture in the development of thermal infrared techniques, both in terms of understanding their geological utility and in developing the technical capability to obtain additional experimental data. Recent analysis of thermal infrared measurements has produced some promising results. However, the results of individual research projects suggest many different directions for future R & D activities. The purpose of the workshop was to review recent research accomplishments in a comprehensive fashion, and to discuss the scope and relative emphasis of future research activities. In addition, the workshop was designed to examine various types of instrumentation required to support future research in the thermal infrared, in light of current and future technological capabilities.

The workshop was organized by NASA Headquarters. It was chaired by Dr. Hugh Kieffer (U. S. Geological Survey) and Dr. Robert Vincent (Geospectra Corporation). Dr. Kieffer served as principal investigator for the Viking thermal infrared experiments and more recently has become involved in the use of thermal infrared in monitoring volcanic activity at Mt. St. Helens. Dr. Vincent has extensive experience in terrestrial remote sensing applications, and he conducted some of the earlier pioneering research in the use of thermal infrared techniques. Invitations were extended to a wide range of geoscientists with prior experience in NASA's Earth applications and planetary exploration programs. Approximately 20 individuals representing a variety of government agencies, private companies, and academic institutions attended the meeting (a list of participants is included in this document). The Workshop was held at the Lunar and Planetary Institute February 11–13, 1980.

Objectives and Description

The workshop served as a planning meeting in which the scope and direction of future research activities could be discussed in a relatively informal setting. The technical objectives of the workshop were as follows:

1. to review the state-of-the-art capabilities of thermal infrared methods from a geological perspective.

2. to identify gaps in current understanding and establish the rationale for future research activities.

3. to discuss the appropriate balance of field experiments, laboratory studies, and theoretical investigations required to address major research objectives.

4. to identify various types of instrumentation required for future laboratory studies and field investigations.

Review of earlier work emphasized the fact that past research efforts sponsored by NASA have focused primarily upon the 8–14 micron wavelength region within the mid-infrared. The 3–5 micron region has been exploited for a variety of military applications, and also for mapping areal variation in surface temperature within specific environments. However, relatively little research has been performed to date to determine the types of geological information which could potentially be derived from remote sensing measurements in the 3–5 micron region.

Discussion of past research accomplishments also emphasized the importance of the field of view and the internal calibration of thermal infrared sensor systems. Infrared imagery acquired in the past has been primarily used in a qualitative fashion to identify relative variations in thermal radiance within a particular scene. The spatial resolution of earlier orbital sensors has been too coarse in many cases to detect subtle variations in thermal emittance which correspond to physical boundaries between different surficial materials. Thermal scanner systems are generally calibrated in a relative sense, and long term variations in internal black-body characteristics are not monitored in a precise, systematic fashion. The coarse spatial resolution and time varying calibration of previous sensors significantly limited attempts to make quantitative use of remote sensing data in the thermal infrared.

In addition to the limitations imposed by earlier instrumentation, discussion of past research also identified limitations in our ability to account for topographic and atmospheric effects in remotely sensed thermal infrared imagery. Large variations in signal-to-noise occur across a natural daytime scene when viewed in the infrared due to natural variations in the intensity and duration of solar insolation at the Earth's surface. Illuminated slopes are characterized by a high signal-to-noise ratio which could potentially be quite useful in using multispectral infrared measurements for rock type discrimination. However, improved methods of analyzing thermal emittance and topographic data must be developed to fully exploit multispectral infrared surveys. Atmospheric absorption and scattering phenomena introduce additional "noise" into thermal infrared observations of the Earth's surface. New methods of combined data analysis are also required to remove spatial and temporal variations in thermal infrared surveys produced by atmospheric effects.

Discussion of future research objectives highlighted the need for a variety of activities, including:

- comparative laboratory studies to assess the accuracy of emissivity spectra measured by reflectance, transmission, and emittance methods.

- *in situ* field studies of the bulk emissivity and thermal inertia of surface cover materials.

- development of theoretical "mixing models" which accurately predict the thermal infrared characteristics of natural surfaces consisting of heterogeneous mixtures of rock, soil, vegetation, water, etc.

- empirical analysis of high spectral and spatial resolution imagery to evaluate the utility of thermal infrared measurements for mapping variations in the emissivity of natural surfaces (specifically, to evaluate tradeoffs between increased resolution and decreased signal-to-noise).

- empirical analysis of repetitive, broadband imagery to evaluate the utility of thermal infrared measurements for characterizing the bulk thermal inertia of surficial materials (specifically, to evaluate tradeoffs between the frequency, time of day, variable viewing geometry, and spatial resolution of remote sensing surveys).

Instrumentation required to address these various research objectives was discussed at the conclusion of the workshop. Workshop participants speculated about the desirable measurement characteristics of future sensor systems for use in both laboratory and field environments. These speculations were tempered by a review of technological capabilities in the thermal infrared which are presently available and those which should become available in the near term. The consensus of the workshop attendees was that top priority should be given to the development of a multichannel airborne scanner which could operate in the 8–14 micron region. Workshop particpants also expressed keen interest in the Portable Field Emission Spectrometer (PFES) instrument which was recently developed at JPL to obtain ground-based, *in situ* measurements of surface emissivity.

Outcome of the Workshop

Workshop discussions emphasized the importance of the thermal infrared as a potential source of geologically useful information. Futhermore, current research results indicated that geological information obtained from thermal infrared measurements generally complement and do not duplicate the types of information derived from spectral reflectance measurements. The summary opinion of the Workshop participants was that the thermal infrared is an under-studied and under-utilized portion of the spectrum from a geological point of view. They felt that the thermal infrared region holds great promise for future research and development. A detailed summary of the findings and recommendations of the Workshop was prepared by Dr. Kieffer. The workshop summary immediately follows this introductory section.

NASA Headquarters has taken several steps to implement the recommendations of the workshop. The following actions have specifically been adopted:

- A six-channel airborne thermal infrared scanner is currently being fabricated. This instrument is designed to operate at approximately 40,000 ft. with a 2.5 milliradian instantaneous field of view and a total field of view of 86°. The scanner will obtain simultaneous measurements of thermal emittance in six bands (8.2–8.6/8.6–9.0/9.0–9.4/ 9.4–10.2/10.2–11.2/11.2–12.2 micrometers) with a noise equivalent temperature difference of 0.4°–0.5° C (NEDT) at 25° C in each band. This scanner will be field tested during the summer of 1982, and will be available for general use by NASA investigators in 1983.

- A program for follow-on investigations of Heat Capacity Mapping Mission data has been initiated in 1981. Plans are being formulated to maintain the capability to produce retrospective HCMM computer compatible tapes (CCTS) and paired day/night infrared scenes through 1983.

- Plans for assessing the utility of broadband thermal infrared measurements to be obtained by the Thematic Mapper are being established.

The Workshop provided a firm rationale for the continued development of thermal infrared techniques and a useful guide to the kinds of R & D activities that should be given priority attention in the future. We would like to thank all those who attended the workshop, especially the chairmen, for their collective time and effort in making the meeting a success.

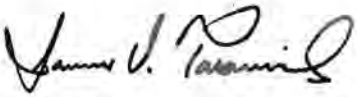

James V. Taranik
Program Chief

Mark Settle
Program Scientist

Non-Renewable Resources Program
Office of Space and Terrestrial Applications
NASA Headquarters

Summary

M. Settle, NASA Headquarters, Washington, DC
H. Kieffer, U.S. Geological Survey, Flagstaff, AZ

This meeting was held to review the current capabilities of thermal infrared techniques, to evaluate their potential utility from a geological perspective, and to discuss the direction of future research and development. The meeting was attended by a variety of individuals, including sensor engineers with experience in instrument design and fabrication and geologists with experience in the analysis and interpretation of remotely sensed data. Consideration of past research was quite wide ranging, including a historical review of early laboratory experiments, discussion of previous airborne remote sensing surveys, and presentation of results from past and present spacecraft missions. Discussion of future research activities also covered a wide range of topics, including laboratory analysis of the emissivity properties of natural surficial materials, theoretical modeling of atmospheric transmission and radiation phenomena, and test site projects involving analysis of ground-based and aerial infrared data.

The consensus of the workshop participants was that NASA should place greater emphasis on the development of thermal infrared techniques in the future. There was a lively exchange of views concerning future R&D priorities. Workshop discussions highlighted the dual need for fundamental studies of the various physical processes which govern the thermal infrared characteristics of natural surfaces, and empirical studies of experimental remote sensing data obtained over a wide diversity of test sites. Workshop participants were seriously concerned that current levels of research support and currently available instrumentation were not adequate to address these two objectives. This section summarizes the scope of workshop discussions and the overall results of the meeting.

Past Applications of Thermal Infrared Techniques

The thermal infrared is conventionally defined as that portion of the electromagnetic spectrum which extends from wavelengths of 3.0 μm to approximately 100 μm. Two atmospheric "windows" within the thermal infrared have been exploited in the past for geological remote sensing. These spectral regions, situated at 3–5 and 8–14 μm, represent wavelength bands within which atmospheric absorption of thermal energy radiated at the earth's surface is minimized. Infrared observations of the earth at wavelengths beyond 20 μm are dominated by atmospheric radiation. Variations in thermal emission at the earth's surface cannot generally be detected at these longer wavelengths.

Past uses of thermal infrared techniques for geological investigations can be categorized as follows:

Ground Temperature Surveys

Broadband measurements (over wavelength intervals of 2.0 μm or greater) are commonly performed to detect variations in surface temperature. Such measurements have been conducted in both the 3–5 and 8–14 micron regions. Daytime measurements of surface radiance at 3–5 μm wavelengths contain a component of reflected solar radiation which represents a potential source of error in determining the intensity of thermal radiation emitted at the ground surface. Infrared surveys conducted at night do not contain this reflected solar component. (Note that the 8–14 μm wavelength band can be used for remote sensing surveys under both day and night time conditions). It is generally difficult to determine absolute surface temperature on the basis of thermal infrared surveys because of intervening atmospheric effects produced by gaseous absorption and emission, particulate scattering, etc. Problems with the precision and stability of sensor calibration procedures have also compromised the accuracy of surface temperatures determined in the past. Calibration problems have been largely

overcome in the current generation of airborne thermal infrared scanners, however. As a result of these various complications, analysis of broadband thermal surveys has usually been performed in a qualitative fashion to determine the relative differences in thermal radiance within a particular scene.

Thermal Inertia Surveys

Multitemporal, broadband measurements of surface radiance at thermal infrared wavelengths can be used in a relative sense to infer variation in ground temperature at different stages of the diurnal heating cycle. Apparent temperature differences can be combined with measurements of surface reflectivity (i.e., albedo) to estimate the bulk thermal inertia of the ground. (Note that the albedo measurement together with ancillary information is used to estimate the amount of solar energy available for surface heating.) The complicating factors mentioned above are equally applicable to thermal inertia mapping. It is particularly difficult to quantify and account for time-varying meteorological phenomena in multitemporal thermal infrared surveys. Additional problems arise in achieving accurate geographic registration of multitemporal imagery.

Emissivity Surveys

The thermal energy radiated from a natural surface is proportional to the temperature and the emissivity of the surface material. Variations in ground emissivity can be detected within remote sensing measurements, and they can be quantitatively estimated, in principle, if the temperature of the surface is known. Variations in the emissivity of geological material occur over relatively narrow wavelength intervals. Consequently, narrowband measurements over spectral intervals of 1.0 micron or less are required to detect areal variations in the spectral emissivity of natural surfaces. Emissivity mapping studies performed to date have been conducted in the 8–14 μm wavelength region, where reflected solar radiation is not a factor in data interpretation.

Various types of information can be derived through the analysis of remotely sensed thermal infrared measurements. These different types of information are potentially applicable to a broad spectrum of of scientific disciplines, and they have immediate, practical utility as well. Past applications of thermal infrared methods are discussed and referenced in this report. They are summarized in outline form below:

GEOLOGY
- Rock type discrimination/identification
- Structural mapping (lineament analysis)
- Geobotany (analysis of vegetation patterns and vegetation stress)
- Heat flow studies (geothermal resource assessment, volcano monitoring)

HYDROLOGY/OCEANOGRAPHY
- Soil moisture/groundwater studies
- Snow pack mapping/glaciology
- Dispersion of pollutants and sediments (lakes, coastal zone, etc).
- Current systems/circulation studies

AERONOMY/METEOROLOGY
- Atmospheric thermal structure
- Aerosol/particle distribution studies
- Boundary layer meteorology (e.g., urban heat island analysis)

Current Status of Thermal Infrared Techniques

Thermal infrared remote sensing methods are currently being employed on a routine basis to detect areal variations in ground temperature. A wide variety of broadband infrared scanners is presently available, and certain meteorological satellites are currently performing regional infrared surveys on an operational basis. It is generally difficult to establish the accuracy of remotely sensed ground temperatures. This difficulty is partly the result of instrumentation limitations. Many sensors are not precisely calibrated in a radiometric sense. Furthermore, sensors which contain internal blackbody sources for calibration purposes may develop internal biases due to long term modification of the emissivity properties of the black bodies resulting from surface oxidation, gas absorption and/or evaporation, etc.

Another major difficulty commonly encountered in evaluating the accuracy of thermal surveys is the disparity between the spatial scale of the remote sensing measurements and contemporaneous ground truth measurements. Aerial and orbital sensors are designed to measure the average radiance of a particular area, generally on the order of $10m^2$ or more. In comparison, ground truth determinations of kinetic surface temperature are generally point measurements. Areas $10m^2$ or larger in size can contain significant spatial variations in vegetation density, soil moisture, surface texture, etc. Consequently, point measurements of surface temperature cannot be directly compared with average areal temperatures inferred on the basis of remote sensing measurements. Statistical procedures must be employed in comparing ground truth measurements obtained at isolated points with airborne or spaceborne thermal scanner data acquired over much larger areas. Several empirical procedures have been employed in the past to provide ground truth calibration of infrared surveys, including the use of inland bodies of water as isothermal points of reference.

Atmospheric effects can introduce additional complications in relating aerial or orbital measurements of surface radiance to actual surface temperatures. This is particularly true for spaceborne sensors with large fields of view which conduct regional surveys over ground swaths of hundreds of kilometers or more. Water vapor content, aerosol concentration, and thermal structure of the atmosphere can vary significantly over distances of several hundred kilometers. These atmospheric variations can contribute to areal or orbital measurements of surface radiance in ways which serve to camouflage the actual thermal energy being emitted at the earth's surface. Atmospheric effects can be accounted for within localized areas through the use of upward-viewing, ground based radiometers.

Instrumentation limitations, difficulties in relating remote sensing data to ground truth measurements, and atmospheric effects have placed significant restrictions upon the absolute accuracy of ground temperature surveys obtained by remote sensing methods. Nevertheless, broadband infrared surveys have proven useful for detecting relative variations in surface temperature which can be correlated with variations in subsurface heat flow, geological structure, rock lithology, soil moisture, etc. Improvements in sensor precision that can be realized with currently available technology and more sophisticated data analysis methods could potentially improve the accuracy of remotely sensed ground temperatures. Research required to address the question of more accurate determination of actual surface temperatures is discussed in the following section.

Only a limited number of thermal inertia surveys has been conducted in the past, primarily for research purposes. A series of experiments was performed in the mid 1970's to test the feasibility of using thermal inertia information for rock type discrimination and geologic mapping. The results of these experiments were encouraging and provided the scientific justification for the Heat Capacity Mapping Mission (HCMM)—an earth applications project conducted by NASA which obtained diurnal measurements of thermal radiance from which variations in apparent thermal inertia could be estimated.

HCMM data were collected during 1978-1980 and analysis of the data is still in progress. The HCMM satellite obtained thermal imagery with a swath width of 760 km and a ground (pixel) resolution of 500 × 500m. Consecutive day-night passes during a particular 24 hour period were acquired over mid-latitude regions at 16 day intervals. Preliminary analyses suggest that the accuracy of orbital thermal inertia surveys could be improved by more precise sensor calibration procedures and greater frequency of observations during the diurnal heating cycle. The utility of future orbital thermal inertia surveys could be improved by increasing the spatial resolution of thermal radiance measurements and decreasing the interval between observational periods.

In a similar fashion, past attempts to utilize thermal infrared methods for detecting areal variations in the emissivity of natural surfaces have been largely experimental. A limited number of airborne surveys has been conducted in the past which possessed sufficiently narrow bandwidth measurement capabilities to test the feasibility of emissivity mapping. (These surveys were performed within the 8–14 μm region with two or more measurement bands, each possessing a bandwidth of 1.0 μm or less.) Past experiments were conducted over semi-arid test sites which contained excellent rock exposures and little vegetative cover. In addition, they were performed near the peak of the daily insolation cycle to maximize the strength of the surface emission "signal" relative to sources of thermal "noise". As anticipated, areal variations in surface emissivity were small (typically less than 10% of the total signal); however, they proved to be detectable. Additional airborne experiments over test sites of greater complexity are needed to fully evaluate the utility of thermal infrared techniques for emissivity mapping.

Future Research

The geological utility of thermal infrared techniques could be significantly improved through more detailed understanding of the various physical phenomena which contribute to the thermal characteristics of natural surfaces as they are observed at aerial or orbital altitudes. A major physical phenomenon which represents a source of "noise" in the geological analysis of thermal infrared data is the earth's atmosphere. Gaseous species within the atmosphere possess distinctive absorption and emission characteristics at thermal infrared wavelengths. Water vapor is a particularly important species because of its strong absorption characteristics at certain infrared wavelengths, and its relative abundance in the lower atmosphere. Suspended particles and aerosols also influence the radiative properties of the atmosphere. Several attempts have been made to model and remove atmospheric effects from thermal infrared remote sensing surveys in specialized cases where simultaneous measurements of atmospheric properties have been obtained. Atmospheric measurements performed at an individual ground station cannot always be extrapolated to other areas, however. It would be useful to investigate how measurements performed by meteorological satellites might be combined with thermal infrared surveys in the future to remove regional atmospheric effects from large scale surveys of surface thermal emission.

Varations in surface relief introduce a measure of thermal variability in an areal infrared survey which is not related to the intrinsic physical properties of the geologic materials exposed at the surface. Surface materials experience very different cycles of solar heating depending upon their orientation with respect to the sun. Variations in the amplitude of surface temperatures on sun-facing and shadowed slopes tend to mask variations in the emissivity or thermal inertia of surface materials. Improved methods of accounting for topographic variations within regional thermal infrared surveys would permit more accurate quantitative analysis of areal variation in surface properties.

Advances in our current capability to characterize and remove atmospheric and topographic effects from thermal infrared surveys will create a need for more sophisticated models of the kinetic temperature of natural surfaces. Theoretical models have been developed in the past which describe the

thermal energy balance at the earth's surface in one or two dimensions. Existing models can account quite accurately for variations in the density, thermal conductivity, and specific heat of subsurface materials. More sophisticated models will be needed in the future, however, to describe the effects of evaporation, precipitation, and ground texture upon the thermal characteristics of natural surfaces. In addition, existing models must be generalized to fully represent thermal flux in a three dimensional sense, in order to investigate the relative contribution of rock, soil, vegetation, and water to remote sensing measurements of average surface radiance at thermal infrared wavelengths.

The research topics described above address several of the fundamental problems involved in the analysis and interpretation of remotely sensed thermal data. Research of a more empirical nature is also required to define the characteristics of thermal infrared sensor systems which would be optimum from a geological perspective. In particular, aerial scanner data must be collected and analyzed over a wider variety of test sites in order to fully evaluate the usefulness of infrared techniques for detecting areal variations in surface emissivity and thermal inertia. In the case of emissivity mapping, additional experiments are needed to examine tradeoffs between spectral and spatial resolution, and the measurement sensitivity that can be achieved at orbital altitudes. Variations in surface roughness produce variations in the effective emissivity of a natural surface, even under circumstances in which the composition of surficial materials is perfectly uniform. Surface roughness effects will become increasingly important as measurement bandwidths become narrower. A greater variety of empirical emissivity measurements under natural field conditions are needed to evaluate the relative improvement that can be achieved in discriminating different types of geological materials with decreasing measurement bandwidth. (Note that atmospheric effects will also introduce a component of noise in narrowband measurements which will become increasingly significant with decreasing bandwidth.)

In the case of thermal inertia mapping, empirical test site experiments are required to determine the optimum spatial resolution, timing, and frequency of infrared surveys of geological mapping. The HCMM satellite obtained diurnal measurements of surface radiance over mid-latitude regions shortly after local noon and midnight. Measurements of this type are useful for determining the diurnal range of surface temperature. Additional measurements of surface temperature during the daily insolation cycle can be used to refine estimates of thermal inertia and place greater constraints on models of subsurface layering, soil moisture, etc. Future orbital missions consisting of two or more spacecraft could be planned to obtain multiple measurements of surface radiance, if such data was shown to be useful. Similarly, the interval between successive diurnal measurements of thermal inertia could be reduced by a multiple spacecraft mission if seasonal variations in thermal inertia proved to be useful for geological mapping.

Finally, workshop discussions highlighted the need for several specialized laboratory and field studies. Only a limited number of laboratory emissivity measurements have been performed on surficial materials to date. Many geological samples that have been examined in the laboratory have been sectioned or polished or otherwise altered from their natural *in situ* condition. The emissivity characteristics of vegetative species remain essentially unknown. Determination of the emissivity properties of surficial materials in their natural state is essential for the detailed analysis and interpretation of narrowband thermal infrared data.

Thermal inertia is a bulk physical property of the ground surface which, in turn, is a function of the density, thermal conductivity and heat capacity of the surficial materials. Extensive laboratory measurements of the specific gravity, intrinsic thermal conductivity, and intrinsic heat capacity of geological materials have been performed in the past. Future *in situ* measurements of bulk thermal inertia are needed under realistic field conditions to determine the extent to which theoretical estimates of thermal inertial-based on laboratory data are actually realized in nature. Past attempts to develop portable instrumentation to measure the *in situ* thermal inertia of natural surfaces should be continued in the future.

Potential Payoff

As described above, thermal infrared techniques hold great potential for geological mapping. In fact, certain types of geological information obtained through the analysis of thermal infrared measurements cannot currently be obtained using other remote sensing techniques. For example, narrowband thermal infrared measurements can be used to differentiate carbonate and silicate rock types found in sedimentary sequences, and to discriminate intrusive igneous rocks found in volcanic terranes.

This type of mineralogical information complements information on clay composition and abundance that can be derived from measurements at shorter wavelengths. Combined analysis of visible-near infrared-shortwave infrared and thermal infrared data acquired over a particular area will provide geologists with a powerful tool for rock type identification and classification. In addition, night time infrared measurements and thermal inertia surveys have revealed the presence of large scale structural features which appear to be related to the porosity and moisture content of near surface materials. As in the case of narrowband surveys, many of these structural features cannot be detected in imaging data acquired at shorter wavelengths.

The various research activities described above were deemed essential by the majority of workshop participants in order to fully exploit the geological potential of thermal infrared techniques. This research will determine the inherent limitations imposed by atmospheric effects and surface topography upon quantitative geological analysis of thermal infrared measurements. Furthermore, it will enable investigators to evaluate the extent to which these effects could be accounted for within remote sensing surveys through the use of ancillary atmospheric and/or topographic data. The program of research outlined above will reveal the relative advantages of increasingly complex methods of data acquisition and analysis. This type of assessment can be performed relatively inexpensively through an aggressive program of laboratory studies, theoretical modeling, and airborne data collection and analysis.

The prime benefit of the foregoing program of research is that it will provide needed justification for the future development of aerial and orbital sensor systems for use by the geological community. Furthermore, it will permit future measurement systems to be designed in a manner which is best suited to geological applications. Research results will specifically enable measurement parameters such as spatial and spectral resolution, number and position of spectral bandpasses, radiometric accuracy, time(s) of day of data acquisition, and multitemporal coverage requirements to be specified from a geological perspective.

Recommendations

There was broad agreement among workshop participants on the following recommendations:

1. Past research and development of thermal infrared remote sensing techniques have not kept pace with R&D efforts devoted to other remote sensing methods, particularly visible/near infrared and microwave (radar) techniques. Limited experimental results obtained to date indicate that thermal infrared methods hold great promise for geological mapping. On the basis of these results, greater effort should be made in the future to redress the imbalance between R&D in the thermal infrared and parallel research in other technique areas. This should be construed as a general recommendation related to long term redistribution of emphasis in remote sensing research and not simply a plea for greater funding in the immediate future.

2. High priority should be placed upon establishing a multispectral airborne measurement capability in the 8–14 μm wavelength region. Combined analysis of multispectral measurements obtained in different portions of the electromagnetic spectrum holds great promise for geologic mapping in general, and rock type discrimination in particular. No aircraft scanners presently exist which can acquire the experimental data needed to fully evaluate the utility of the 8–14 μm region for geological applications. The next generation aircraft sensor to operate in this wavelength interval should, at a minimum, possess the capability to obtain measurements of emitted thermal radiation in three distinct channels with a precision (noise equivalent temperature difference) of 0.5 K and ground resolution of 10m.

3. The characteristics and current availability of data collected by the Heat Capacity Mapping Mission (HCMM) should be more widely publicized within the geological community. HCMM data represents the only orbital set of thermal infrared imagery that will be available to geologists prior to the launch of Landsat D. Even with the advent of Landsat D, HCMM will be the only source of nighttime infrared imagery acquired at moderate spatial resolution during the mid to late nineteen eighties. Greater effort should be made to alert geologists to the various ways in which HCMM can be used and the procedures that have been established for data distribution. The results of the HCMM principal investigators program should also be prominently publicized within the geological community as they become available.

Historical Development of Multispectral Thermal Infrared Techniques for Geological Mapping

Robert K. Vincent, Geospectra Corporation

Most geological applications of thermal infrared scanner data to date have employed broad bandwidth sensors operating in the 8μm–14μm wavelength region (an atmospheric "window"). Several investigators have reported encouraging results in attempting to discriminate different types of minerals, rocks, and soils through the analysis of data acquired by narrow-band infrared spectrometers and medium-band multispectral infrared scanners. Coblentz (1901, 1906) was the first to show that silicate rocks characteristically display spectral emittance minima which can be observed in the 8μm–12μm region. His measurements were performed with a laboratory infrared spectrometer. It was over 30 years later that Saksena (1940) positively identified the emittance minima of quartz in the 8.1μm–10.1μm and 12.0μm–13.0μm wavelength regions as being caused, respectively, by Si-O and Si-Si stretching modes in SiO_4 tetrahedra. The first serious study of the emittance minima of silicates in the context of geological remote sensing was performed by R. J. P. Lyon (1963, 1964) of Stanford University in the mid-1960's. His laboratory studies indicated that the transmittance minima of silicate mineral powders occur at slightly different wavelength positions for different silicate minerals (Lyon, 1963), as shown in Figure 1. He also demonstrated (Lyon, 1964) that thermal infrared emittance minima for mafic and ultramafic (quartz-poor) rocks generally occur at longer wavelengths than emittance minima of felsic (quartz-rich) rocks, as shown in Figure 2.

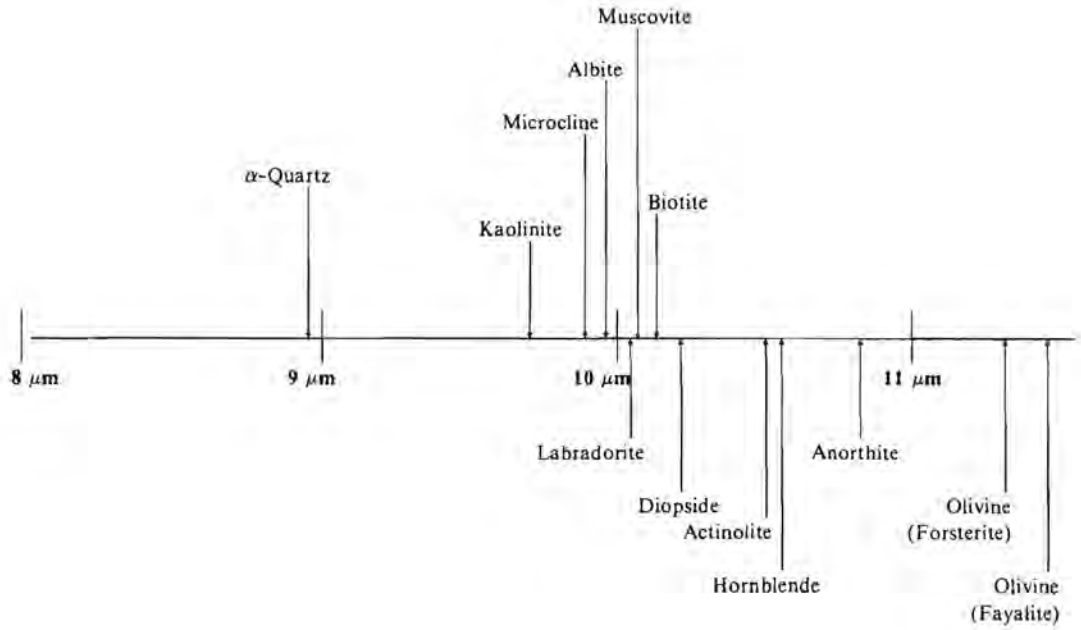

Figure 1. Spectral Positions of Transmission Minima of Selected Silicate Mineral Powders (After Lyon, 1963).

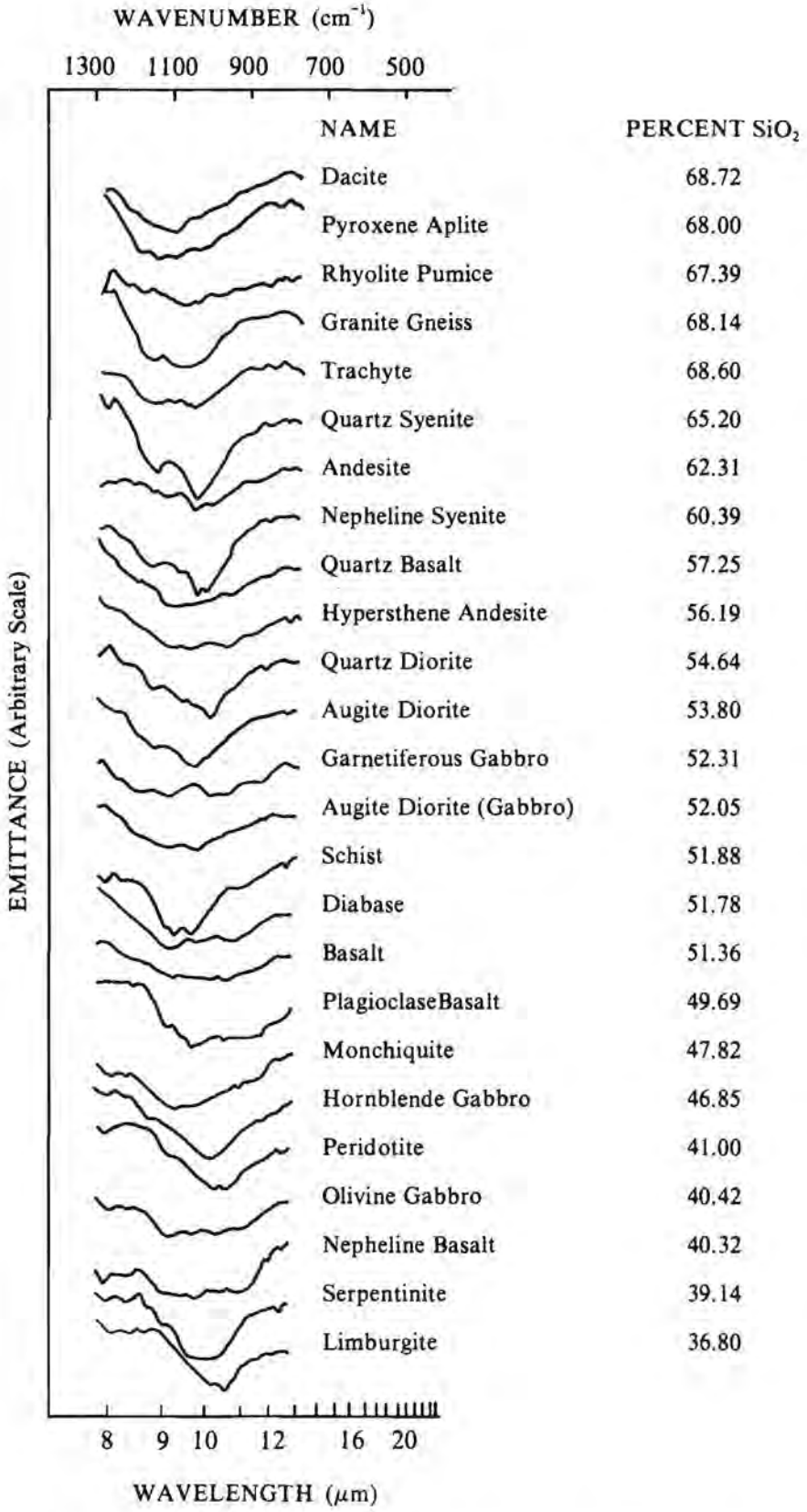

Figure 2. Emittance Spectra of Silicate Rocks. (After Lyon, 1964).

In the mid-1960's through the early 1970's, thermal infrared spectroscopy was applied to the moon and planets through ground-based and balloon-borne telescopes. Hunt (195, 1966), Hunt and Salisbury (1964a, 1964b, 1969), and Salisbury and Hunt (1968) investigated thermal infrared spectra of the Moon and Mars. Goetz (1968) compared the infrared spectra of various lunar sites on the basis of ground-based telescopic measurements. In 1970, balloon-borne measurements of the Moon were made and interpreted by Salisbury, *et al.* (1970). J. W. Salisbury, G. R. Hunt, R. K. Vincent and L. M. Logan at the Lunar-Planetary Research Branch of Air Force Cambridge Research Laboratory performed a number of experimental studies on the thermal infrared spectral emittance and reflectance properties of rocks and minerals in the late 1960's and early 1970's (Vincent and Hunt, 1968; Hunt and Vincent, 1968; Logan and Hunt, 1970; Hunt and Logan, 1972; Hunt and Salisbury, 1974, 1975, and 1976; Hunt, 1976).

Vincent and Thomson (1971) produced the first thermal infrared spectral ratio image in the early 1970's. They analyzed multiple channel data acquired over a test site near Mill Creek, Oklahoma by an airborne scanner operated by the University of Michigan Willow Run Laboratories (now known as the Environmental Research Institute of Michigan, ERIM). This was the first time that multispectral thermal infrared data related to rock composition was produced in the form of an image. Quartz sandstone outcroppings near a sandstone quarry were discriminated from limestone overburden and other terrain features such as vegetation, water, etc. Vincent and Thomson (1972) followed this study with further investigation of thermal infrared ratio images over an area near Pisgah Crater, California. They successfully discriminated intermediate (dacite) from basic (basalt) silicate rocks, though they could not discriminate clay-rich playa sediments from basaltic lava by the two-channel ratio imaging method. Non-imaging airborne spectrometer data flown by Lyon (1972) over the same area confirmed the infrared ratioing results of Vincent and Thomson. This work was followed by laboratory and theoretical studies on igneous silicate rocks by Vincent (1972, 1973, and 1975). Dillman and Vincent (1974) later produced a color composite image of three ratio images obtained in the visible, reflective IR, and thermal IR wavelength regions using airborne multispectral scanner data acquired over Halloran Spring, California. The results of this experiment indicated that granite, gneiss, andesite and quartz monzonite could be discriminated from one another in that area. The mapping accuracy for the experiment was 78% when very sparsely vegetated regions of the color ratio image were compared with a geologic map.

The most recent and definitive example of the utility of multispectral thermal infrared data for geological remote sensing was provided in 1979 (A. B. Kahle, D. P. Madura, and J. M. Soha) by an experiment with the now defunct NASA 24-channel multispectral scanner over the East Tintic Mining District, Utah. Six channels of the thermal IR data (8.3–8.7μm, 8.8–9.3μm, 9.4–9.9μm, 10.1–11.0μm, 11.0–12.0μm, and 12.0–13.0μm) were collected, and the first, second, and fourth of these channels were used to produce a color composite with an inverse principal components transformation enhancement method. In the resulting color image it was possible to discriminate quartz latites from latites and monzonites; sandy limestones from nearly pure limestones; clays from most other soil or rock types; and quartz-rich silicates from carbonates. In general, it appeared as though quartz content was the principal compositional constituent being mapped. An image of the same area from an airborne Landsat D thematic mapper simulator, which has only one thermal infrared channel, showed distinctly different spectral patterns on the ground, proving that a division of the 8–14μm thermal infrared region into several medium-width channels provides unique spectral information that cannot be duplicated in the visible/reflective infrared wavelength regions.

References

Coblentz W. W. (1901) Selected radiation from various solids, 2. *Nat. Bur. Stand. U.S. Bull.* **6**, 301.

Coblentz W. W. (1906) *Investigation of infrared spectra*. Carnegie Inst. of Wash. Pub. No. 65, Washington.

Dillman R. and Vincent R. K. (1974) Unsupervised mapping of geologic features and soils in California. In *Proc. Ninth Symp. on Remote Sensing of Environ.*, p. 2012-2025. Environmental Res. Inst. of Michigan, Ann Arbor.

Goetz A. F. H. (1968) Differential infrared lunar emission spectroscopy. *J. Geophys. Res.* **73**, 1455-1466.

Hunt G. R. (1965) Infrared spectral emission and its application to the detection of organic matter on Mars. *J. Geophys. Res.* **70**, 2351-2357.

Hunt G .R. (1966) Rapid remote sensing by a spectrum matching technique. 1. Description and discussion of the method. *J. Geophys. Res.* **71**, 2919-2930.

Hunt G. R. (1976) Infrared spectral behavior of fine particulate solids. *J. Phys. Chem.* **80**, 1195-1198.

Hunt G. R. and Logan L. M. (1972) Variation of single particle mid-infrared emission spectra with particle size. *Appl. Opt.* **11**, 142-147.

Hunt G. R. and Salisbury J. W. (1964a) Lunar surface features: mid-infrared spectral observations. *Science* **146**, 641-642.

Hunt G. R. and Salisbury J. W. (1964b) Determination of compositional differences on the lunar surface using ground based infrared spectroscopy. *Report of Third Annual Meeting of Working Group on Extraterrestrial Resources*, p. 31-46. Kennedy Space Center.

Hunt G. R. and Salisbury J. W. (1969) Mid-infrared spectroscopic observations of the Moon. *Phil. Trans. Roy. Soc. London* **264A**, 109-139.

Hunt G. R. and Salisbury, J. W. (1974) *Mid-infrared spectral behavior of igneous rocks*. AFCRL-TR-74-0625 Environmental Research Paper 496, 142 pp.

Hunt G. R. and Salisbury J. W. (1975) *Mid infrared spectral behavior of sedimentary rocks*. AFCRL-TR-75-0356 Environmental Research Paper 520, 49 pp.

Hunt G. R. and Salisbury J. W. (1976) *Mid infrared spectral behavior of metamorphic rocks*. AFCRL-TR-76-0003 Environmental Research Paper 543, 67 pp.

Hunt G. R. and Vincent R. K. (1968) The behavior of spectral features in the infrared emission from particulate surfaces of various grain sizes. *J. Geophys. Res.* **73**, 6039-6046.

Kahle A. B., Madura D. P., and Soha J. M. (1979) *Processing of Multispectral Thermal IR Data for Geologic Applications*. JPL Publ. 79-89, Jet Propulsion Laboratory, Pasadena, Calif., 39 pp.

Logan L. M. and Hunt G. R. (1970) Emission spectral of particulate silicates under simulated Lunar conditions. *J. Geophys. Res.* **75**, 6539-6547.

Lyon R. J. P. (1963) *Evaluation of Infrared Spectrophotometry for Compositional Analysis of Lunar and Planetary Soils*, NASA Rpt. NASA-TN-D-1871, 1-115.

Lyon R. J. P. (1964) *Evaluation of Infrared Spectrophotometry for Compositional Analysis of Lunar and Planetary Soils, Part II. Rough and Powdered Surfaces*, NASA Rept. CR-100, 172pp.

Lyon R. J. P. (1972) Infrared spectral emittance in geological mapping: airborne spectrometer data from Pisgah Crater, California. *Science* **175**, 983-986.

Saksena B. D. (1940) Analysis of the Raman and infrared spectra of alpha-quartz. *Proc. Indian Acad. Sci.* **12A**, 92-139.

Salisbury J. W. and Hunt G. R. (1968) Martian surface materials: effect of particle size on spectral behavior. *Science* **161**, 365-366.

Salisbury J. W., Vincent R. K., Logan L. M., and Hunt G. R. (1970) Infrared emissivity of lunar surface features, 2. Interpretation. *J. Geophys. Res.* **75**, 2671-2682.

Vincent R. K. (1972) Emission polarization study on quartz and calcite. *Appl. Opt.* **11**, 1942-1945.

Vincent R. K. (1973) *A Thermal Infrared Ratio Imaging Method for Mapping Compositional Variations Among Silicate Rock Types*, Ph.D. Dissertation, Dept. of Geol. and Mineral., Univ. of Mich., Ann Arbor.

Vincent R. K. (1975) The potential role of thermal infrared multispectral scanners in geological remote sensing. *Proc. IEEE* **63**, 137-147.

Vincent R. K. and Hunt G. R. (1968) Infrared reflectance from mat surfaces, *Appl. Opt.* **7**, 53-59.

Vincent R. K. and Thomson F. (1971) Discrimination of basic silicate rocks by recognition maps processed from aerial infrared data. In *Proc. Seventh Inter. Symp. on Remote Sensing of Environ.* p. 247-252. Enviromental Res. Inst. of Mich., Ann Arbor.

Vincent R. K. and Thomson F. (1972) Rock type discrimination from ratioed infrared scanner images of Pisgah Crater, California, *Science* **175**, 986-988.

Heat Capacity Mapping Mission: Interim Results and Achievements

James V. Taranik, NASA Headquarters

Technical Background

The Heat Capacity Mapping Mission (HCMM) was an experimental space project sponsored by NASA's Office of Space and Terrestrial Applications. The HCMM satellite was launched April 26, 1978 and placed in a high inclination (97.6°), near circular orbit at an altitude of 620km. The satellite carried a scanning radiometer which obtained broadband measurements of spectral radiance in the visible (0.55–1.1 micrometer wavelength) and thermal infrared (10.5–12.5 micrometer) portions of the electromagnetic spectrum. This instrument viewed the surface of the Earth as it passed beneath the satellite and obtained simultaneous measurements of reflected solar radiation and emitted thermal radiation in its visible and infrared channels, respectively.

The field of view of the HCMM radiometer was mechanically rotated through a scan angle of 60° producing imagery with a nominal swath width of 720km. The ground resolution of the radiometer was 600 × 600 meters in the thermal channel and 500 × 500 meters in the visible channel immediately beneath the spacecraft (i.e. at nadir). Data obtained in the two channels can be spatially cross registered to an accuracy of 0.2 resolution elements or better. Measurement precision in the two channels was limited by the analog telemetry system to a Noise Equivalent Radiance (NER) of 0.2 mw/cm^2 in the visible and a Noise Equivalent Temperature Difference (NEDT) of 0.4°K at 280°K in the thermal infrared.

Because HCMM was an experimental mission, it was not designed to obtain global coverage of the Earth's surface. The HCMM satellite did not possess an onboard tape recorder system. Consequently, it was only able to obtain useful scientific data when within range of certain ground receiving stations. HCMM data have been acquired over extensive areas of North America, Europe, and Australia. (HCMM Data Users Guide, associated catalogs, and data in both image and digital format, are now available from the National Space Science Data Center, Code 601.4, NASA Goddard Space Flight Center, Greenbelt, Maryland 20071).

Scientific Investigations

HCMM was designed to experimentally evaluate the usefulness of remotely sensed surface temperature measurements for a wide variety of applications in geology, botany, ecology, hydrology, and meteorology. The orbital characteristics of the satellite permitted repetitive observations of mid-latitude regions over the course of the diurnal heating cycle. Repetitive coverage at mid-latitudes occurred at times of maximum and minimum surface temperature (roughly 1:30 p.m. and 2:30 a.m. local time, respectively). This type of coverage is optimal for observing temporal and spatial thermal contrast within surficial materials.

HCMM thermal infrared measurements can be used to examine the amplitude of day/night variations in surface temperature on a regional basis. Furthermore, simultaneous measurements of surface reflectivity obtained at visible wavelengths during daytime HCMM passes can be used to estimate surface albedo and thus infer the amount of solar energy available for surface heating. Combined analysis of regional variations in albedo and day/night temperatures allow the bulk thermal properties of near surface materials to be evaluated, specifically thermal inertia which is a function of bulk density, thermal conductivity, and heat capacity.

Most other Earth viewing satellite systems, such as Landsat, only obtain measurements in the visible (0.4–0.7 micrometer) and reflected infrared (0.7–2.5 micrometer) portions of the electromagnetic spectrum.

Table 1. Domestic HCMM Investigations

Principal Investigator and Affiliation	Test Site Location	Objectives
Mr. James C. Barnes Environmental Research and Technology, Inc. Concord, Massachusetts	Sierra Nevadas, California; Central Arizona Mountains	Use HCMM data to study snow hydrology, thermal mapping of snow, operational snow cover mapping and runoff prediction.
Dr. Toby N. Carlson Department of Meterology Pennsylvania State University University Park, Pennsylvania	Washington, DC; St. Louis; Houston; Los Angeles	Utilize data from HCMM as input to mesoscale wind model to study urban heat islands.
Dr. J. C. Harlan Remote Sensing Center Texas A & M University College Station, Texas	West/Central Oklahoma	Demonstrate the feasibility of using HCMM-derived plant canopy temperature and soil moisture data as a measure of cultivated crop condition in ungrazed dryland farming areas where temperature and precipitation measurements normally do not exist.
Dr. Ray D. Jackson U.S. Deparment of Agriculture Water Conservation Laboratory Phoenix, Arizona	Central California	Demonstrate the use of spacecraft temperature and albedo data to assess soil moisture over large areas to improve agricultural resources management practices.
Dr. Anne B. Kahle NASA/Jet Propulsion Laboratory Pasadena, California	Death Valley, California; Walker Lane, Nevada; Pisgah, California	Investigate the feasibility of using thermal inertia inferred from remotely sensed temperature data for reconnaissance geologic mapping and mineral exploration.
Professor Ronald J. P. Lyon Dept. of Applied Earth Sciences Stanford University Stanford, California	Yerington, Nevada	Investigate the utilization of thermal sensing in rock discrimination and mineral exploration. Evaluate thermal modeling techniques.
Dr. Donald G. Moore Remote Sensing Institute South Dakota State University Brookings, South Dakota	South Dakota	Develop a remote sensing method for rapid and accurate detection and monitoring of regions with shallow water tables which are susceptible to ground water contamination.
Dr. Terry W. Offield U.S. Geological Survey Branch of Uranium and Thorium Resources Denver, Colorado	Wyoming; Arizona	Map thermal inertia for discrimination of geologic units and energy or mineral resource areas and evaluate thermal modeling and satellite mapping techniques.
Dr. Ernest I. Rich School of Earth Sciences Stanford University Stanford, California	Northern California	Identify rock types via seasonal thermal changes, identify linear features buried under alluvial fill.
Mr. John R. Schott Calspan Corporation Buffalo, New York	Lakes Erie and Ontario; plus Rochester, Buffalo and Syracuse	Study the thermal properties of the Great Lakes as they relate to water quality, lake hydrology and energy exchange. Study urban heat islands (Buffalo, Rochester and Syracuse).
Dr. Craig L. Wiegand U.S. Department of Agriculture Agricultural Research Service Weslaco, Texas	South Texas	Use day and night HCMM data for freeze damage assessment, planting date advisory and evapotranspiration studies.
Mr. Donald R. Wiesnet National Oceanic and Atmospheric Administration National Environmental Satellite Service Environmental Sciences Group Suitland, Maryland	Adirondack Mountains; Potomac River Estuaries; Luverne, Minnesota; East/Central California	Chart tidal currents in estuaries; evaluate thermal inertia soil moisture measurements and study of the thermal emission of snow.

Measurements of reflected solar radiation can only be used to infer information about the surface properties of ground materials. HCMM is unique in that it acquired data which can potentially be used to obtain information about the bulk physical properties of surficial materials.

Twelve domestic (U.S.) investigators and twelve foreign investigators from a variety of scientific disciplines were selected by NASA to analyze and evaluate the HCMM data. (A listing of domestic investigators is provided in Table 1.). Data collection activities have been in progress for approximately two years. However, most domestic investigators did not begin receiving substantial amounts of data until the spring of 1980 and their studies are consequently in preliminary stages of completion. A brief summary of HCMM results and findings follows.

Geological Applications

HCMM data were analyzed by geologists from the U. S. Geological Survey and were found to be useful for the delineation of subtle, large landscape features which had not previously been observed by field geologists. Although field work is in progress by the USGS to determine the geologic significance of some of the long lineaments observed on HCMM imagery, these features appear to be related to discontinuities (faults) in consolidated rock which may have influenced mineralization in the northern Rocky Mountains and Great Plains. These features were not observed on Landsat or other remote sensing imagery and appear to be related to subtle differences in soil moisture which affect the thermal conductivity and heat capacity of rocks. Geologists from the Federal Republic of Germany developed a technique for displaying reflected energy and day/night temperature images in color. Such a display provided new information on geologic units in Africa which were not obvious on Landsat imagery. The German geological remote sensing team also developed a technique for merging Landsat data with HCMM data to allow both surface properties and body properties of rocks to be analyzed using a color encoded image. The higher resolution reflectance data from Landsat when combined with HCMM thermal emittance data allowed even more geological information to be extracted because the data types are complementary.

Agricultural Applications

Scientists from the U. S. Department of Agriculture and Remote Sensing Institute of South Dakota reported that analysis of data allowed detection of subtle differences in soil moisture, because the amount of water contained in soils and plants has a significant effect on the amount of heat these landscape cover types store and reradiate on a daily basis. The South Dakota investigators were able to delineate cool areas on summer imagery that were related to shallow groundwater sources which are of great importance to farming and land development in the midwest. The form and extent of the shallow groundwater system was not previously known and could not be detected on Landsat data. Aircraft thermal data and ground investigations confirmed the presence of the features. Scientists from Canada and Europe had great difficulty in detecting crop moisture stress because of the cloudy and wet conditions that prevailed in their countries during much of their investigations, and the repeat coverage cycle of HCMM. In semiarid areas like Texas and Arizona detection of crop moisture stress may be feasible, but the short duration of the HCMM mission and problems with data distribution have not yet allowed this feasibility to be successfully demonstrated.

Urban Heat Island Studies

HCMM is able to quantify the degree to which cities are warmer than suburbs and rural areas. This quantification is leading to new insights which may prove most valuable in studies of urban microclimate. Indications are that absence of vegetation and evapotranspiration is responsible for high summer

temperatures, rather than the heat capacity of the asphalt, concrete, and steel environment. Studies of the micrometerology just now beginning may provide guidance on how to use open spaces to best moderate urban temperatures.

Oceans and Lakes

The low spatial resolution and broad coverage of HCMM have made it an ideal system for investigation of circulation patterns of lakes and oceans. In these studies, only temperature measurements and not the temperature differences are required. HCMM thus supplements the data acquired by other satellites.

Future Studies

The data gathering phase of HCMM is complete. The analysis of the data will continue for several more years. As a proof of concept, HCMM has been successful. Modeling studies and field measurements based upon the knowledge gained from this mission will lead to an improved understanding of the utility of thermal measurements for resource applications.

Orbital Sensors Capable of Obtaining Thermal Infrared Measurements of the Earth's Surface

Orbital Sensor	Satellite Mission	Resolution		Ground Coverage	Repeat Cycle	Data Availability			Notes
		Spectral	Spatial			Archive Location	Dates	Data Product	
AVHRR-Advanced Very High Resolution Radiometer	Tiros-N, NOAA 6	Band 3: 3.55–3.93μm Band 4: 10.5–11.5μm	1 km[a] 4 km[b]	300 km swath width/global coverage	diurnal	SDSD/National Geophysical and Solar Terrestrial Data Center	12/78 to present[c]	CCTs, Photographic prints	[a] Local area coverage [b] Global coverage [c] Availability not continuous
AVHRR/2	NOAA 7, NOAA D through NOAA G	Band 3: 3.55–3.93μm Band 4: 10.3–11.3μm Band 5: 11.5–12.5μm	1 km[a] 4 km[b]	3000 km swath width/global coverage	diurnal	SDSD	8/81 to present	CCTs, Photographic prints	[a] Local area coverage [b] Global coverage
CZCS - Coastal Zone Color Sanner	Nimbus 7	Band 6: 10.5–12.5μm	825 m	1566 swath width/global coverage[a]	6 days	SDSD/NSSDC	2/79 to present	CCTs, Photographic prints	[a] Prime operational areas are U.S. and European coastlines, Gulf of Mexico, Mediterranean & Arctic/Antarctic
HCMR-Heat Capacity Mapping Radiometer	HCMM	IR: 10.5–12.5μm	0.6 km	716 km swath width/85° N – 85° S coverage	diurnal, every 5–16 days	NSSDC	4/26/78–10/20/80	CCTs[a], Photographic prints	[a] Registered day/night or individual radiance data
MSS-Multispectral Scanner	Landsat 3	Band 8: 10.4–12.6μm	238 m	185 km swath width/global coverage	18 days[a]	EDC	3/78–3/79 [a]	CCTs[b], Photographic prints	[a] Data is very scanty due to sensor difficulties [b] Contains all MSS bands
OLS-Operational Linescan System	DMSP Block 5-D F1–F4	IR: 8.0–13.0μm	0.5 km[a] 2.8 km[b]	2890 km swath width/global coverage	diurnal	SDSD/NSSDC/WDC-A	3/79 to present[c]	IR mapped images	[a] High resolution mode [b] Low resolution mode [c] Little data currently being received
SR-Scanning Radiometer	ITOS-1, NOAA 1–5	IR: 10.5–12.5μm	7.4 km	4000 km swath width/global coverage	diurnal	SDSD	4/70–6/71[a] 12/72–3/78[b]	Corrected images and mosaics, stereographic photographic prints/CCTs	[a] ITOS-1 & NOAA-1 [b] NOAA 2–5
VHRR-Very High Resolution Radiometer	NOAA 2–5	IR: 10.5–12.5μm	0.87 km	2580 km swath width/global coverage[a]	diurnal	SDSD	9/78–2/79[b] 11/72–2/79[c]	CCTs[b] Photographic prints[c]	[a] Selected regions/times [b] Dates CCTs are available [c] Dates photo products available
VIR-Visible and Infrared Radiometer	Seasat-A	IR: 10.5–12.5μm	5 km	2280 km centered on nadir/75° N to 75° S coverage[a]	36 hours	SDSD	7/5/78–8/25/78	GDR CCT[a]	[a] Data processed for these areas only: 57°–61° N, 90°–16° W
VISSR-Visible/Infrared Spin-Scan Radiometer	GMS	IR: 10.5–12.5μm	5 km	full disk image/global coverage	30 minutes	SDSD	4/78 to present	GMS FGGE data set CCT; Photographic prints	
VISSR	SMS, GOES	Band 8: 10.36–12.12μm	8 km	full disk image/global coverage	30 minutes	SDSD	6/74 to present	Photographic prints, movie loops, CCTs[a]	[a] Digital synoptic sectors
TM-Thematic Mapper	Landsat-D	Band 6: 10.4–12.5μm	120 m	185 km swath width/global	16 days	EDC	7/30/82[a]	CCTs, Photographic prints	[a] Proposed launch date

Archive Location:

SDSD:
Satellite Data Services Division
NOAA/EDIS/NCC
Room 100, World Weather Building
Washington DC 20244
(301) 763-8111 or FTS 763-8111

Supplemental DMSP data:
WDC-A for Glaciology,
CIRES, Campus Box 449,
University of Colorado
Boulder, CO 80309
(303) 492-5171, FTS 323-5311

Supplemental Data for NOAA operational satellites:
National Geophysical and Solar Terrestrial
Data Center
Boulder, CO 80302
(303) 499-1000

NSSDC
National Space Science Data Center
Code 601.4
Goddard Space Flight Center
Greenbelt, MD 20771
(301) 344-6695

Researchers who reside outside of the U.S.
should direct data requests to:

World Data Center A for Rockets and Satellites
Code 601
Goddard Space Flight Center
Greenbelt, MD 20771 USA
(301) 344-6695

EDC
EROS Data Center
U.S. Geological Survey
Sioux Falls, SD 57198
(605) 594-6111

Tiros-N - Television and Infrared Observing Satellite
NOAA - National Oceanic and Atmospheric Administration
Nimbus 7 - (NASA experimental satellite)
HCMM - Heat Capacity Mapping Mission
Landsat - Land Satellite
DMSP - Defense Meterological Satellite Program
ITOS - Improved TIROS Observing Systems
Seasat - Sea Satellite
GMS - Geostationary Meteorological Satellite
SMS - Synchronous Meteorological Satellite
GOES - Geostationary Operational Environmental Satellite
CCT - Computer Compatible Tape
GDR - Geophysical Data Record
FGGE - First Global GARP Experiment (Global Atmospheric Research Program)

ABSTRACTS

Development of an earth resource pushbroom scanner utilizing a 90-element 8-14 micrometer (Hg,Cd)Te array

Thomas J. Brown
HONEYWELL
Defense Electronics Division
Electro-Optics Center
2 Forbes Road
Lexington, Massachusetts 02173

Abstract

Thermal infrared Pushbroom scanners being developed for NASA's earth resources survey experiments in the middle to late 1980's offer high spectral, spatial and temporal resolution, and high reliability through design simplicity. This mode of operation does not require moving optics; has integral chopping and calibration, and consequently, the Pushbroom scanner is lighter, simpler and more compact than its electromechanical predecessors.

This paper describes the development of a 90 linear element, 8-14 micrometer, photoconductive (PC) (Hg,Cd)Te, IR/CCD/MUX Pushbroom Field Test Instrument.

Introduction

The 90-element IR/CCD Pushbroom Field Test Instrument was developed to demonstrate pushbroom scan imagery in the 8-14 micrometer spectral region and will be tested under aircraft flight simulated conditions on laboratory targets as well as on outdoor target terrain. On the basis of these demonstrations, NASA plans to test pushbroom imagery with the focal plane/dewar mounted in a fixed wing aircraft. The instrument is shown in Figure 1.

The pushbroom scanning concept is based on scanning a straight-line path with a linear array of high sensitivity, solid-state infrared detectors. The array elements are activated sequentially in the cross track direction while being swept forward along the flight path as shown in Figure 2. At an altitude of 10 kilometers, the current system can sweep a 7 kilometer wide strip. The length of the strip map depends on the duration of the flight.

Background

It has long been recognized that the technology for making self-scanned multi-element infrared detector focal planes was needed. The invention of charge coupled devices in 1969 sparked an enthusiasm for such focal planes using both monolithic (CCD as the detector) and hybrid (detector connected to the CCD) approaches. The ultimate realization of such a focal plane would employ multi-elements closely packed, moderate operating temperature, high IR sensitivity and low power consumption. These goals are now readily achievable for the thermal (10.5 to 12.5 micrometer) infrared in hybrid focal planes employing (Hg,Cd)Te photodiodes and silicon charge coupled devices.

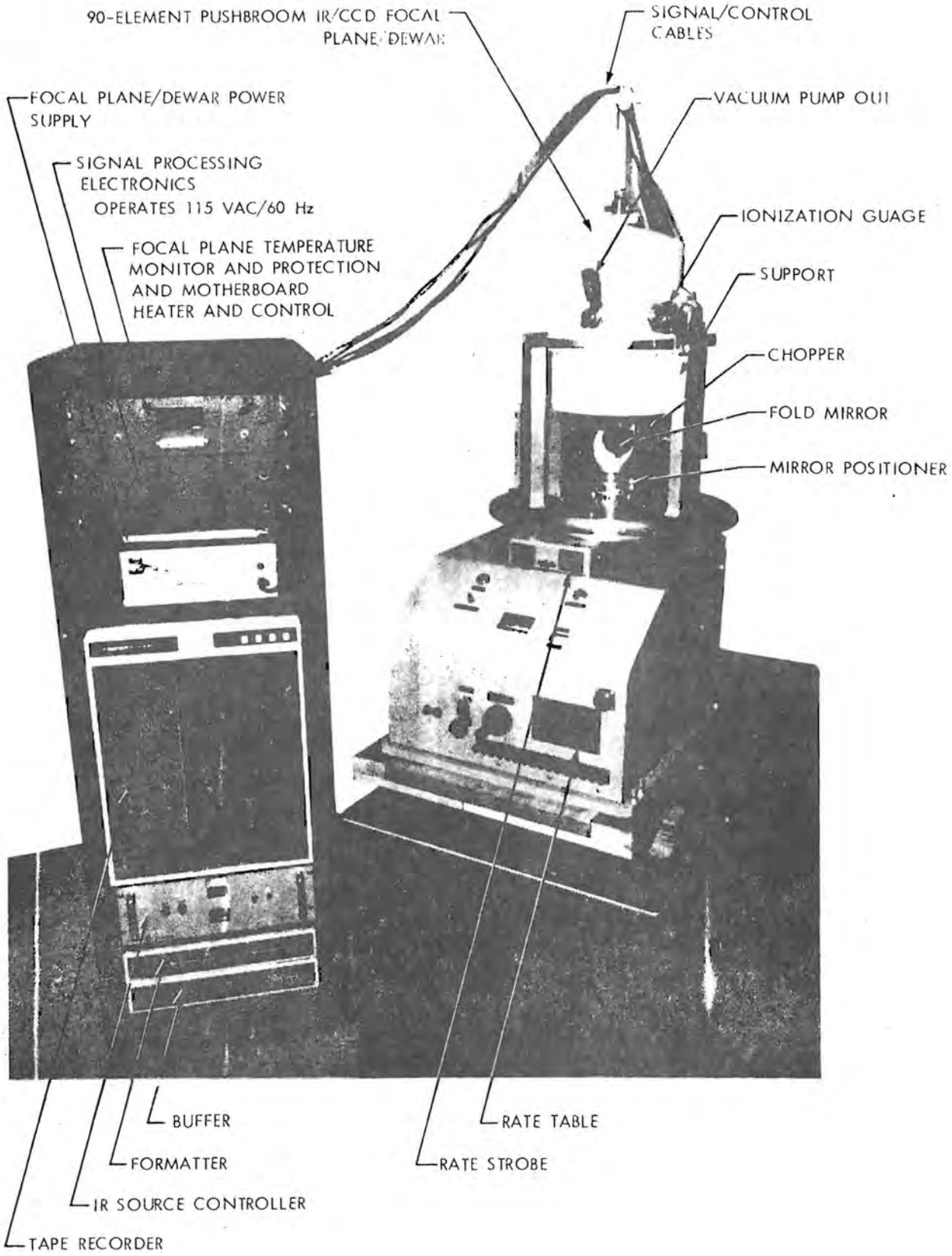

Figure 1. 90-element IR/CCD pushbroom field test instrument.

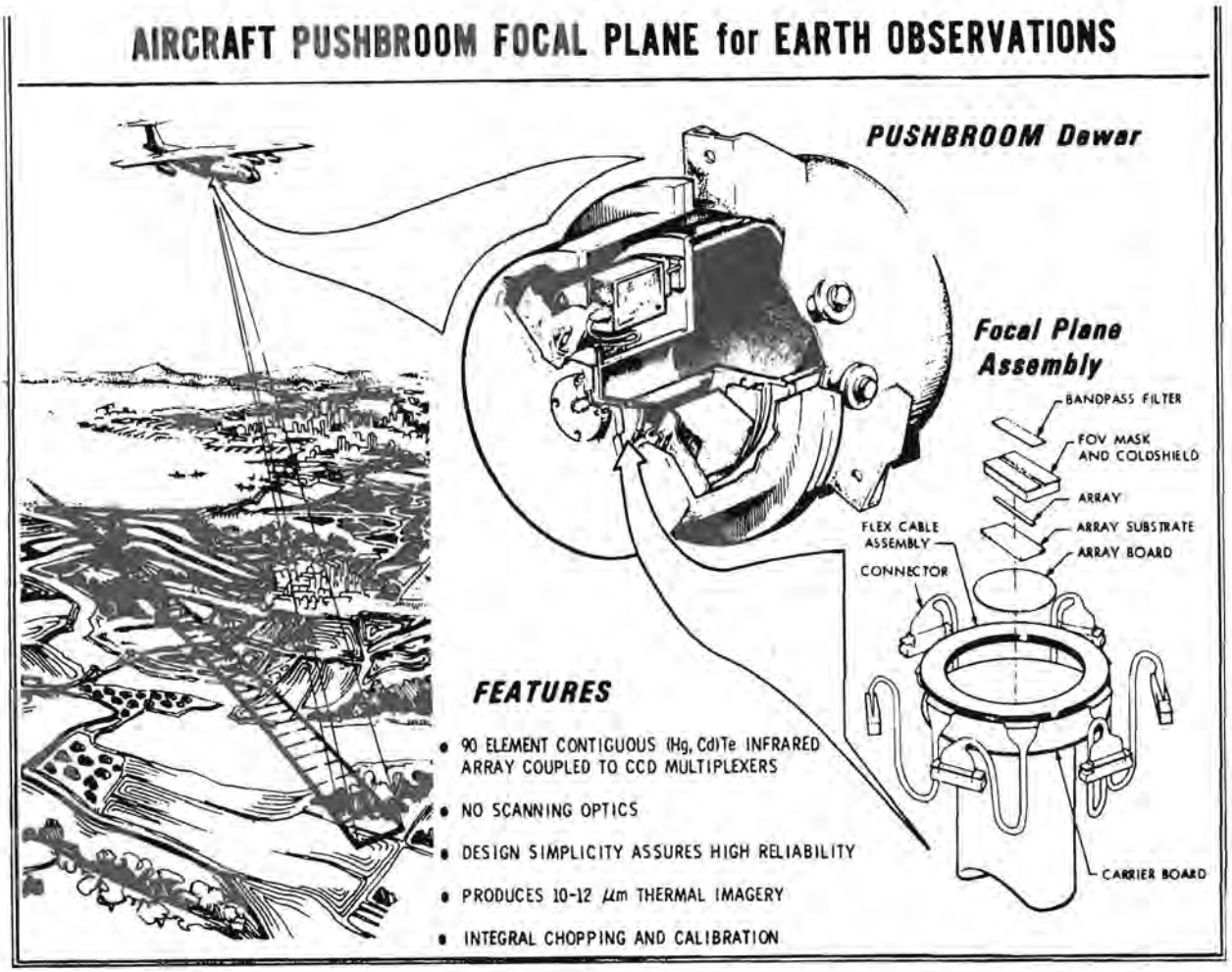

Figure 2. Pushbroom scanning concept.

A simple 9-element focal plane detector array and signal processing electronics was developed and delivered to NASA/Goddard Space Flight Center in December 1977. The feasibility of pushbroom was verified in the laboratory with this 9-element system. Since (Hg,Cd)Te photodiodes (sensitive in the 10.5 to 12.5 micrometer region) having sufficiently high performance for direct coupling to CCD's were unavailable at the time, an array of (Hg,Cd)Te photoconductive detectors was parallel-coupled to the CCD through cryogenically cooled preamps. An array of high performance detectors was mounted in a variable temperature (80 to 120 K) test dewar along with 9-matched preamps and a 30-channel CCD multiplexer. A self-contained system was designed and fabricated, as depicted in Figure 3. Tests showed a 9-channel average D^*_λ peak value of 7.5×10^9 cm $Hz^{1/2}W^{-1}$ (17 Hz, 60° FOV, 1 Hz, 105 K) at the output of the CCD multiplexer. This exceeded the work statement objective by a factor of 5. The detector array alone exhibited an average D^*_λ peak of 9.6×10^9 cm $Hz^{1/2}W^{-1}$ and, hence, the total S/N degradation suffered in the multiplexing electronics was limited to only 22 percent.

This 9-element IR/CCD focal plane and electronics has since been integrated into a thermal infrared imaging system at NASA/GSFC using LSI microprocessor image processing and a CRT display. After two years of operation

and repeated dewar evacuations using an oil diffusion pump, the focal plane has shown only a 5 to 10 percent reduction in responsivity. This speaks well for the reliability and performance of such focal planes.

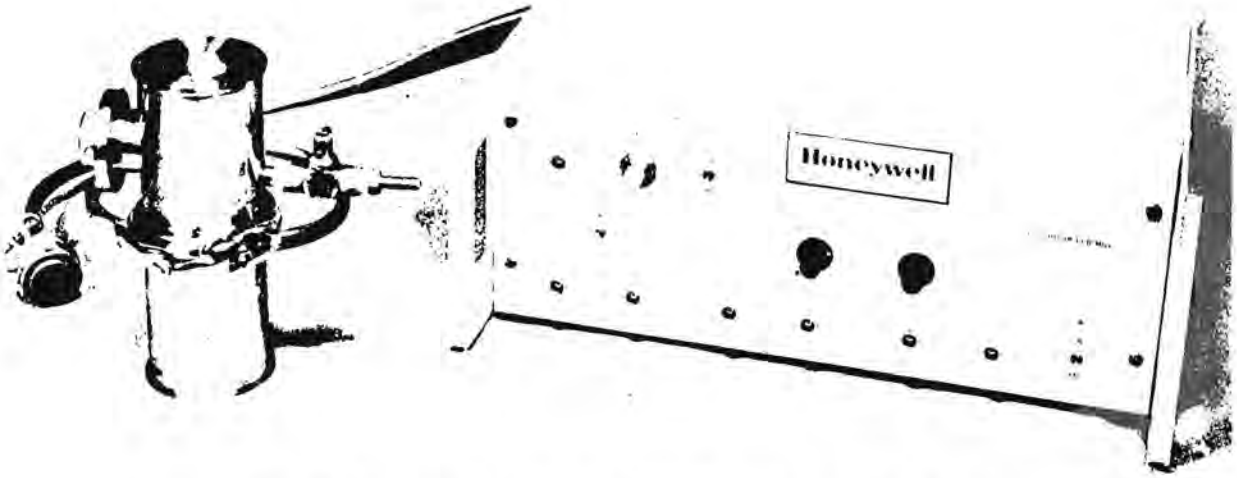

Figure 3. The 9-channel 10μm PC (Hg,Cd)Te IR/CCD MUX breadboard.

On the basis of the 9-channel Pushbroom PC IR/CCD (hybrid) breadboard, NASA/GSFC funded the 90-element Aircraft Pushbroom IR/CCD Focal Plane development program in October 1977. Nearing the completion of the 90-element program in July 1979, NASA/GSFC initiated the construction of a 90-element IR/CCD Pushbroom Field Test Instrument and image processing facility. The objective of this project was to demonstrate thermal infrared Pushbroom hard-copy imagery.

The development of the 90-element system from October 1977 to the present is the subject of this paper.

System description

The 90-element IR/CCD Pushbroom Field Test Instrument was designed to simulate flight motion and pushbroom scanning operation on the NASA/GSFC CV-990 or C-45 Airborne Laboratories. The ground based test instrument consists of the 90-element linear (Hg,Cd)Te photoconductive focal plane and dewar assembly together with NASA/GSFC supplied electronics which provides power to the dewar electronics and controls for the operation of the CCD electronics and the additional system components shown in Figure 1.

The field test instrument has been complemented with an image processing facility which permits an immediate "in-house quick look" at infrared tape recordings of natural and artificial scenes taken in the laboratory and out of doors. The field test instrument is shown in Figures 1 and 4 and the image processing facility is shown in Figure 5.

The components specified for the system included a rate table, fold mirror, mirror positioner, reference blackbody source, tuning fork chopper, system mount and a focal plane temperature monitor and protector, and motherboard heater and temperature control.

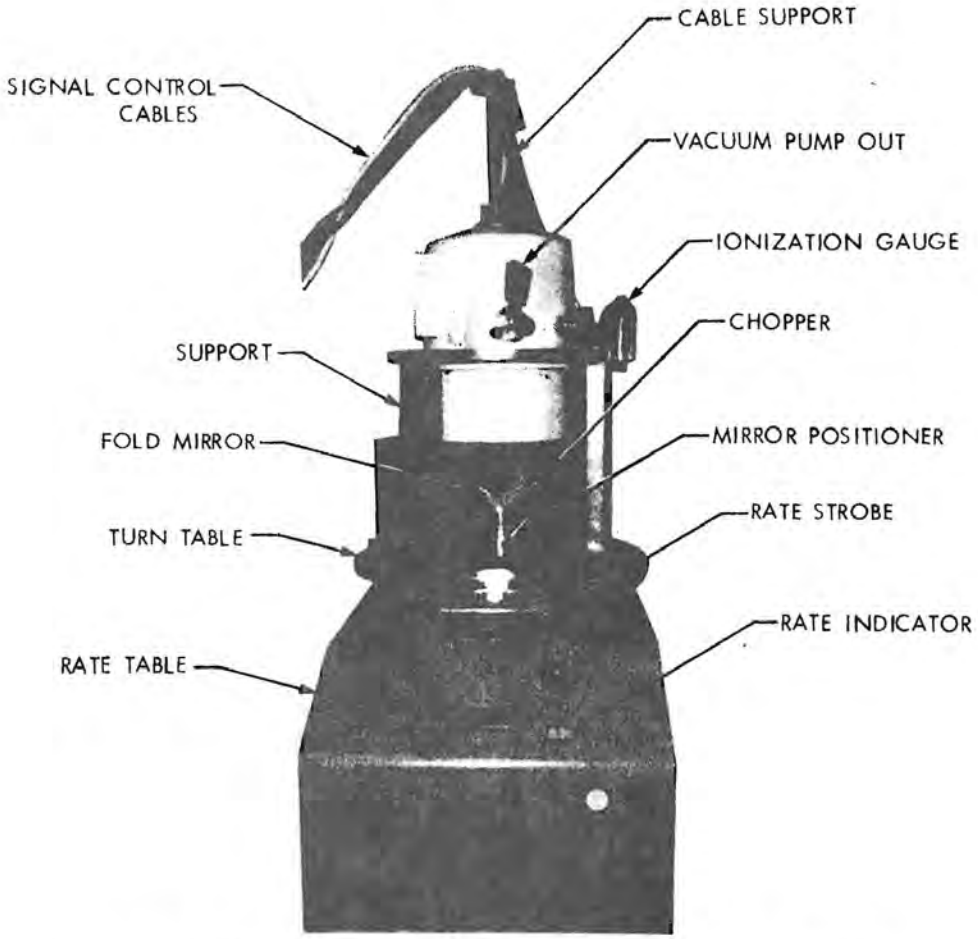

Figure 4. 90-element Pushbroom IR/CCD focal plane/dewar and rate table.

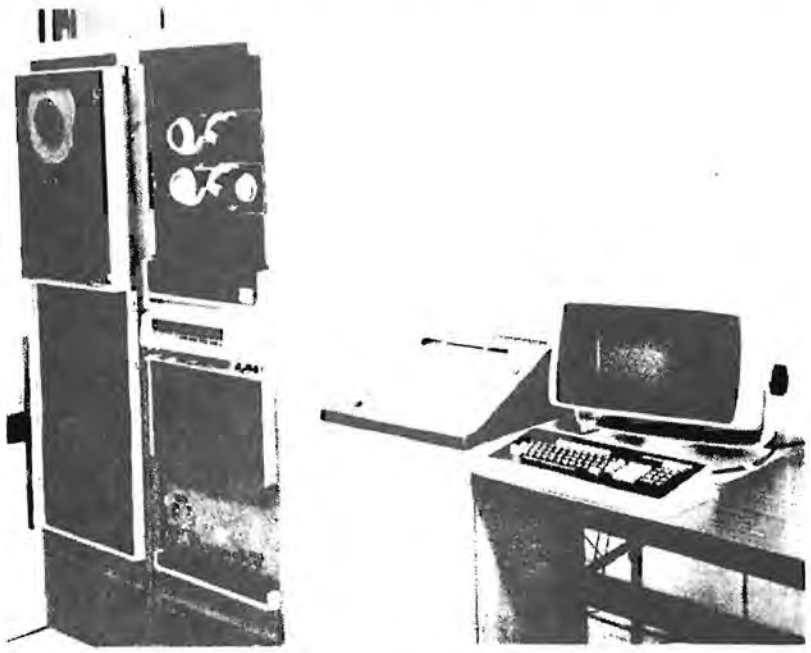

Figure 5. Image processing facility.

System operation

The system operation can best be explained by referring to the system schematic in Figure 6. The focal plane dewar is operated in a vertical downward position to insure liquid nitrogen (77 K) cryogenic cooling for the detectors. The 90 elements are projected vertically to the scene or 30° to the blackbody source by the fold mirror and an f/2.25 germanium lens cell. A 30 Hz tuning fork chopper modulates the input radiation and provides a syncronizing pulse to the signal processing electronics. The leading or trailing edge of the chopper blade initiates the sampling of the chopper blade reference temperature or of the scene, respectively. The system will be calibrated using the five inches square blackbody source against the blade temperature. Calibration tapes will be run with the rate table stopped. Imagery of the blackbody source is expected to be lightly striped, due primarily to the non-uniformities of responsivity of the detectors. A master "striping correction" algorithm will be generated from these data. The power supply provides detector bias power and power to the motherboard heater. The local plane and motherboard temperatures are monitored and the detector bias power is interlocked to a thermal monitor to prevent detector damage above 85 K.

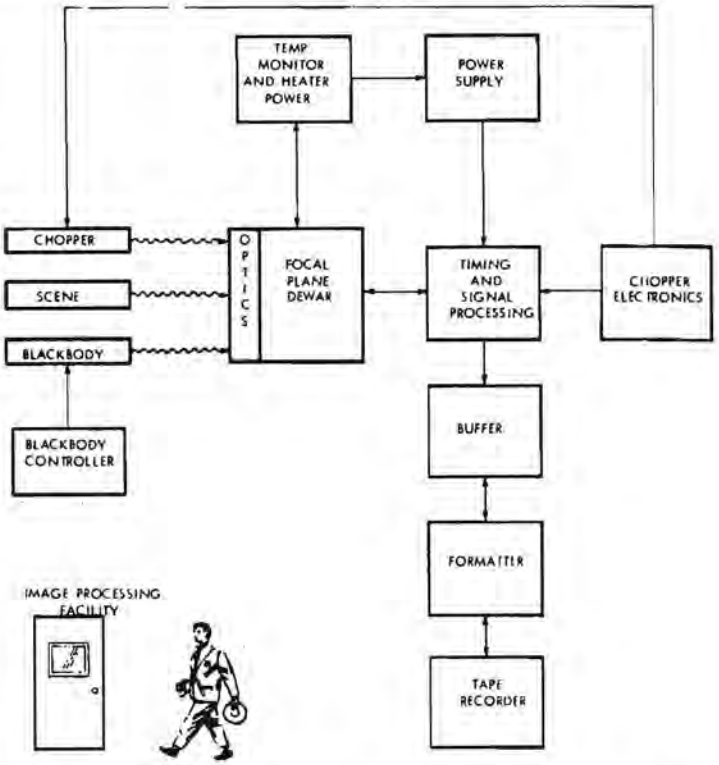

Figure 6. Schematic diagram of the pushbroom IR/CCD field test instrument and image processing.

Each photoconductive (Hg,Cd)Te detector element has a discrete component preamplifier, which is coupled to one of six 15-channel CCDs (6 x 15 = 90 elements). Each CCD takes every 6th detector/preamp signal output, i.e. CCD#1 takes elements number 1,7,13,19,25, etc. while CCD#2 takes elements numbers 2,8,14,20,26, etc. A description of the operation of the Honeywell CCD multiplexer number 2178 SSC will not be discussed at this time; however, in this application, the chopper frequency is 30 Hz, the sample rate is 180 Hz, the CCD clock rate is 2.7 KHz, the data rate is 6,120 bytes per second, and there are six data lines as mentioned before. The CCD analog output is converted A/D and fed to a buffer, formatter and finally to a 9 track, 75 IPS, tape recorder with dual density. The signal flow from the scene to the tape recorder is shown graphically in Figure 7.

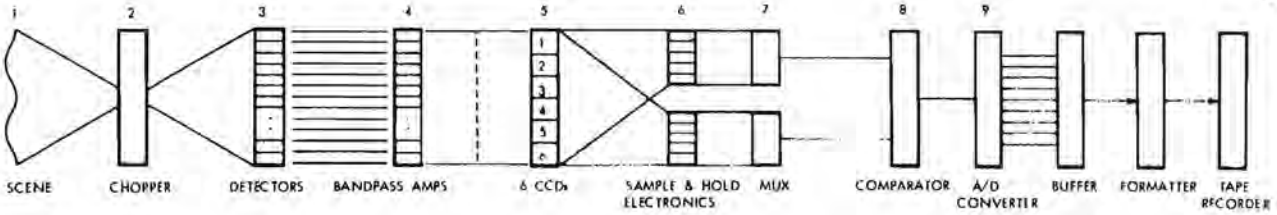

SIGNAL DESCRIPTIONS

1. SCENE RADIANCE $N_\lambda(T, \epsilon)$
2. TUNING FORK CHOPPER FREQUENCY IS 30 Hz
3. DETECTOR CURRENT $I_D(N_\lambda, S_\lambda)$, WHERE S_λ IS SPECTRAL RESPONSIVITY OF DETECTOR
4. AMPLIFIER OUTPUT CURRENT $I_A = I_D A_f$, WHERE A_f IS CURRENT GAIN
5. CCD CHARGE $Q = I_A H$ WHERE H IS INTEGRATION TIME; TWO OUTPUTS V_o $Q/C + V_{reset}$ AND V_{reset}
6. ELECTRONICS SAMPLE AND HOLD BOTH SIGNAL AND RESET VOLTAGES
7. SIX PARALLEL ANALOG SIGNAL AND RESET VOLTAGES ARE MULTIPLEXED SEPARATELY
8. COMPARATOR OUTPUT, $V_{signal} = V_o - V_{reset}$
9. A/D CONVERTER OUTPUT IS 8 PARALLEL BITS

Figure 7. Pushbroom IR/CCD/MUX signal flow.

The Pushbroom System operation sequence is shown below.

Time	Operation
24 hours	Cool down and turn on heater for electronics (stabilize motherboard)
20.0 min	Turn on blackbody source (if calibration only)
10.0 min	Set mirror to appropriate position (0° for scan 120° CCW for calibrate)
5.0 min	Turn on rate table (scan only)
4.0 min	Turn on tape equipment and mount tape
2.0 min	Power up electronics and chopper
1.0 min	Engage Rate Table (scan only)

Electronic signal processing and data records and file lengths are covered in subsequent paragraphs.

System specification and performance

The 90-element Pushbroom IR/CCD Focal Plane specifications and performance data, the output signal description, flight simulation conditions, scan motion and effects of table speed on file lengths are shown in the following tables of specifications and data.

System design

The 90-element Pushbroom IR/CCD Field Test Instrument radiometric performance, scan motion, electronic signal processing and image processing design studies are discussed in the following sections.

Table 1. 90-Element Pushbroom IR/CCD Field Test Instrument Specifications and Data

Focal plane specifications

Element size	0.002" x 0.002" Nominal
Spacing between elements	0.0002" Nominal
Number of Elements	90
Array Configuration	Linear
Spectral Range	8 to 14 micrometers
Scene Dynamic Range	260 to 320 K
Scene Resolution	0.5 K at 300 K
Operating Temperature	77 K
Dewar Hold Time	> 18 hours
IFOV	5.5 mr

Detector focal plane performance data

Bias power dissipation	1.25 mW/detector (average) 113 mW(total)
Average D* (500 K, 1000 Hz)	$9.1 \pm 1.2 \times 10^9$ cm $Hz^{1/2}W^{-1}$
Average D* (13.2 μm, 30 Hz)	6.78×10^9 cm $Hz^{1/2}W^{-1}$
Calculated NEΔT (300 K)	0.569 K (no oversampling)

Output signal description

Sample Frequency	180 Hz
Chopper Frequency	30 Hz
Samples Recorded per Chopper Cycle	2
Output Word Length	8 Bits
Number of Gray Levels	256
Record Length	1632 bytes
File Lengths (Depending on Table Speeds)	
2.42 degree/s	417792 Bytes
1.45 degree/s	835584 Bytes
0.94 degree/s	1671168 Bytes

Table 2. System Operation Parameters

	ALTITUDE, (FT)	VELOCITY, (FT/s)	IFOV FOOT-PRINT (FT)	DETECTOR DWELL TIME PER IFOV, (MILLISEC)	SCAN SWATH WIDTH,(FEET)	DEMONSTRATION SCAN RATE, (DEGREES/s)	OVERSAMPLING FACTOR	RESULTANT NEΔT AT 300 K (K)	FILE LENGTH REQUIRED FOR 180° SCAN, (STRIPES)	FILE LENGTH (MEGA BYTES)	NUMBER OF GOOD DATA STRIPES/ IMAGE
MAXIMUM SCAN RATE FOR UNIT SAMPLING FACTOR (ONE SAMPLE PER CHOPPER DWELL)	3*	-	0.20 inch	33.3	2.25	9.45	1.00	0.569	512	0.104	512
C45 TWIN BEECH	6000	150	33	130	4400	2.42	3.90	0.[illegible]	2048	0.418	1997
C45 TWIN BEECH	10000	150	55	217	7300	1.45	6.50	0.773	4096	0.836	3228
CV 990 AIR BORN LABORATORY	35000	340	192	335	25500	0.94	10.00	0.180	8192	0.671	5120
RESOLUTION LIMIT OF 8 BIT A/D CONVERTER	-	-	-	-	-	-	-	0.234	-	-	-

* MINIMUM DEPTH OF SYSTEM FOCUS

Radiometric performance

The radiometric resolution of thermal scanners is frequently characterized by their noise equivalent differential temperature which is the temperature differential between adjacent elements of the scene that will yield a signal equal to the system noise. The NEΔT can be expressed in terms of the noise equivalent radiance NER and the differential radiance due to a unit change in temperature dN/dT:

$$NE\Delta T = \frac{NER}{dN/dT}$$

The noise equivalent radiance can be described by:

$$NER = \frac{\sqrt{A_D}(\Delta f)^{1/2}}{A_c \Omega_c D^* \tau_o (\nu_p/\nu_s)}$$

where quantities required for the calculation are enumerated in the following paragraphs.

The reduction of the test data on the 90 elements in the detector array yielded an average detectivity of D^* (1000 Hz, 500 K) = $0.90 \times 10^{10} \pm 0.12 \times 10^{10}$ cm-Hz$^{1/2}$ W^{-1}. Data were also taken for the spectral response on six of the elements which showed that the wavelength at peak response was approximately λ_p = 13.2 micrometers. The factor to convert the blackbody D^* to the detectivity at the wavelength at peak response is 2.38, so:

$$D^* \text{ (1000 Hz, 13.2 } \mu\text{m)} = 2.14 \times 10^{10} \text{cm-Hz}^{1/2} \text{ W}^{-1},$$

The chopper frequency for the Pushbroom system is 30 Hz, which suggests a reduction in the D^* due to 1/f noise. Eleven detectors on the array were tested to determine the typical noise spectrum of the elements. The average increase in the detector noise level in going from a 1000 Hz to a 30 Hz chopping frequency was a factor of 3.16. Correspondingly, the detectivity will be reduced by this factor,

$$D^* \text{ (30 Hz, 13.2 } \mu\text{m)} = 6.78 \times 10^{9} \text{ cm-Hz}^{1/2} \text{ W}^{-1},$$

The IFOV of each of the 90 elements on the detector array is nominally 5.5 milliradians which yields a solid angular subtense of:

$$\Omega_c = (5.5 \text{ mr})^2 = 3.03 \times 10^{-5} \text{ ster.}$$

The dimension of the individual detector elements are 2 x 2 mils or $\sqrt{A_D} = 5.08 \times 10^{-3}$ cm.

The optics included two optical filters and a f/2.25 lens cell.

The lens cell has three antireflection coated germanium lenses each with an average transmittance over the 8 to 14 micrometer spectral region of approximately 0.91. The two filters each have nominal transmittances over this spectral region of about 0.80. So, the optical efficiency of the filters and lenses is:

$$\tau_o = (0.9125)^3 \, (0.800)^2 = 0.486$$

The diameter of the entrance aperture of the lens cell is 4 mm, so the area of the aperture is $A_c = \pi(0.2 \text{ cm})^2 = 1.26 \times 10^{-1}$ cm^2.

The bandwidth of the CCD sampling electronics is Δf = 90 Hz, 1/2 of 180 Hz sampling frequency, according to Shannon's Sampling Rate Theorem.

The degradation in NER due to the signal processing is included in the factor (v_p/v_s). A factor of $(1/2)(4/\pi)(1/\sqrt{2}) = 0.45$ arises when the RMS fundamental component is extracted from 30 Hz square wave resulting from the chopped radiance signal.

There will be an additional factor resulting from inefficiencies in the signal processing circuitry. The CCD's integrate the current output of the preamps. The integration time per sample is $\tau_i = 1/f_{sample}$. Of the six integrations (samples) taken over each chopper period only two are processed and recorded, one of the scene and one of the chopper blade reference. These are eventually subtracted from one another. Ideally, all six integrations should be used to give the best signal to noise ratio. This nonoptimized situation results in the signal voltage level being lower by a factor of 3 and the noise voltage level being lower by a factor of $\sqrt{3}$ (noise power will be lower by a factor of 3). This results in a lowering of the signal to noise ratio by a factor of $\sqrt{3}$, or in effect, (v_p/v_s) has a factor of $1/\sqrt{3}$ included for an overall value of:

$$(v_p/v_s) = 0.45/\sqrt{3} = 0.260$$

The above quantities yield a noise equivalent radiance of:

$$NER = 1.47 \times 10^{-5} \text{ W/cm}^2\text{/Ster.}$$

The value of dN/dT can be exactly determined by the evaluation of the integral:

$$dN/dT = \int_{\lambda_1}^{\lambda_2} \frac{\partial N_\lambda}{\partial T} S(\lambda)\, d\lambda$$

which can be reduced to the following approximation:

$$dN/dT = \frac{S N_\lambda c_2}{\lambda T^2} \Delta\lambda$$

Here, c_2 is one of Planck's radiation constants. The normalized spectral responsivity S is close to unity because the detectors are operating near their peak spectral response. The spectral radiance of a blackbody at temperature T, N_λ is calculated from Planck's radiation equation to be:

$$N_\lambda(T) = \frac{c_1}{\pi\lambda^5 \left(e^{c_2/\lambda T} - 1\right)}$$

$N\lambda(260\text{ K}) = 4.85 \times 10^{-4}$ W/cm^2/ster/μm
$N\lambda(300\text{ K}) = 9.28 \times 10^{-4}$ W/cm^2/ster/μm
$N\lambda(320\text{ K}) = 1.21 \times 10^{-3}$ W/cm^2/ster/μm

The differential radiance is:

$dN/dT\ (260\text{ K}) = 1.80 \times 10^{-5}$ W/cm^2/ster/K
$dN/dT\ (300\text{ K}) = 2.58 \times 10^{-5}$ W/cm^2/ster/K
$dN/dT\ (320\text{ K}) = 2.96 \times 10^{-5}$ W/cm^2/ster/K

So the noise equivalent differential temperature is:

$$NE\Delta T\ (T) = \frac{NER}{dN/dT(T)}$$

$$NE\Delta T\ (260\ K) = 0.818\ K$$
$$NE\Delta T\ (300\ K) = 0.569\ K$$
$$NE\Delta T\ (320\ K) = 0.497\ K$$

These values of NEΔT are irrespective of any oversampling that may occur if the rotary table angular speed is less than some value related to the chopper frequency and the IFOV,

$$(30\ \text{samples/s}) \times (0.314°/\text{sample}) = 9.42°/\text{s}$$

The necessary table angular speeds to adequately simulate the flight speeds of the C45 and CV990 aircraft can be defined by an over sampling factor F at a given table speed w,

$$F = \frac{w\ (\text{No Oversampling})}{w\ (\text{Oversampling})}$$

Correspondingly, the signal to noise ratio for the particular pixel in an image will be increased by a factor of $\sqrt{F}$ (signal increases by factor of F and noise increases by a factor of $\sqrt{F}$). Therefore, the NEΔT will decrease by a factor of $\sqrt{F}$. The effect of oversampling is summarized in Table 2.

GSFC supplied electronics

The sampling frequency is nominally 180 samples per second, and the chopper frequency is 30 Hz; therefore, six samples per chopper cycle are taken. The leading and trailing edge of the chopper signal begins the simultaneous sampling of the CCD wells. The first sample is dumped because it may occur while the chopper aperture is not fully open (closed).

The outputs of the CCD wells are fed into six 8-bit analog to digital converters which produce parallel words. These six words are then multiplexed into a single 8-bit data line. The output of the electronics includes the 8-bit parallel word and the appropriate control inputs to the buffer, formatter and 9 track tape recorder.

Record and file lengths

Each sampling of the complete 90-element array are accompanied by six housekeeping bytes and six blank characters for a total of 102 bytes. A stripe is defined as two consecutive samplings of the 90 elements (one of the scene and one of the chopper blade reference) yielding a total of 204 bytes/stripe. To use the two 2048 byte buffer memories most practically, it was decided to use eight stripes per record or 1632 bytes per record.

It is required that, independent of scan rate, a 90 x 512 pixel image is produced with each scan which represents a (512 pixels) x (0.315°/pixel) = 161° scan angle. Also, each scan will yield a single file. This means that the slower the scan rate, the greater the file length. Table 2 shows the relationships between the

aircraft being simulated, required table speed, and oversampling factor. The amount of good data stripes in a 161 degree scan file is (oversampling factor) x (512 stripes). For simplification the lengths of files written on tape will be 2^m stripes or 2^m x 204 bytes where m is an integer such that 2^m is the number of good stripes. The remainder of the file is filled with data, but will be ignored in the image processing. The file lengths and the number of good data stripes for the desired table speeds are also summarized in Table 2.

Image processing study

A tradeoff was made to determine the most optimum way to process the data. The basic choice was whether to use a Control Data CDC6600 via remote terminal to Bethesda, Md., or to use an in-house system used for image processing for another application. It was ultimately decided that the advantages of being in-house outweighed any other factors and we proceeded with the necessary software modifications. The resulting software has the advantage that it provides an immediate "quick look" at IR data tapes and is general enough to handle almost any input format. It will be useful for more advanced image processing in the future.

"Striping correction" algorithm and rehistograming programs were written. The "striping correction" program features a main program plus a number of utility subroutines for creating an artificial diagonal striped and graded gray scale test picture, Figure 8, for a line averaging check and for resampling algorithms for n^{th} order oversampling. Additional programs permit average and standard deviation calculations of the signal amplitude for the 90 elements for a uniform input signal and for scene input signals.

The details of the 90-element IR/CCD Pushbroom Image Processsing Facility will be covered in a separate paper.

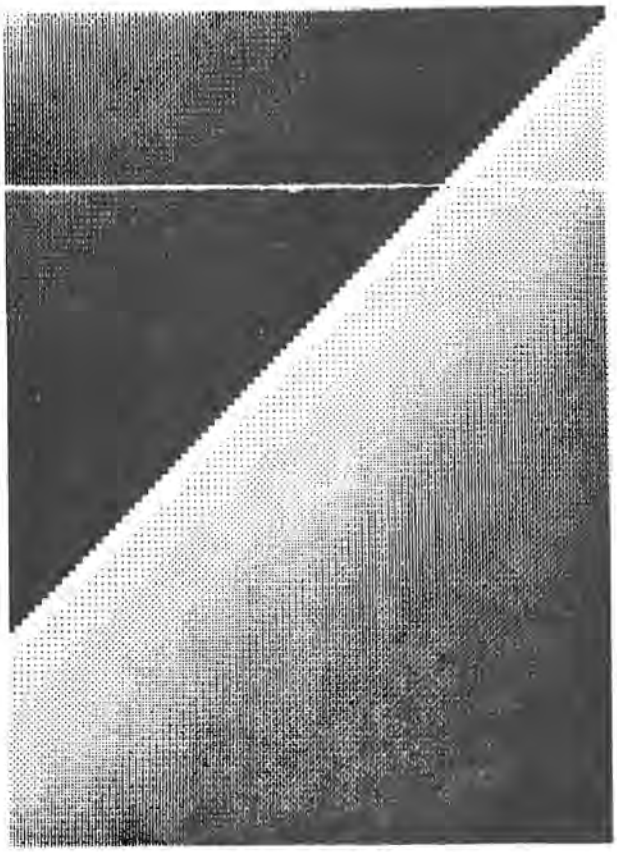

Figure 8. Test gray scale image.

A 120 element array was selected. The array is shown in Figure 9, with a close-up shown in Figure 10. One advantage of the selected array was that it had 30 more elements than required and provided flexibility should outages occur due to manufacturing defects or should performance vary significantly across the array. The detector array assembly was designed for this flexibility (see Figure 11). All 120 elements were good and the center 90 were used.

A key design feature was the six circular flex cables that interfaced between the carrier board and the tape-to-wire adapter board. All 120 detector element leads were brought out to pads on the edge of the carrier board that were sequenced around the periphery. Each flex cable was attached to 15 detector element pads at intervals of six elements. The cables then route the elements to a grouped pattern on the tape-to-wire adapter board. This pattern connected to a wire bundle cable with a connector attached. This, in turn, connected to the preamplifier assembly, bringing the detector elements in contact with the inputs of the preamplifiers. The reason behind the six groups of 15 elements was that the CCD shift register had only 16 inputs. Using 15 of the 16 inputs required six separate CCD shift registers. The CCD's are clocked simultaneously and six outputs are sampled and held and then sequentially multiplexed in order to get six outputs in one CCD clock period. The adjacent inputs to any one CCD are tied to detector elements separated by intervals of six elements to permit an "unscrambled" serial presentation of the imaged data.

The circular tape cables and tape-to-wire adapter board could be assembled in any angular position relative to the carrier board; however, the best 90 (center) consecutive elements within the 120 element array were used.

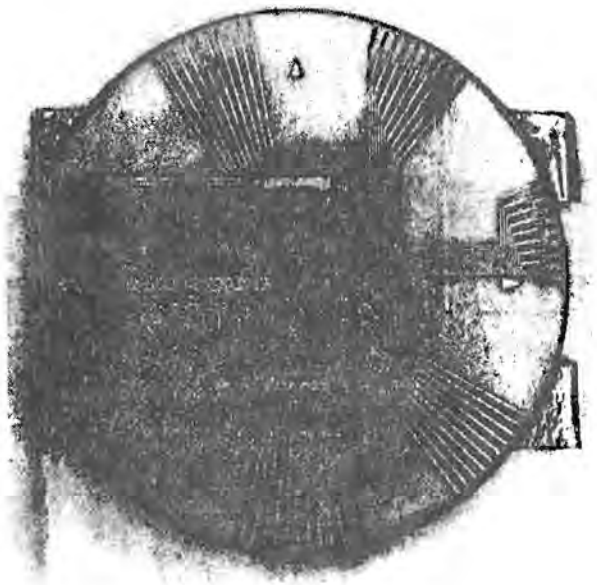

Figure 9. 90 (120) - element pushbroom (Hg,Cd)Te focal plane array.

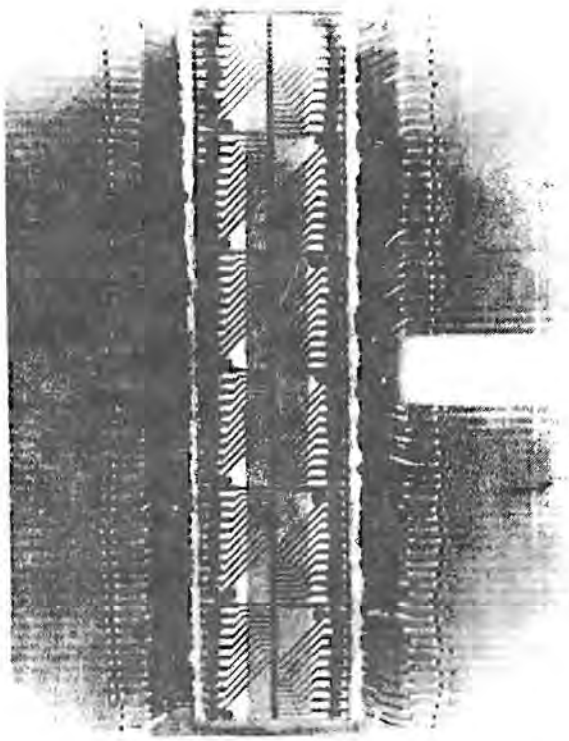

Figure 10. 90 (120) - element pushbroom (Hg,Cd)Te focal plane array close-up.

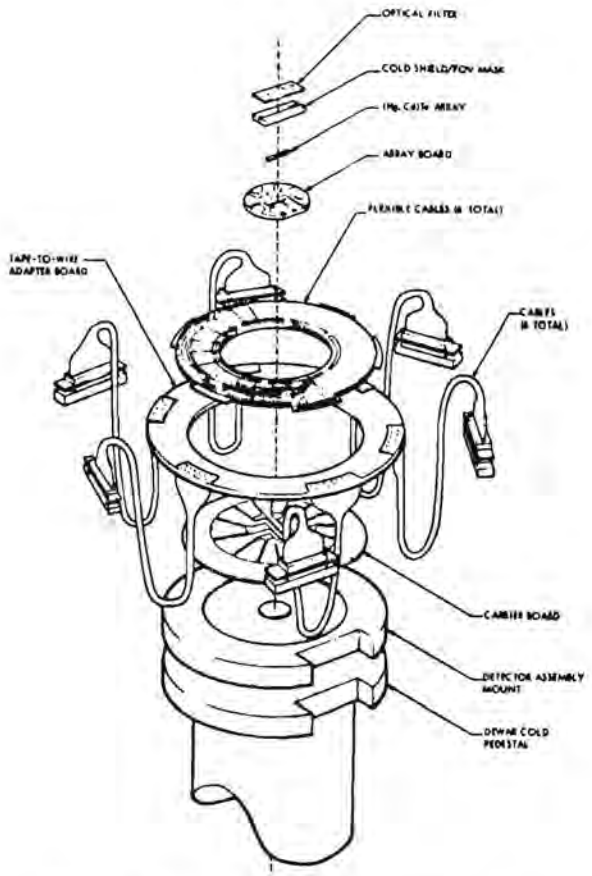

Figure 11. Detector array assembly.

The array board contains the detector array, the combination field-of-view mask, cold shield and bandpass filter and the printed circuit fiducial marks which were aligned with those of the carrier board as the array board was being bonded to the carrier board.

The carrier board consists of a ceramic printed circuit board bonded to an aluminum plate which interfaces to the cold finger of the dewar. This method was chosen, instead of directly bonding the carrier board to the dewar cold finger, because the wire connections from the array board to the carrier board was made by thermocompression bonding.

Preamplifier assembly

The preamplifier assembly design was based on double-sided printed circuit board technology and was configured as six modules containing 15 preamplifiers each with all modules connected to a common motherboard. Three preamplifiers were packaged on a single printed circuit card and five identical cards are contained in each module. See Figure 12.

The preamplifier cards were mounted orthogonal to the motherboard and held in place as follows. Wire leads from the preamplifier board were placed around all five boards comprising a module, with grooves in the side pieces to constrain side-to-side motion. A metal cover was installed on the frame with spring clips bonded to the inside surface to provide a compression force for the preamplifier cards. See Figure 13.

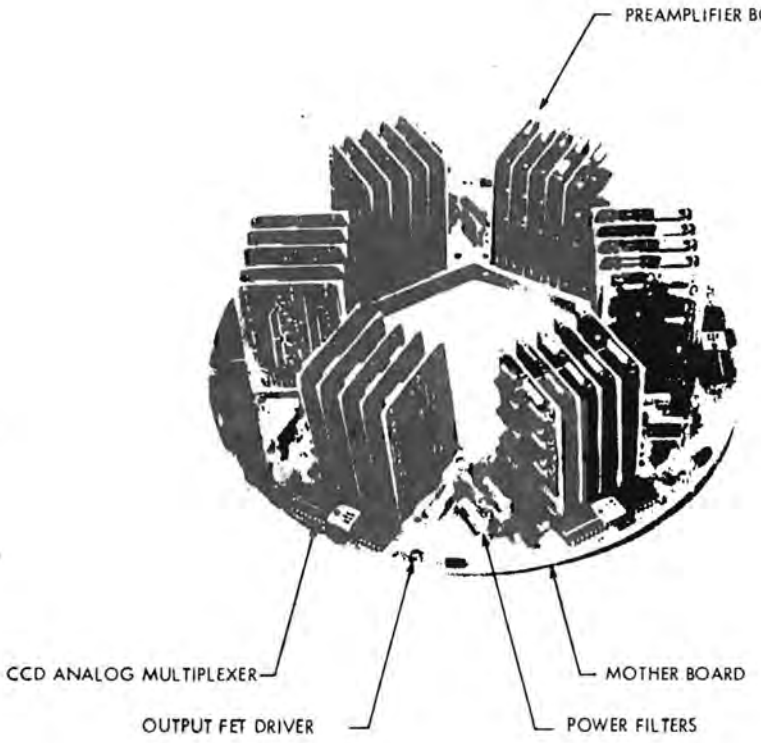

Figure 12. Preamplifier assembly without metal frame.

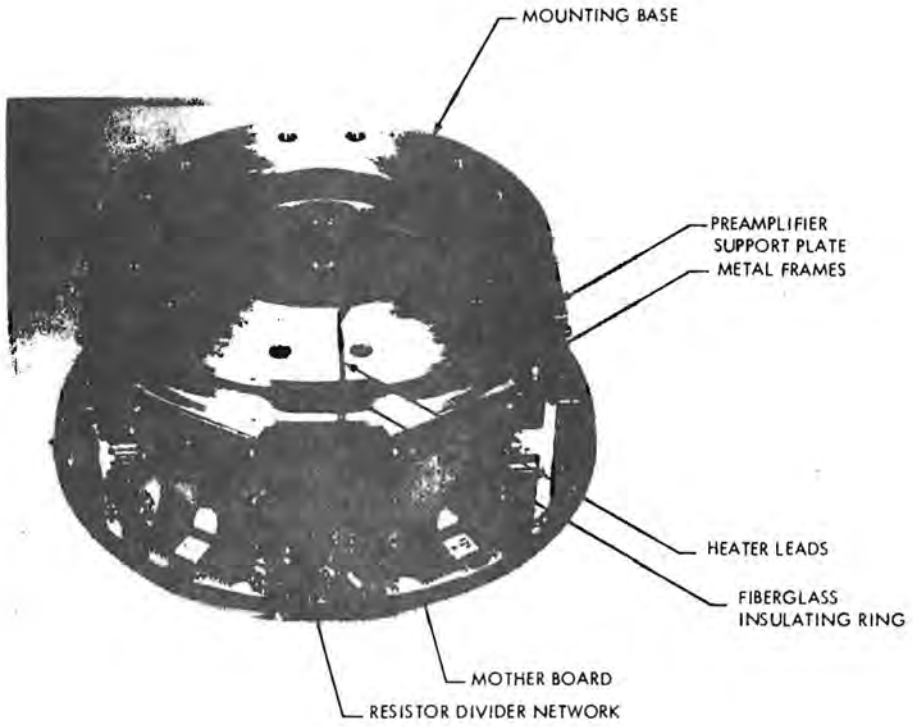

Figure 13. Preamplifier assembly with metal frames.

The CCD shift registers, with output FET source follower, were mounted on the motherboard, one for each preamplifier module.

The key to the preamplifier assembly design was not as much the packaging approach as it was the thermal design. The dewar cold finger and platform operate at 77 K to maximize the detector array performance. Operating the electronics close to 77 K would have degraded the component performance and reliability; therefore, the preamplifier mount assembly was made of two aluminum rings separated by a fiberglass cylinder which was bonded to each ring. The preamplifier assembly was attached to the upper ring, and the lower ring was clamped to the dewar cold platform. The dimensions of the fiberglass cylinder was designed to provide a thermal conductance that would allow the preamplifier assembly to operate at 200 K. The heat generated by the preamplifiers provide the thermal source with thermal paths to the cold dewar through the fiberglass cylinder, connecting cables and radiation. The preamplifier assembly was shielded from the dewar warm inside walls with aluminized mylar. See Figures 14 and 15.

The preamplifier mount assembly contains a printed wire heater bonded to the underside of the upper plate and provisions to cold strap across the fiberglass cylinder.

Dewar feed-thrus

One vacuum feed-thru connector handles all electrical signal and power inputs and electronic signal outputs to the GSFC supplied power supply, signal processing, logic and timing circuits. A second vacuum feed-thru was used for the motherboard heating tape power input and for temperature sensor monitors.

Component trade-offs: limitations on system configuration

The previous section discussed some of the mechanical, electronic and optical requirements of the Pushbroom system. However, an important consideration was the 40 degree field-of-view of the focal plane which put

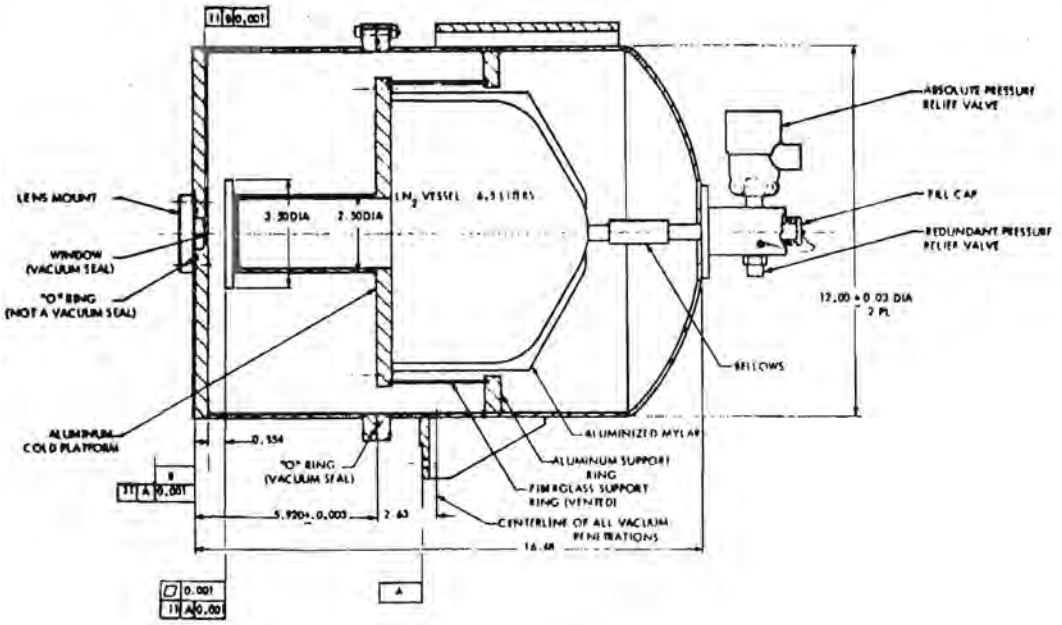

Figure 14. Dewar design.

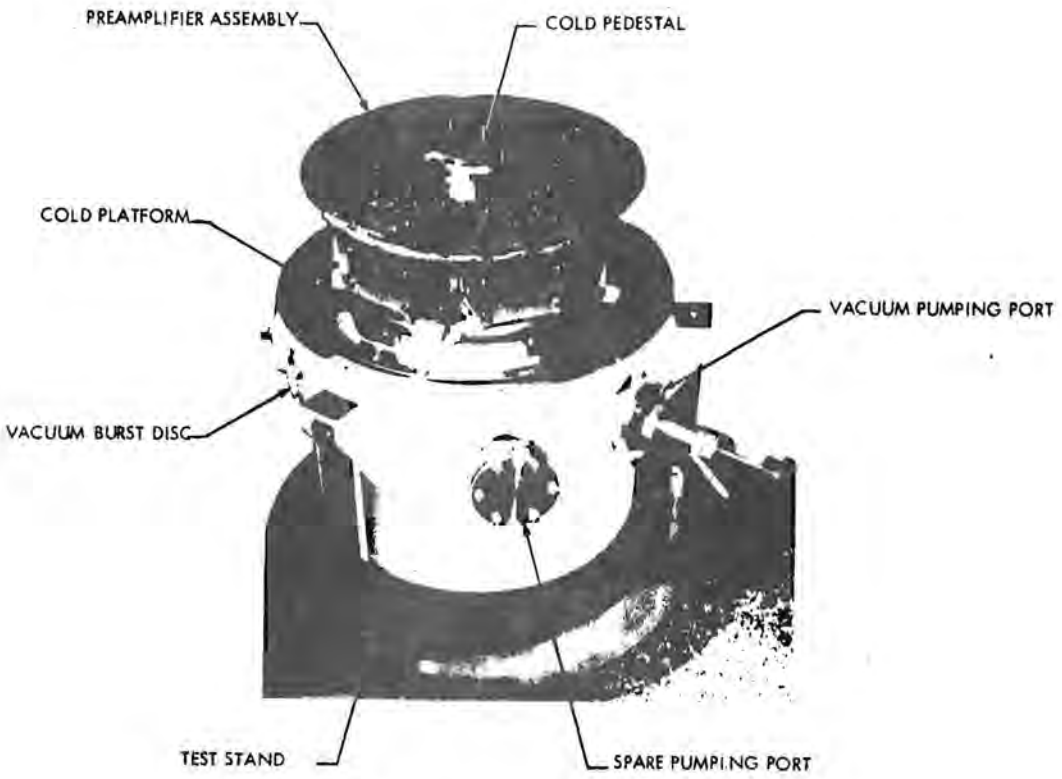

Figure 15. Dewar with cover removed.

limitations on the system configuration. As a result of this, size became an important design consideration and the system configuration was significantly modified from the preliminary concepts.

Chopper

Initially, rotary motion variable speed choppers were considered but, in all of the motor driven choppers considered, the problem arose with the drive motor obstructing a portion of the 40 degree FOV. An alternate choice was to consider a tuning fork chopper. A drawing of the chopper is shown in Figure 16.

Rotating mirror and positioner

The function of the rotating mirror includes the reflection of the image of the 90-element array into the blackbody source. This reduces the size of the holding fixture required for mounting the dewar and the other components. The mirror is rotated 120° counter clockwise from the forward looking scan position to image the array at a 30° angle across the emitting plate of the reference source. The reflective surface was diamond turned and coated with SiO to provide approximately 97 percent reflectivity in the 8-14 micrometer spectral region.

Reference and calibration source

The major trade-offs were performance, overall size of source, emitting area, cost, and weight. The requirements for reference and calibration sources were met with a 5 inches x 5 inches emitting surface blackbody source.

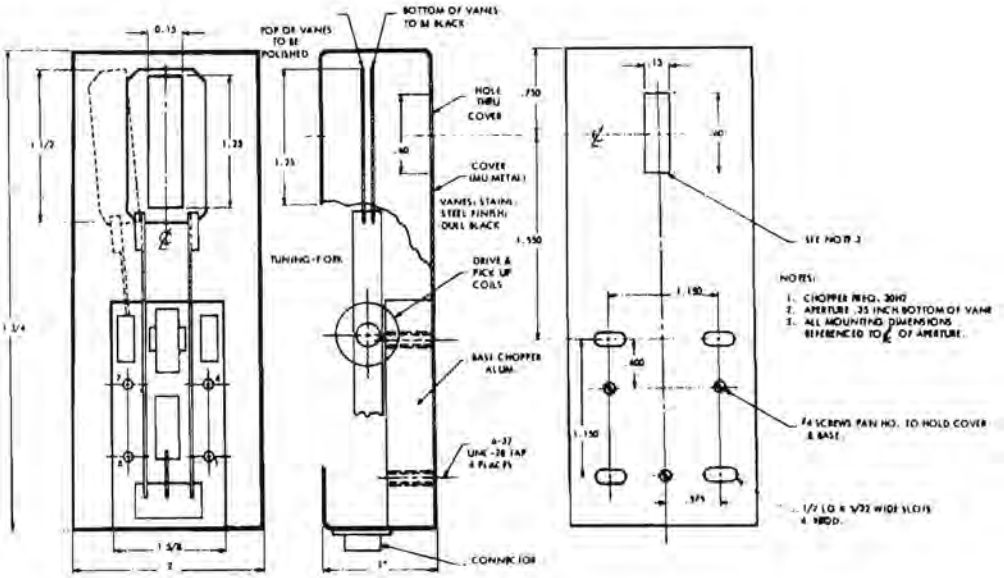

Figure 16. Final chopper drawing.

Dewar holding fixture

The dewar holding fixture was designed to accommodate all the system components and to operate satisfactorily when subjected to the torque motion of the rotary table. The mounting pads of the dewar rest on the top of the fixture flange; see Figure 4. The blackbody source was mounted on a flat rectangular alignment plate. The rotation stage with mirror was bolted to a removable center base plate. When the fixture is eventually installed in an aircraft, the center baseplate with the rotation stage and mirror will be removed leaving a clear downward viewing aperture.

Rotary table

The table was required to accommodate a load of 125 pounds and to meet the requirements on scan motion set out in a previous section. It met all the speed and accuracy requirements, and has a 24 inch turntable.

Systems test: calibration with blackbody source

The Pushbroom system will be tested over the range of the thermal source (283-333 K). The position of the mirror will be 120° counter clockwise from the forward looking scan position. The rate table will not be used. A number of files of uniform calibrated input will be used to determine the final "striping correction" algorithm factors.

Spatial resolution

Spatial resolution will be checked using a bar chart pattern, with a spatial interval of 0.4 inch minimum at 3 feet distance, 0.09 cycles per milliradian.

Simulation of flight conditions

Using the rate table, the C45 and CV990 aircraft motion will be simulated and 90 x 512 pixel byte files will be created. This will be repeated several times using various scenes. Typical scenes may be a group of people or objects in the lab, or a building outside. The resulting pictures will be analyzed to check the resolution of the objects and the overall quality of the images.

Conclusion

The successful developments of the 9-element and 90-element thermal infrared hybrid imaging systems using photoconductive (Hg,Cd)Te has verified the operational concept of 8-14 micrometer pushbroom scanners.

Ideally, photovoltaic (Hg,Cd)Te diodes are best for larger focal planes, since they permit direct coupling (no pre-amplifiers) and consume very little power. In 1977, to test the direct coupling concept, a 5 micrometer photovoltaic (Hg,Cd)Te detector was directly connected to a Si CCD MUX. No degradation in signal-to-noise-ratio was experienced and a D* peak value of 1.6×10^{11} cm $Hz^{1/2}$ W^{-1} (BLIP) was obtained after the CCD multiplexer, when the photodiode at 77 K was irradiated by the 300 K background with 180 degree field of view. That historic achievement represented a major milestone towards the realization of a hybrid focal plane. Today these PV (Hg,Cd)Te IR/CCD Pushbroom focal planes are a reality and there is a high probability that they will be selected for use in NASA's next generation earth resource satellites. A conceptual drawing of such a focal plane is shown in Figure 17.

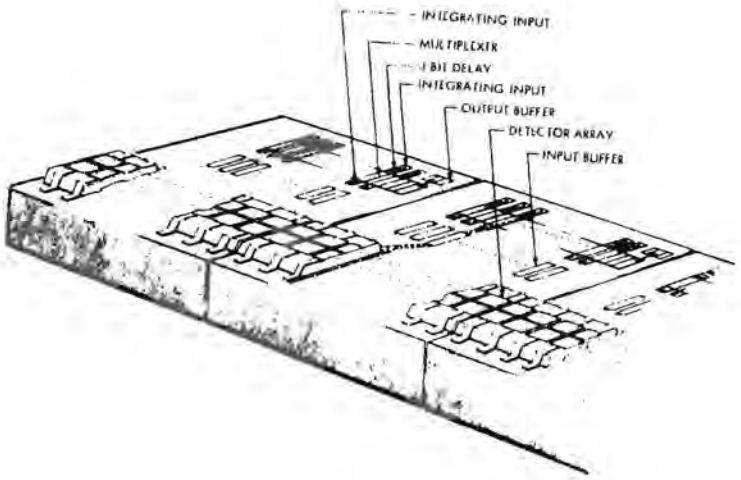

Figure 17. Photovoltaic (Hg,Cd)Te IR/CCD pushbroom focal plane concept.

Acknowledgements

The author wishes to thank H. Ostrow and L.Thompson of NASA for their support and guidance, and is indebted to J. Spera, P. O'Sullivan, and H. Hackney for the system; to M. Harris and F. Frazier for the image processing, and finally to K. Twohig, W. Rae, S. Iwasa, J. Stobie and R. Bombard for the focal plane dewar assembly.

This work was supported under NASA/GSFC 5-24323 and NASA 5-25662.

References

1. Thompson, Leslie L., Tracy, Richard A., and Frankel, David G., "On-board radiometric preprocessing for multispectral linear arrays (MLA)", Proceedings of the Society of Photo-Optical Instrumentation Engineers, Vol. 178, Smart Sensors, April 17-18, 1979, Washington, D.C. pp 83-90.

2. Thompson, L.L., "Remote Sensing Using Solid State Array Technology," Photogrammetric Engineering and Remote Sensing, Vol. 45, No. 1, January 1979, pp 47-55.

3. Gurnee, M.N., and Iwasa, S., "Experimental Verification of High Detector/CCD Performance with Direct Coupled Non-BLIP PV Detectors at Thermoelectric Cooler Temperatures", Proceedings of IRIS Detector Specialty Group, June 1978.

4. Foss, Norm A., and Gregorick, David, "Direct Coupled PV Detector/CCD Interfacing for Non-BLIP Focal Planes", Proceedings of IRIS Detector Specialty Group, June 1978.

5. Schnetzler, Charles C. and Thompson, Leslie L., "Multispectral Resource Sampler: An Experimental Satellite Sensor for the Mid-1980's", Proceedings of the Society of Photo-Optical Instrumentation Engineers, SPIE Technical Symposium, Vol. 183, May 22-24, 1979, Huntsville, AL.

6. Barbe, D.F., "Advanced Infrared Focal Plane Array Concepts", Electro-Optical Systems Design, April 1977, pp 50-58.

SOME SENSITIVITY CONSIDERATIONS FOR A THERMAL IR MULTISPECTRAL SCANNER. Alexander F. H. Goetz and Alan R. Gillespie, Jet Propulsion Laboratory, California Institute of Technology, Pasadena, CA 91103.

The encouraging results obtained by Kahle and Rowan (1980) using multispectral thermal infrared images for the mapping of silicates and carbonates in the East Tintic mining district, Utah, have provided renewed impetus for the construction of an aircraft thermal IR MSS. The following is a somewhat elementary discussion of some of the important design considerations for such an instrument.

The principal parameters affecting the signal received from the ground by the instrument are: (1) ground temperature, (2) atmospheric transmission and emission, and (3) spectral emissivity. Ground temperature and atmospheric effects play a much greater role on the signal value received by the instrument than does spectral emissivity, the desired quantity.

Temperature Effects

Figure 1 demonstrates the range of radiance values that can be expected. Using Planck's law and assuming a uniform spectral emissivity across the 8-12 μm region, the dynamic range of signal, or the difference between the maximum and minimum signal expected, is a little more than a factor of two for a 40°K range in temperatures. All values in these plots are given per micrometer wavelength interval. The second plot in figure 1 shows the change in radiance per degree Kelvin for a range of temperatures as a function of wavelength. From these data the equivalent change in temperature for a change in emissivity of 0.01 can be calculated. This parameter is then readily compared to the sensitivity of scanner systems commonly given in units of noise equivalent change in temperature or NEΔT. For a one micrometer bandwidth the NEΔT for a 0.01 change in spectral emissivity ranges from approximately 0.5° at 8 μm to 0.8° at 12 μm. The total range of spectral emissivities expected is approximately 0.15 (Kahle et al., 1980). Therefore a maximum apparent temperature change of only 8° associated with variation in spectral emissivity can be expected.

Atmospheric Effects

Calculation of the effect of the atmospheric emission and absorption for various elevations was made using the LOWTRAN 4 program (Selby et al., 1978). Figure 2A shows the values of the total radiation received at the sensor as a combination of the surface contribution attenuated by the atmosphere, and the emission from the atmosphere. The standard case is developed from the U.S. Standard Atmosphere with a visibility of 23 km, the surface at 2 km above sea level and the sensor at 5 km above the surface. The atmospheric emission term constitutes approximately 8% or less of the energy arriving from the surface. Also, figure 2A shows the radiation received in the presence of a tropical summer atmosphere. This illustrates one of the extremes one would expect in atmospheric effects. Figure 2B shows the standard case and the effect of looking 45° off the nadir, simulating the effect of scan angle. The total signal varies less than 3% from nadir to 45° off nadir. This variation is significant, however, easily defined and compensated during data reduction.

Figure 2C portrays the atmospheric effects that can be expected from satellite altitude. Significant absorption occurs in the 8-9.5 μm region. The effect of the 9.6 μm ozone band is seen clearly as an absorption of nearly one-half of the signal from the surface. None of the effects described preclude mid-IR spectral imaging from orbit.

The question of system sensitivity requirements can be calculated theoretically, but the interpreter's perception of the information content in an image cannot be quantified. The following is a description of an empirical method, using existing data, to determine the sensitivity requirements for thermal spectral imaging.

Simulations

Kahle et al. (1980) constructed a "color enhanced radiance composite" picture from three channels of thermal scanner data (Table I) in which changes of reststrahlen band intensity and wavelength were exploited to display varying concentrations of silica over a test region in the East Tintic mining district of central Utah. Here we model and simulate the effects of changing the signal/noise ratio and detector size on the interpretability of this color radiance composite picture.

Table I: Mid-IR channels on NASA's 24-Channel Scanner. Stars denote channels selected by Kahle et al. (1980) to use in constructing color radiance composite picture

Channel	Band Limits (Micrometers)
17*	8.3 - 8.8
18*	8.8 - 9.3
19	9.3 - 9.8
20*	10.1 - 11.0
21	11.0 - 12.0
22	12.0 - 13.0

Kahle et al. (1980) created the color radiance composite by principal component transformation of radiance data from channels 17, 18, and 20, followed by non-linear contrast stretches in each of the now uncorrelated principal component images, a technique they considered to yield optimum results for color display. The contrast stretches were chosen to cause each principal component image histogram to resemble a Gaussian distribution. Subsequently, the inverse transformation was applied to recreate the correlated channels 17, 18, and 20, now stretched for display as blue, green, and red components of an additive color composite.

We simulated the effects of noisy detectors on this color radiance composite by adding normally distributed random noise to channels 17, 18, and 20, and then performing the same procedure utilized by Kahle et al. (1980) to produce a color composite for comparison. Table II lists the standard deviation of the noise (in DN) necessary to simulate noisy images with the specified NEΔT's.

Table II Equivalent DN values and filter sizes required to simulate different NEΔT's

NEΔT (°K)	1.00	0.50	0.32	0.106	0.053
Channel 17	9.6	4.4	2.4	[3x3]	[6x6]
Channel 18	11.2	5.2	2.7	[3x3]	[6x6]
Channel 20	9.5	3.8	0	[3x3]	[6x6]

To simulate data with lower NEΔT than measured for NASA's 24-channel scanner which varied from 0.2 to 0.32°K, the data were first adjusted to a uniform NEΔT of 0.32°K, and then neighboring pixels were added together to produce a smaller picture, with fewer pixels but increased IFOV. In theory, adding pixels together reduces noise by $N^{-1/2}$ where N is the number of pixels. The size of the neighborhood used is reported in brackets in Table II. In practice, this simulation corresponds to increasing the detector size and increasing dwell time. Each of these changes reduces noise, so if the detector size is doubled and the dwell time is doubled, the NEΔT should decrease by

$$\frac{1}{\sqrt{4}} \times \frac{1}{\sqrt{2}}$$

to about 35%. Actually, the realized NEΔT will be somewhat greater than 50% of the original, because detector behavior is not ideal. Thus our simulation (NEΔT reduced to 50%) should be fairly accurate.

Figure 3 presents four of the simulations we studied. Figure 3C shows the basic composite of Kahle and Rowan (1980), except that the NEΔT in each channel has been increased to 0.32°K. Figure 3D shows the same composite, except that the "detector size" has been increased to 6 x 6 pixels to drop the NEΔT to 0.053°K. The increased pixel size and loss of spatial resolution is clearly visible, and color contrast has been increased. This is because the noise-free histograms are more peaked (lower standard deviation) than histograms of noisy data, so contrast stretching to fit the Gaussian distribution used by Kahle et al. (1980) actually is harsher than the stretch they used.

In Figure 3A, NEΔT has been increased to 1.0°K. The most noticeable effect is the loss of color resolution compared to the less noisy images. This is caused by loss of contrast in the stretched principal component images as the histograms are broadened by the addition of random noise. As shown in Figure 3B, further increases of the contrast in the principal component images restores some of the lost color differences, but also makes speckle from the added noise more evident.

Summary

Sensitivity calculations can be made by theoretical means as well as demonstrated by simulations using real data. The simulations show that in order to measure and portray meaningful surface spectral emissivity variations, a system with 0.5 μm widebands requires a NEΔT at 300°K of 0.4° or better. This value is similar to the one obtained by theoretical calculation.

Acknowledgments

This research was carried on at the Jet Propulsion Laboratory, California Institute of Technology and was sponsored by the National Aeronautics and Space Administration under contract NAS7-100.

REFERENCES

Kahle, A. B. and L. C. Rowan, Evaluation of multispectral middle infrared aircraft images for lithologic mapping in the East Tintic Mountains, Utah, Geology in press, May 1980.

Kahle, A. B., D. P. Madura and J. M. Soha, Middle infrared multispectral aircraft scanner data: Analysis for geological applications, Applied Optics, in press, July 1980.

Selby, J. E. A., F. X. Kneizys, J. H. Chetwynd, Jr., and R. A. McClatchey, Atmospheric transmittance/radiance: Computer code LOWTRAN 4, Air Force Geophysics Lab., Rpt. # AFCL-TR-78-0053, Hanscom AFB, Mass. 01731, 100 pp, 1978.

Figure Captions

Figure 1 Theoretical calculations of (a) blackbody spectral radiance for various temperatures. Ordinate W is displayed in relative units. (b) Change in radiance as a function of temperature and wavelength. (c) Equivalent temperature change for a change in spectral emittance of 0.01.

Figure 2 Theoretical radiance at the sensor for a variety of conditions using the LOWTRAN 4 program. The values plotted are the surface radiance at the surface, the atmospheric emission from the column extending from the surface to the sensor and the total radiation reaching the sensor which is the sum of the two components modified by the atmospheric transmission. (A) Standard case using the U.S. standard atmosphere, 23 km visibility, ground at 2 km above sea level and sensor 5 km above ground level. For tropical summer the same visibility and elevation conditions prevail only the standard tropical summer atmosphere is used. (B) Standard conditions showing the effect of off-nadir viewing. (C) Standard conditions except that sensor has been placed above the atmosphere.

Figure 3 Color enhanced radiance composite pictures showing the effect of changing NEΔT and detector size. (A) NEΔT = 1.0°K. (B) NEΔT = 1.0°K but contrast in principal components has been boosted. (C) NEΔT = 0.32°K. (D) NEΔT = 0.053°K (detector size = 6 x 6 pixels).

Figure 1

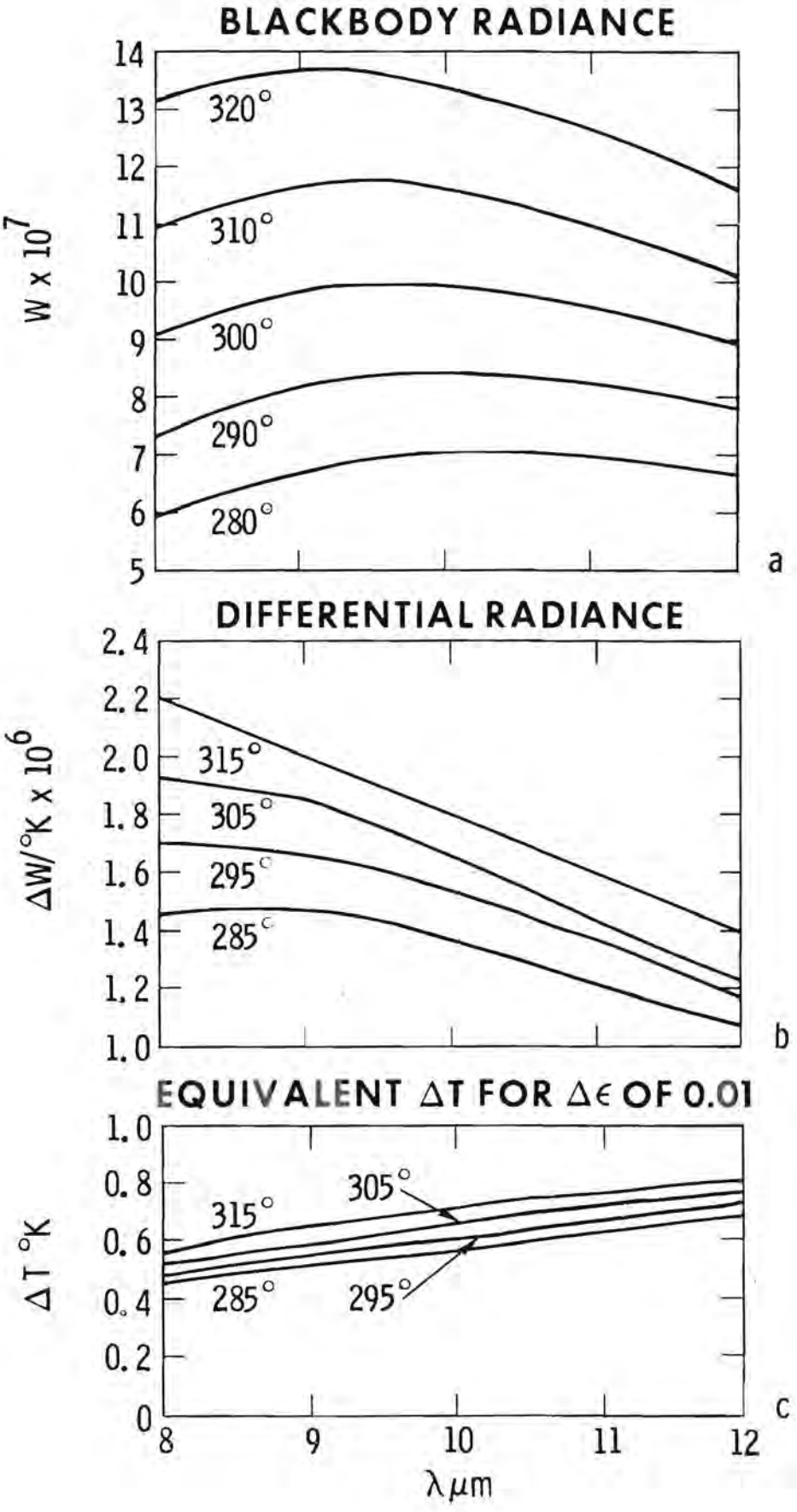
BLACKBODY RADIANCE
W x 10^7
14
13
12
11
10
9
8
7
6
5
320°
310°
300°
290°
280°
a
DIFFERENTIAL RADIANCE
ΔW/°K x 10^6
2.4
2.2
2.0
1.8
1.6
1.4
1.2
1.0
315°
305°
295°
285°
b
EQUIVALENT ΔT FOR Δε OF 0.01
ΔT °K
1.0
0.8
0.6
0.4
0.2
0
315°
305°
285°
295°
c
8
9
10
11
12
λμm

THEORETICAL SCANNER RADIANCE VALUES A

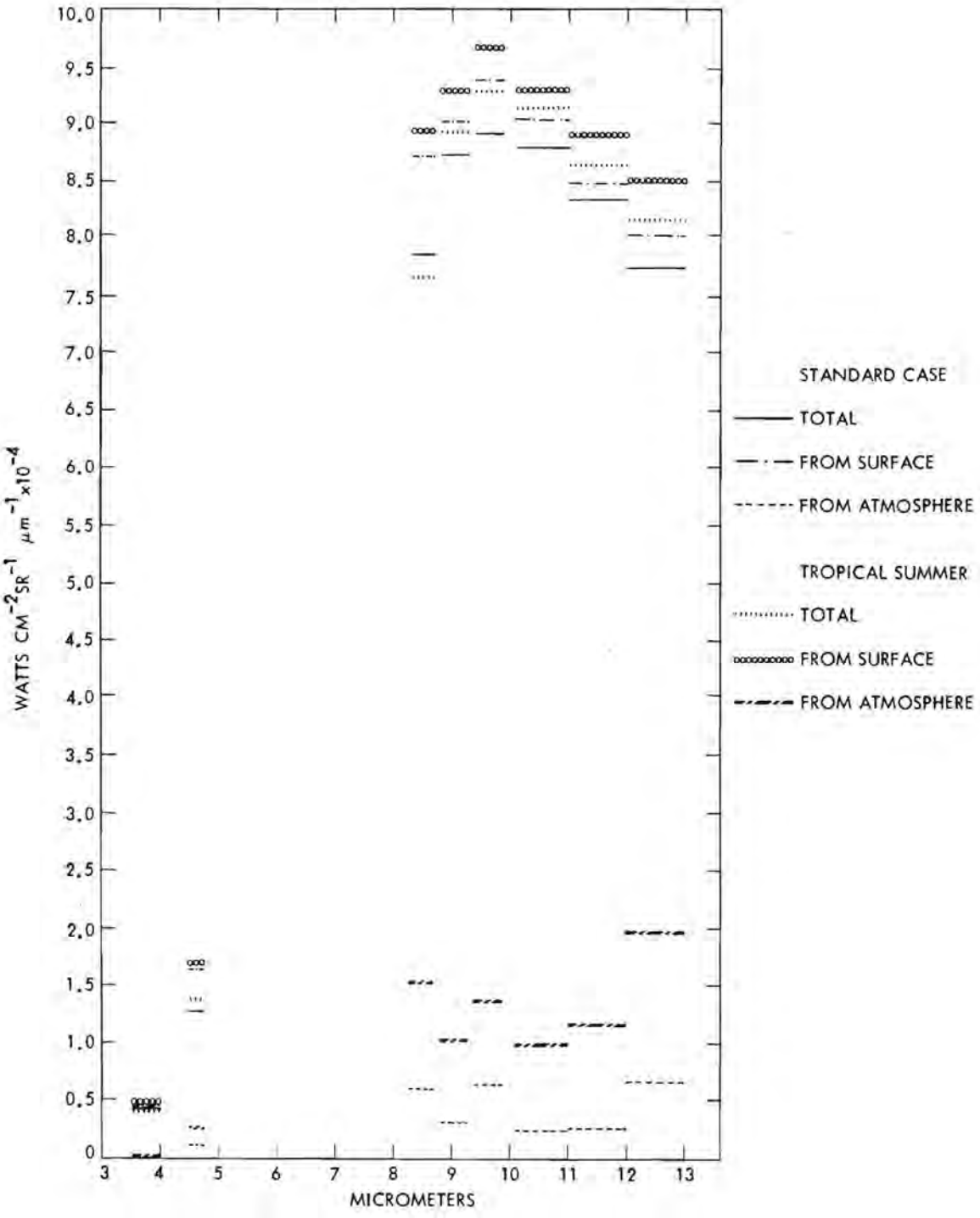

FIGURE 2A

THEORETICAL SCANNER RADIANCE VALUES B

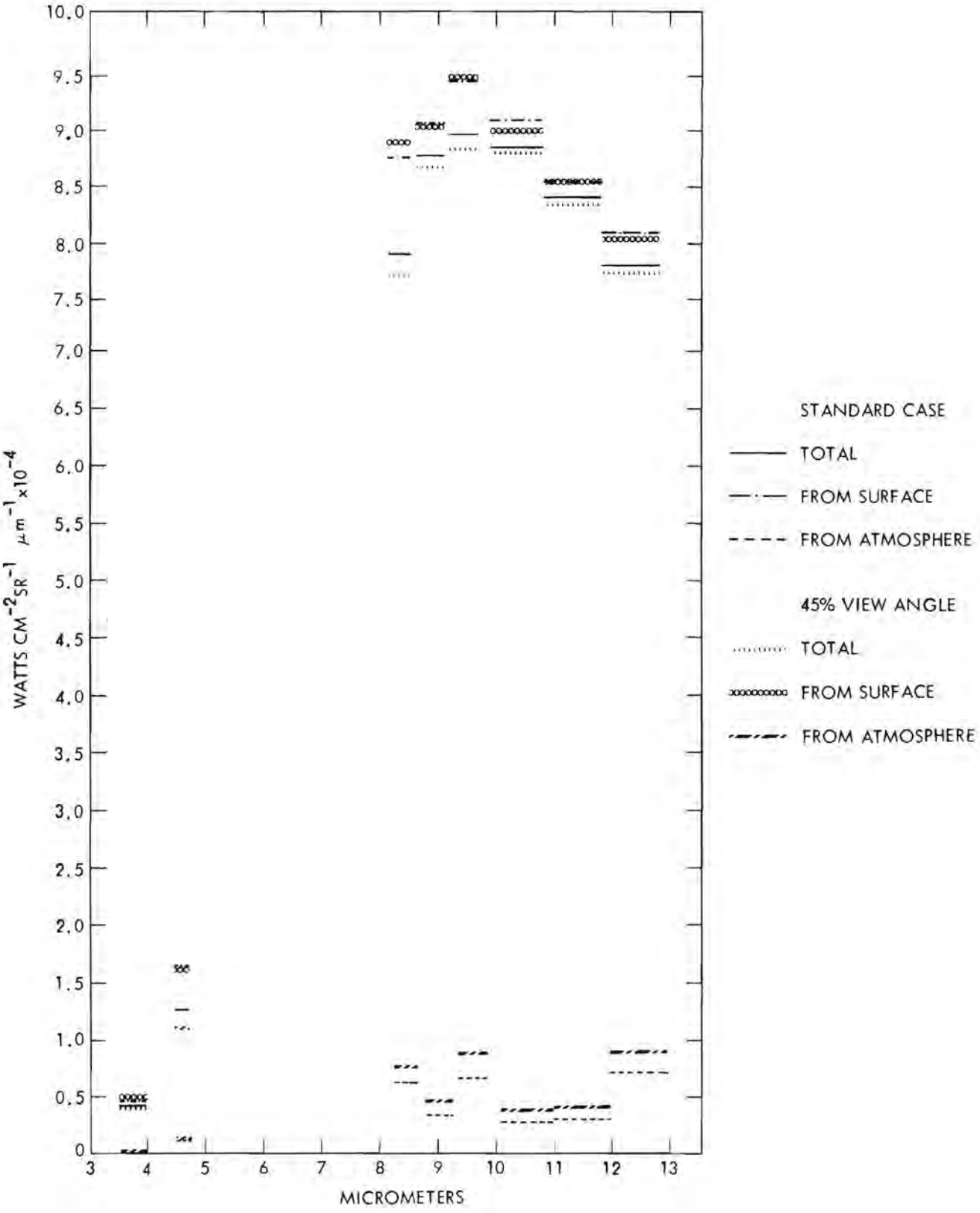

FIGURE 2B

THEORETICAL SCANNER RADIANCE VALUES C

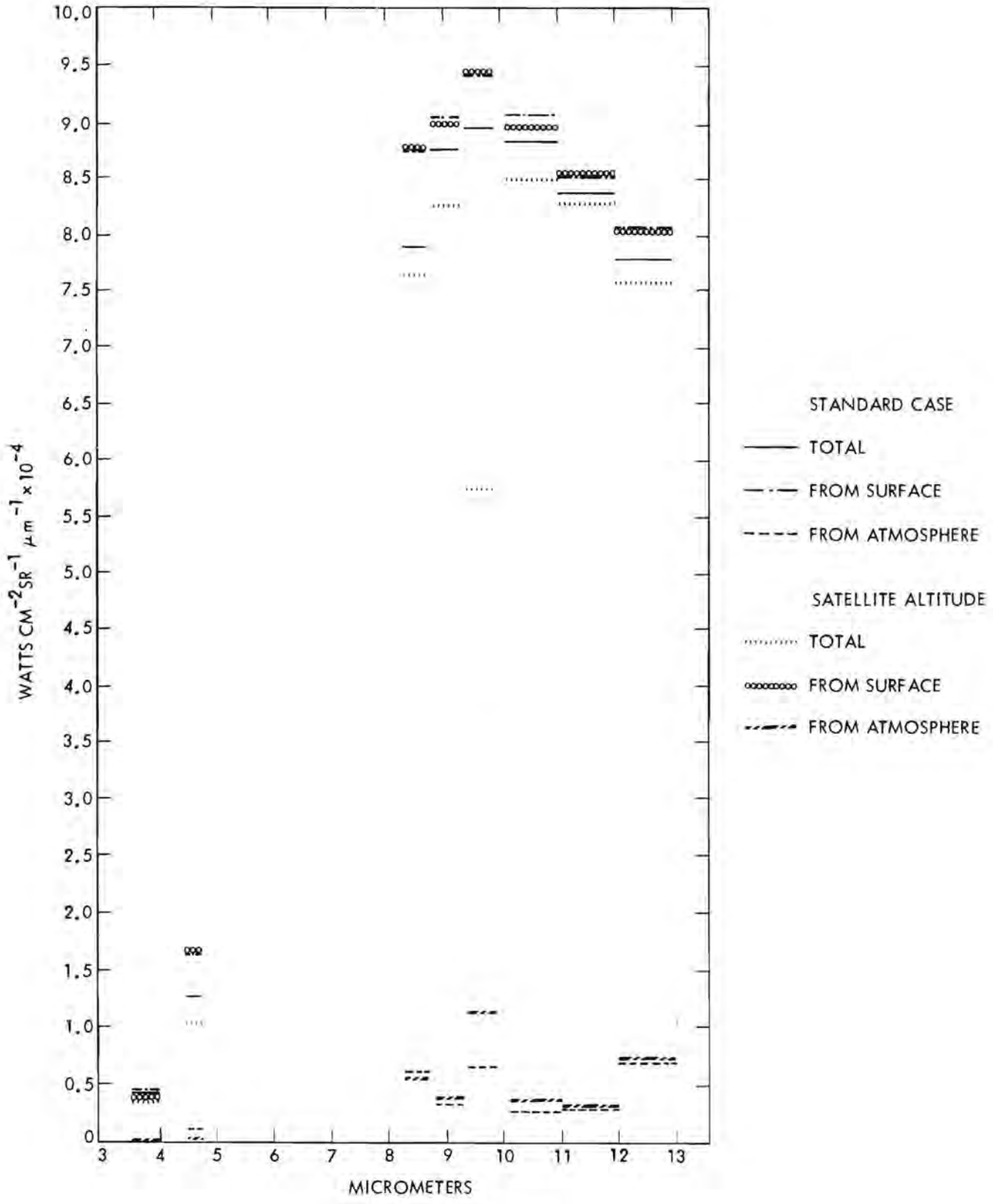

FIGURE 2C

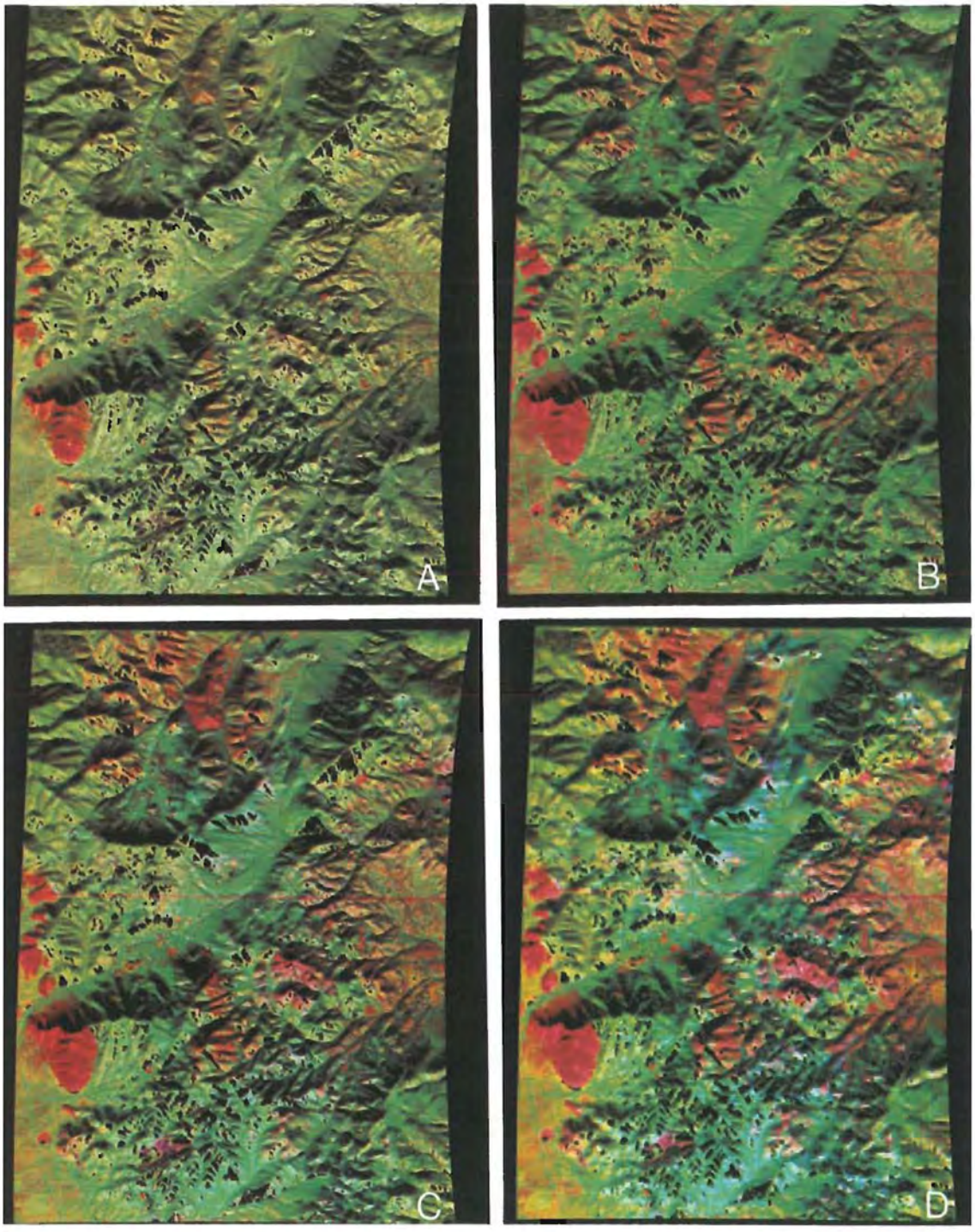
A
B
C
D

EMISSION SPECTRA IN THE THERMAL INFRA-RED REGION,

G. R. Hunt, U.S. Geological Survey, Denver, CO 80225

Spectral measurements in the thermal infra-red region are capable of yielding excellent bulk compositional diagnostic information for geologic materials, provided there is freedom to choose sample conditions and environment, technique, and instrumentation to collect the data. This situation has been demonstrated repeatedly in numerous publications, for minerals (e.g., Lyon, 1964) and rocks (e.g., Hunt and Salisbury, 1974), primarily using transmission and reflection techniques. However, the need exists to define the spectral characteristics of emission from geologic materials under natural conditions.

The type of information available in transmission spectra for silicates is illustrated in Figure 1, and silicates as a class are readily distinguished from other geologic materials such as carbonates, sulfates, oxides, etc. Unfortunately, the idealized conditions used to produce most of these data are not found in remote-sensing situations, especially when applied to the Earth's surface. The specific vibrations that cause the maxima and minima that occur in silicate spectra are summarized in Figure 2.

Many of the existing data were produced in studies directed at the lunar and planetary surfaces which exist under unique conditions and environments, and are not directly transferable to studies of the Earth's surface, primarily because of the presence and nature of the terrestrial atmosphere. Not only does the atmosphere obscure specific spectral regions because of absorption and scattering, but it also governs the thermal regime at and in the surface materials, and its behavior is temporally highly variable.

Although the precise locations of the characterizing resonance frequencies for geologic materials are known or can be determined, the manner in which they are expressed in emission spectra is dependent upon many parameters. The fact that so few successful studies have been published attests to the difficulty of acquiring and interpreting <u>meaningful</u> spectral emission data both in the laboratory and under remote-sensing conditions. The accepted position is that the magnitude of spectral effects in broadbandpass experiments is such that the Earth's surface may be regarded as behaving like a black- or gray-body, implying that any genuine spectral information occurs only as a small perturbation of the much greater thermal effects.

The remote-sensing problem of discriminating among different geologic materials consists, first, of determining the form, magnitude, and location of spectral information under natural or simulated terrestrial conditions, and then developing methods to separate these spectral effects from those of thermal differences caused by different irradiance (depending on time of day, solar declination, and topography) and background (atmospheric) conditions.

Some very preliminary and incomplete laboratory emission data are presented only to illustrate some of the difficulties that exist and must be resolved by further investigations. These data were acquired both from some well-characterized samples and

from rocks and soils collected[1] from the East Tintic Mountains, in an area imaged by the airborne NASA 24-channel multispectral scanner.

Emission spectra were recorded using a Fourier Transform Interferometer Spectrometer, which has the advantages of large energy throughput and records all wavelengths simultaneously. The "emission" spectra shown were generated by dividing the emission intensity of the sample by that from a standard black-body source which matched it in intensity somewhere in the 7 to 25 μm range.

In the laboratory, the initial problem is that of heating the sample. Several methods were explored including: 1) Heating the sample in an air furnace, removing and recording sequential spectra as it cooled. 2) Heating the viewed surface with hot air. 3) Heating the viewed surface with unfiltered radiation from a quartz iodide lamp. 4) Heating as in (3) except that the IR radiation was filtered out. Methods 1 and 2 are subject to difficulties of controlling and maintaining a steady surface temperature. Using method 3, features due to reststrahlen reflection were apparent in the 10 μm range, even for particulate samples. Even with method 4, some effects were still observable due to emission from the filter. Typical curves generated by dividing the emission from a sample of rough-cut quartzite at various temperatures as it cooled after heating in the furnace by that of a black body at 153° C are shown in Figure 3.

Spectra were recorded to illustrate the effects of physical condition and to compare transmission and emission spectra of the same sample. Figure 4 shows the emission spectra of some well-characterized 74-250 μm particle size samples.

Emission spectra of field samples of a quartzite and some sandy limestones are shown in Figure 5. The quartzite samples were collected from the same (small) area and the curves are for the samples under different physical conditions, i.e., sand, sand and chips, natural rock surface, and fresh rough-cut rock surface. The appearance of the diagnostic "quartz" feature near 12 μm in the fresh-cut rock is not surprising because of the freshly exposed surface, nor is the decrease in spectral contrast in progressing from the fresh-cut (lowest) to the deep sand (top) sample. However, the variation in the appearance of the bands in the 10 μm region (where the extinction coefficients of the fundamental Si-O stretching vibrations have extremely high values) requires further study and explanation. The limestone spectra in the lower half of the figure all display a well-defined band near 11 μm due to the carbonate fundamental mode, which is diagnostic of carbonates and readily distinguishes them from silicates.

In Figure 6, transmission spectra[2] (dashed curves) of crushed clay and quartzite samples embedded in potassium bromide pellets are compared with emission spectra (solid curves) of the same samples from the Tintic area in their natural form. It is obvious that only general agreement exists between transmission and emission spectra for these particular samples and that the agreement is better at longer wavelengths than in the 10 μm region.

These preliminary data are presented to emphasize the need for both experimental and theoretical studies to define the spectral characteristics of emission from geologic materials under natural conditions. Of immediate importance is the need to develop appropriate methods for simulating the natural environment in the laboratory and using the data acquired to develop models to relate the spectral emission behavior to the fundamental properties of geologic materials.

References

Lyon, R. J. P., 1964, Evaluation of Infrared Spectrophotometry for Compositional Analysis of Lunar and Planetary Soils: Rough and Powdered Surfaces: Stanford Research Institute Final Report Part II, Contract NaSr 49(04), 176 p.

Hunt, G. R., and Salisbury, J. W., 1974, Mid-Infrared Spectral Behavior of Igneous Rocks: AFCRL-TR-74-0625, 144 p.

1/ Samples supplied by A. Kahle and K. Baird of J.P.L.

2/ Spectra recorded by K. Baird, J.P.L.

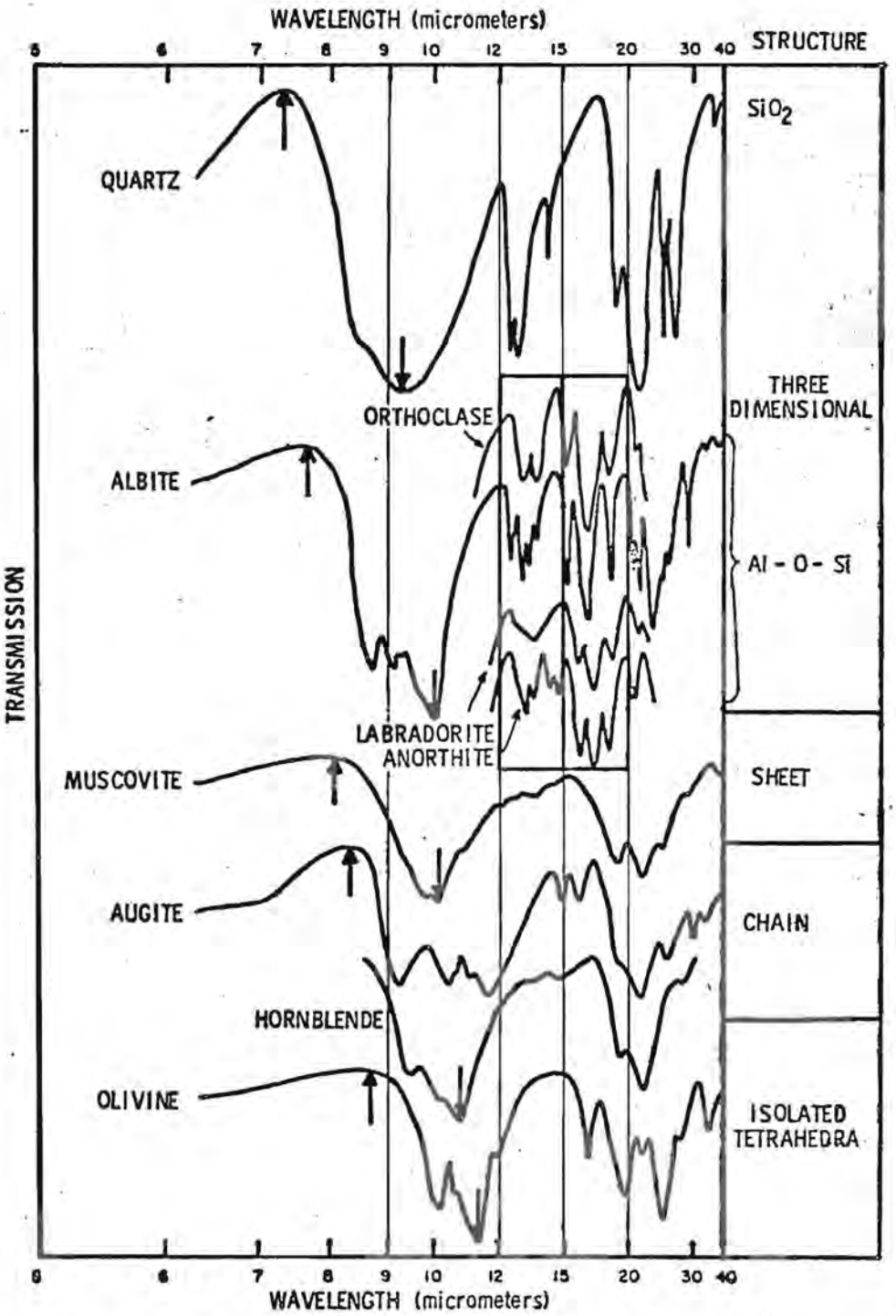

Figure 1. Transmission spectra of silicates illustrating differences that occur as a consequence of structure.

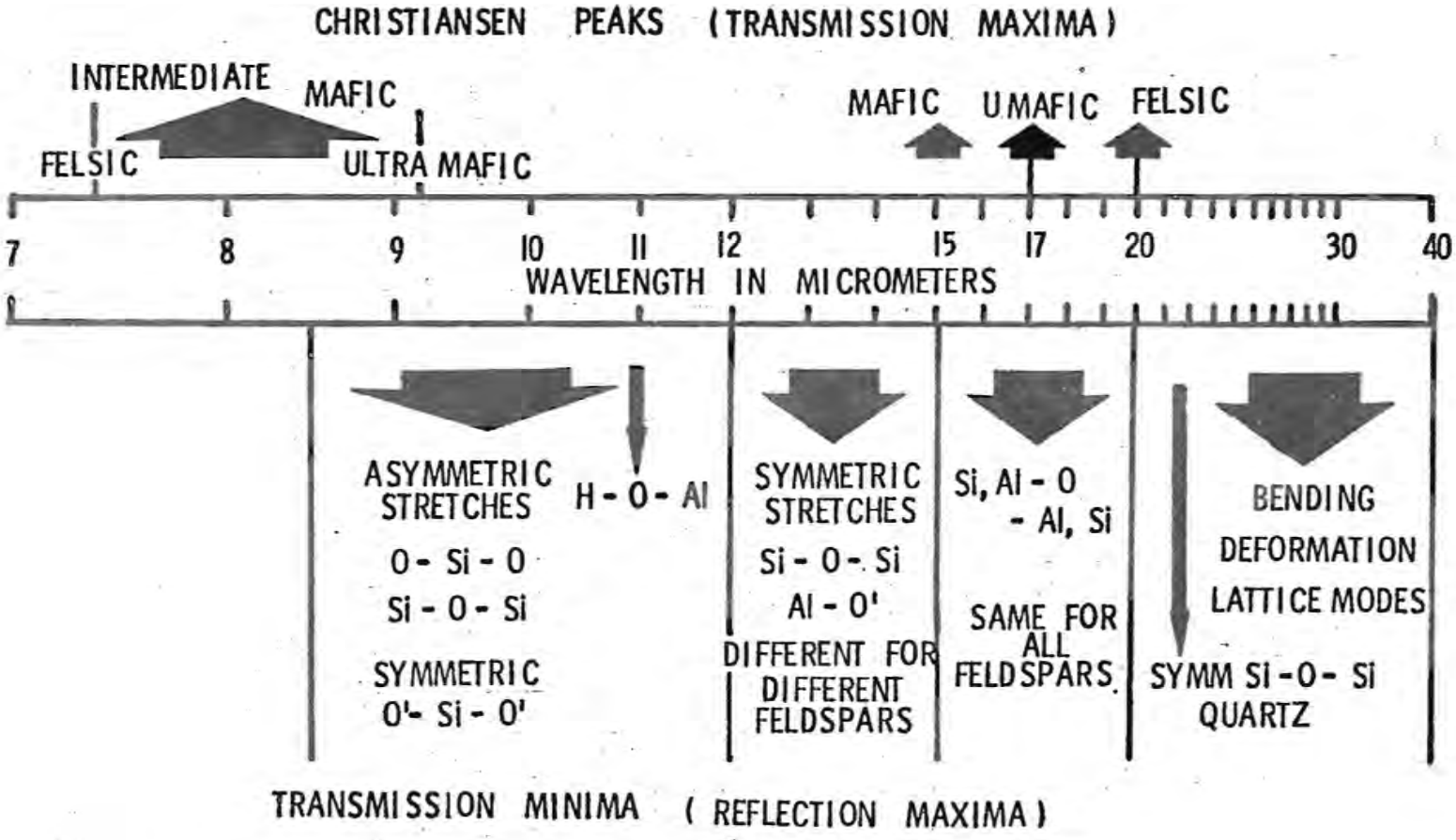

Figure 2. Diagram indicating the location of maxima and minima in transmission and reflection spectra of silicates, and a summary of specific vibrations which cause them.

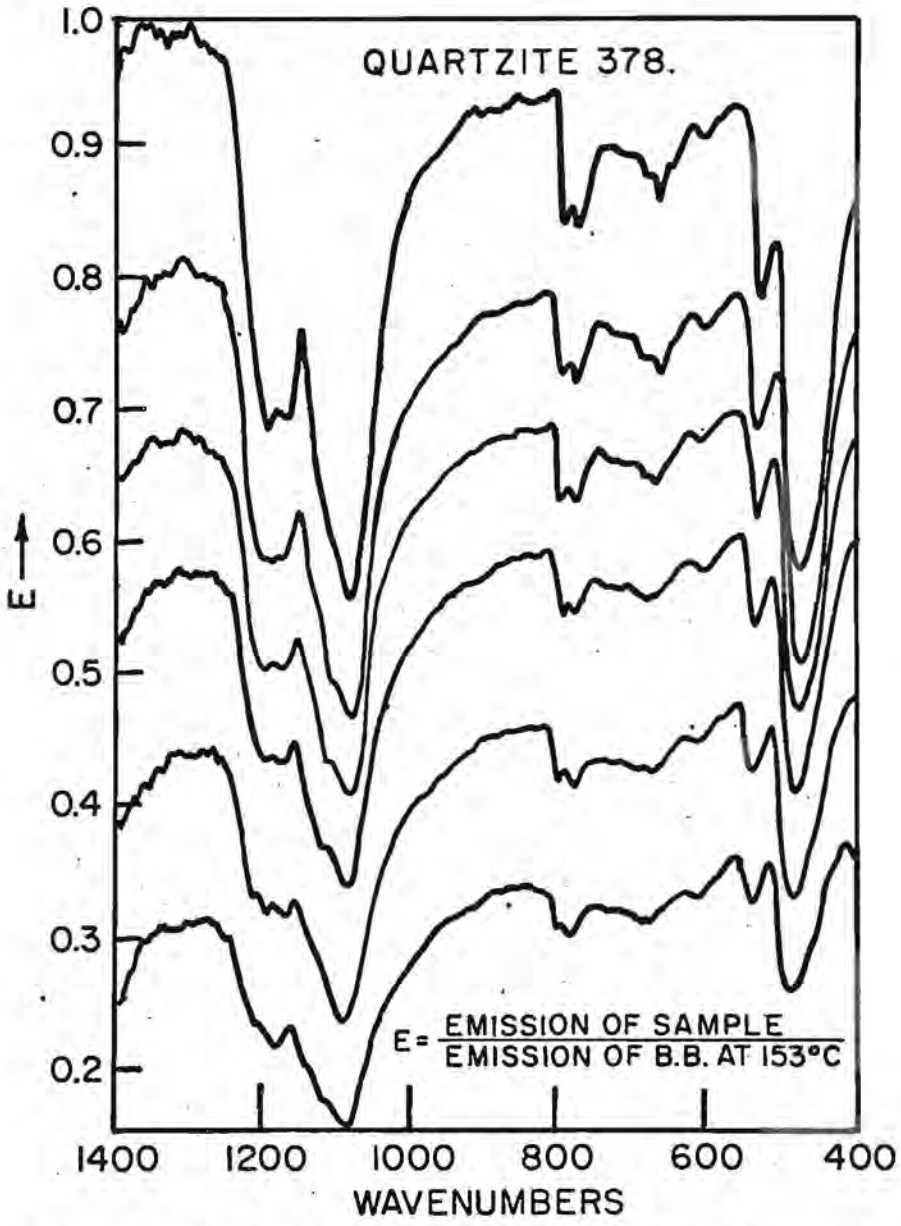

Figure 3. Curves produced by dividing the emission from a quartzite sample as it cooled (hottest at top, coolest at bottom) by that of a black body at 153° C.

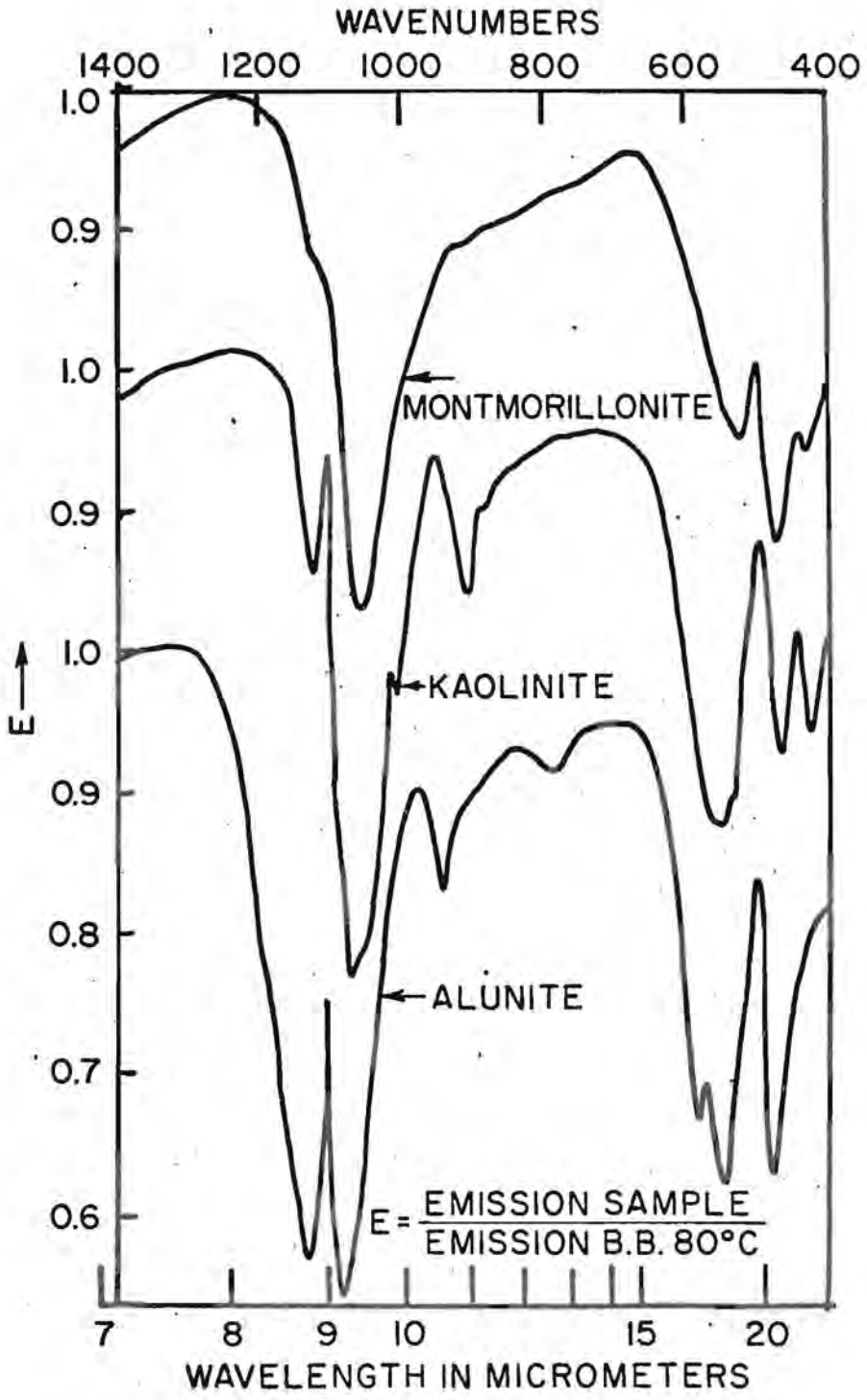

Figure 4. Emission spectra of well characterized particulate clay samples.

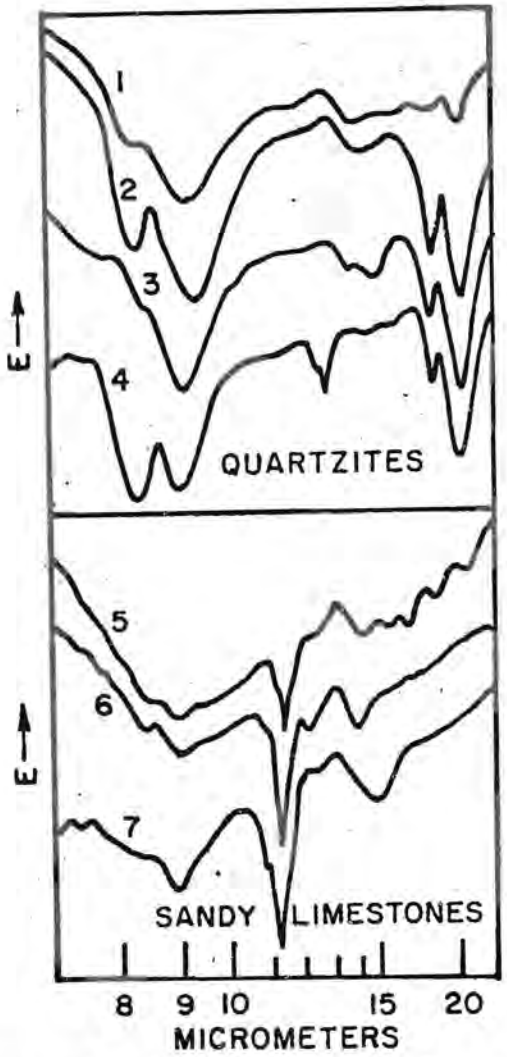

Figure 5. Emission spectra of a quartzite sample (top) and some limestone samples (bottom). The conditions of the quartzite sample are for curve (1) thick layer of sand; (2) thin layer of sand covering rock chips; (3) natural rock surface; and (4) a rough cut rock surface. The curves in the bottom half are (5) limey aluvium sand; (6) dolomite sand; and (7) limestone rock.

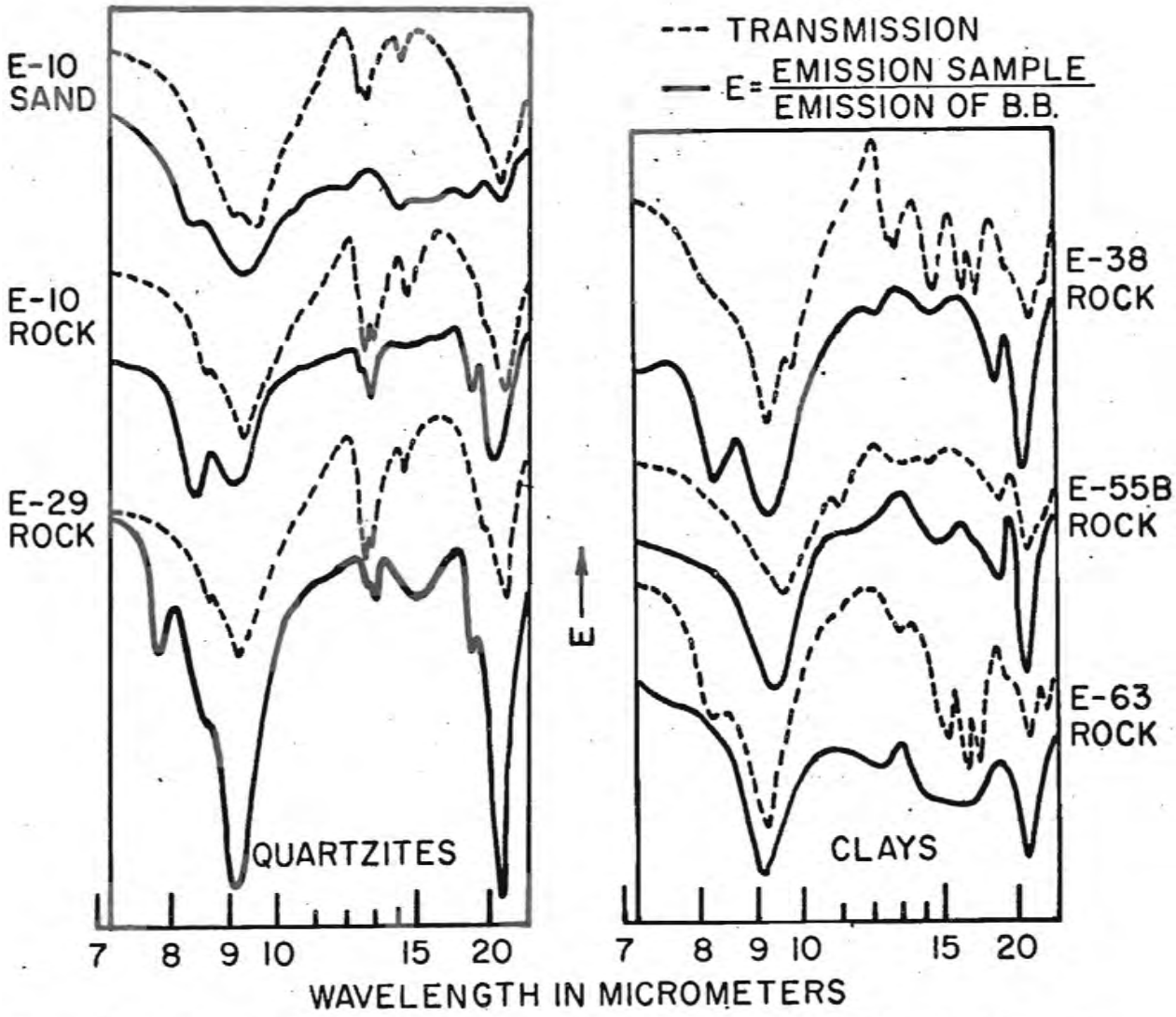

Figure 6. Quartzite (left) and clay (right) transmission and emission spectra. E-10 is quartzite; E-29 is a quartzite rock with a heavy iron stain; E-38, a silicified rock containing halloysite and quartz; E-55, B-clay altered from latite; E-63, opalized quartz.

REMOTE SENSING OF THE EARTH USING MULTISPECTRAL MIDDLE INFRARED SCANNER DATA. Anne B. Kahle, Jet Propulsion Laboratory, California Institute of Technololgy, Pasadena, CA 91103

Laboratory measurements of middle infrared (MIR) (5-40μm) spectra of rocks and minerals show many diagnostic features. The region between 8 and 14μm holds the most promise for remote sensing because this is an excellent atmospheric window and also the region of maximum thermal emission at terrestrial surface temperatures. Within this spectral range, the most prominent spectral features are due to silicon-oxygen stretching vibrations. These change location and intensity with varying composition and structure (Hunt and Salisbury, 1974, 1975, 1976; Lyon, 1965).

The possibility of exploiting these spectral features for remote sensing of rock type from aircraft or satellite has been suggested by many authors (Vickers and Lyon, 1967; Vincent and Thomson, 1972; Vincent, 1975). However, owing to lack of adequate multispectral scanners (Vincent, 1975), very few tests of the technique have been possible. Hovis and others (1968) and Lyon (1972) flew nonimaging spectrometers over areas in California They concluded that even though atmospheric effects were significnt, the reststrahlen bands of silicates were observable. Two tests using a two-channel imaging spectrometer have been reported. Vincent and others (1972) and Vincent and Thomson (1972) flew a scanner having a bandpass between 8.2 and 10.9μm and another bandpass between 9.4 and 12.1μm over a sand quarry near Mill Creek, Oklahoma and over Pisgah Crater, California. By ratioing the spatially registered images, they produced images on which they could distinguish between the quartz sand or sandstone and the nonsilicate surface material at Mill Creek, and at the Pisgah Crater area, were able to distinguish dacite from basalt and rhyolitic tuff from the surrounding alluvium. However, until now the lack of adequate imaging multispectral scanners has precluded further validation of the use of spectral emittance data gathered from aircraft.

Recently we acquired multispectral MIR (8-13μm) scanner data of the East Tintic Mountains in central Utah from the now defunct Bendix 24-channel scanner, flown on the NASA C-130 aircraft. These data consist of six channels of calibrated scanner images of moderate spectral resolution (0.5μm to 1.0μm bandwidth), available in digital format on computer compatible tapes (CCT's). This flight provided an unprecedented opportunity to analyze multispectral MIR image data in a geologically complex area. The district, in an area of high relief and moderate vegetation, consists mainly of Tertiary silicic igneous rocks and Paleozoic quartzite and carbonate rocks that have been locally hydrothermally altered.

The six channels of aircraft data (8.3 - 8.7μm, 8.8 - 9.3μm, 9.4 - 9.9μm, 10.1 - 11.0μm, 11.0 - 12.0μm, and 12.0 - 13.0μm) were contrast enhanced and displayed as black and white images. Because the radiance emitted from the surface is highly dependent upon surface temperature, these images were dominated by temperature (and hence topography). Display of the much more subtle spectral emissivity differences between the channels due to variations in the surface materials required more elaborate image processing.

Using onboard calibration, a simple atmospheric model, and an assumed constant surface emittance of 0.93 in the 11-12μm range, we derived a surface-temperature image from the 11-12μm radiance data. (The 12-13μm data were not used to derive a temperature because of excessive noise.) We could then de-

rive surface-emittance images for the remaining four channels between 8 and 11 μm.

Several additional images were prepared from the multispectral radiance and emittance data, including color composites, ratios, color-ratio composites, and principal component transformations. The most satisfactory image product for separation of rock types, Fig. 1, was produced from the radiance data in channels (8.27-8.7μm), (8.8-9.3μm), and (10.1-11.0μm). The color-enhancement procedure consisted of a nonlinear transformation in which each of the three output channels forming the final color triplet was a function of all three input values. The transformation consists of a principal component rotation, followed by "Gaussian" contrast enhancement and then by an inverse rotation (actually performed by table lookup). This transformation was chosen to remove the correlation that existed between the original components, thus fully utilizing the available color range. A useful feature of the final display is that, although emittance differences appear as variations in color, the intensity of any element of the enhanced scene remains a function of local temperature, just as for the original components. Because temperature is largely topographically controlled, these intensity variations reflect local topography, thus aiding interpretation.

Evaluation of the MIR color composite images was conducted by comparing the distribution of colors in the image with the occurrence of rock units in a generalized lithologic map based on work by Morris, 1964a,b and by field checking critical areas (Kahle & Rowan, 1980). In general, areas shown as red to pink and purple in the image are underlain by rocks in which quartz is a major constituent, whereas blue and green represent rocks that have minor quartz content; green also represents dense vegetation.

The most vivid red areas, A and B, in the image represent quartzite. Slightly less intense and uniform red areas (C, D, and E) consist of interbedded sandstone, limestone, quartzite, shale, dolomite and chert. Silicified altered rocks, F, also appear red to pink in the image. Many small red areas correspond to mine dumps and cleared ground around mines, G, all of which have a high quartz content. The largest exposed mine area, H, the Dragon mine, is exceptional, however, in that it is purple in the image and has a high clay content (halloysite). Several other areas of argillized rocks, I, have a similar appearance. These differences in color suggest that the red areas indicate the presence of large amounts of quartz, whereas the purple denotes higher proportions of clay minerals.

One of the most surprising contrasts seen in the MIR color-composite image is the separation of quartz latitic-quartz monzonitic rocks from latitic-monzonitic rocks: the former unit appears pink, J, whereas the latter unit is blue, K. Important exceptions occur where the rocks are argillized or silicified and, hence, appear purple or red; or where vegetation is dense, in which case the area is green, L. Calcitic quartz latitic rocks also appear pink, M, which might be expected because the quartz content was not affected by the alteration process and the calcite has been leached from the surface.

Carbonate rocks generally appear green, N, in the color composite image. However, in some places, O, they are blue or blue-green and therefore similar to the latitic-monzonitic rocks. Preliminary field examination suggests that the blue and blue-green areas correspond to high proportions of sandy soil. Hydrothermal dolomite is compositionally similar to unaltered

dolomitic rocks in the study area and, therefore, also appears green and blue-green in the image, P. Mining and milling operations appear bright yellow, Q.

The image-processing procedures used to generate the image, although chosen to maximize the differences among surface materials, make it difficult to relate the image color to these spectral differences. However, some general relationships can be noted. Red is consistently related to the presence of quartz-bearing rocks and therefore implies an intense absorption band centered between 8 and 10μm as expected for quartz. In contrast, green appears to represent generally spectrally flat materials such as carbonate rocks and vegetation. In general, the blue correlates with latite and monzonite, both silicate rocks but without quartz as a major constituent.

Examination of spectral-emittance curves derived from the image data suggests that the principal difference we are seeing among the surface materials is in the depth of the spectral features and that variations in the position of the absorption band used in other areas to distinguish among silicate materials (Vincent and Thompson, 1972) appear to be less important here. These results suggest that both intensity and position of the spectral bands need to be studied.

Some distinctions that are not possible in these MIR images can be made in visible and near-infrared (NIR) color-ratio composite images that were previously produced from NASA 24-channel scanner data specifically for mapping hydrothermally altered rocks and vegetation distribution. Although both carbonate rocks and vegetation lack significant absorption bands in the 8-12μm region, the fact that they are readily distinguishable in the visible and NIR color-ratio composite images allows mapping of the carbonate rocks. Argillized rocks and quartz latitic rocks are not consistently distinguishable in the MIR image, but are clearly separable in the visible and NIR image owing to their spectral contrast in the 2.2μm region. Thus, use of color-composite images from both the MIR and the visible and NIR, combined with limited field checking, permit mapping of quartzite, carbonate rocks, quartz latitic and quartz monzonitic rocks, latitic and monzonitic rocks, silicified altered rocks, and argillized altered rocks.

Hovis, W. A., Jr., L. R. Blaine and W. R. Callahan, Appl. Optics, 7, 1137-1140, 1968. Hunt, G. R. and J. W. Salisbury, Air Force Cambridge Research Lab., AFCRL-TR-74-0625, 1974, AFCRL-TR-75-0356, 1975, AFCRL-TR-76-0003, 1976. Kahle, A. B., D. P. Madura and J. M. Soha, Jet Propulsion Lab. Publ. 79-89, 1979. Kahle, A. B. and L. C. Rowan, to be published in Geology, May, 1980. Lyon, R. J. P., Science, 175, 983-986, 1972. Morris, H. T., U. S. Geological Survey Bull., 1142-K, 29 p., 1964a, 1142-L, 1964b. Vickers, R. S. and R. J. P. Lyon, pp. 585-607, Thermophysics of Spacecraft and Planetary Bodies, G. B. Heller, Ed., Academic Press, Inc., New York, 1967. Vincent, R. K, Proc. IEEE, 63, 137-147, 1975. Vincent, R. K. and F. Thomson, J. Geophys. Res., 77, 2465-2472, 1972. Vincent R. K., F. Thomson and K. Watson, J. Geophys. Res., 77, 2473-2477, 1972. Vincent, R. K., L. C. Rowan, R. E. Gillespie and C. Knapp, Remote Sensing of Environment, 4, 199-209, 1975.

Figure 1. *Color composite image of the East Tintic Mountains, Utah, based on principal component transformations of MIR multispectral data. A, B—quartzite. C, D, E—interbedded sandstone, limestone, quartzite, shale, dolomite and chert. F—silicified rocks. G—mine areas. H—Dragon mine. I—argillized rocks. J—quartz latite and quartz monzonite. K—latite and monzonite. L—vegetated areas. M—calcitic quartz latite. N, O—carbonate rocks. P—hydrothermal dolomite. Q—mine tailings and ponds.*

INFRARED THERMAL MAPPING OF MARS: DESIGN, OBSERVATION AND ANALYSIS, Hugh H. Kieffer, U.S. Geological Survey, Flagstaff, Az. 86001.

The Viking Infrared Thermal Mapper (IRTM) was designed to measure martian surface temperatures with modest spatial resolution and coverage (seven 5 mrad fields of view sampled each second). The instrument field of view and integration time, the scan platform motion rates, and the orbital velocity are such that at ranges of 1500 km or greater, approximately contiguous uniform coverage is acquired. In order to cover the full range of martian temperatures with good temperature resolution, and to allow mapping of spectral emission units, if significant spectral variations were found, four broad bands were used in the mid-infrared. To allow estimation of thermal inertia from individual observations, and to enable an energy balance study of the polar caps, a very broad reflectance channel was included. A single detector to measure stratospheric temperatures was added during instrument development.

Observations of Mars began in June 1976 and continue on the surviving Viking orbiter. Due to the highly eccentric Viking orbits, surface resolution ranges from 1.5 x 5 km (smeared down-track) to 150 km; most of Mars has been observed with resolution of 25 km or better at several times of day. Observations have covered two Mars' years, including times of atmospheric clarity and of large atmospheric opacity due to dust.

Several different methods of data analysis have been used (excluding study of the atmosphere or polar condensates);

1. Mapping of predawn temperatures, without regard to albedo
2. Single-observation estimates of thermal inertia, using simultaneous measurement of temperature and albedo
3. Determination of thermal inertia and albedo using observation throughout Martian local hour made at many different times.

Each of these has advantages and all have proven useful. Nearly all analysis of thermal data is done relative to a thermal model which predicts surface temperature for Mars' "average" properties as a function of hour (time of day), latitude, and season. Large variations in surface physical properties have been found, as well as an unexpectedly rapid cooling in the afternoon that occurs over much of the planet. The mapped thermal inertia does not have a close correlation to any other mapped property of Mars. The thermal inertia results have been used in several studies of Mars geology, particularly study of the probable eolian history of the martian surface.

Mapping of surface spectral emissivity has thus far been precluded by the effects of dust in the atmosphere. An extensive analysis of the effects of atmospheric dust on thermal radiation is in progress, but the combined difficulties of dust opacity, anisothermality of the surface due to a range of particle and rock sizes, and an intrinsic small surface spectral emissivity variation indicate that the geologic use of spectral mapping will be very limited.

A variety of data handling and display techniques have been utilized to facilitate processing and analysis of IRTM data on a modest computer. The raw observations and geometry were acquired on about 3000 magnetic tapes, and ultimately reduced to 14 40-megabyte disk packs that contain the temperatures, solar band brightness, observation geometry and thermal models for all on-planet, non-redundant data in the order acquired (TSDR; time sequential data record). Since all observations of an area are desirable for thermal inertia mapping, these data have also been sorted into 90 latitude strips each 2° wide. Another major data base is the average, standard deviation and number of observations for each of the 6 IRTM bands (4 surface,

1 atmosphere, 1 solar) for 90 latitude strips, 24 hour bins, 3 air mass factors (emission angle ranges), 4 longitude bins (based on regional thermal behavior) and about 20 martian seasons (chosen to isolate different phases of the martian dust storms and clear periods). These 10 million values ("megabins") provide the basis of studies of the general properties of the martian atmosphere, condensates, and surface. The TSDR is used for local and topical studies. The latitude sorted data base is used for global mapping and seasonal variation of specific regions.

8-13 MICROMETER SPECTRA FROM HIGH ALTITUDE (RB57) UNDERFLIGHTS COMPARED WITH CONCURRENT S191 DATA FROM SKYLAB SL-3 MISSION. Ronald J. P. Lyon, Director, Stanford Remote Sensing Laboratory, Stanford University, Stanford, California.

Use of the S-191 spectrometer system aboard the SKYLAB SL3 mission showed that geologically-meaningful spectra can be extracted from the data by which terrain targets can be differentiated. The Si-O bond in all silicates (which form most surface rocks) produced an emission minimum which is characteristic of a mineral, or a set of minerals in a rock. The underflight RB57 mission was far more successful, primarily because of its much slower velocity allowing a higher signal/noise, and hence better spectral resolution for any given area of terrain. With the RB57 spectra not only could areas be differentiated, but significant differences in rock targets could be demonstrated, even to indicating the immediate source (geological provenance) of some alluvial outwash in the nearby mountains over which the aircraft also flew its flight strip.

Objective

To demonstrate that differentiation between geologically-significant materials could be made from high altitudes (RB57), and that comparable data could be extracted from space flight, using the pointing and tracking capability of the S-191 spectrometer system. Inherent in this design is a pair of data sets--a RB57 underpass with the Infrared Pallet (spectrometer and radiometer) and a closely concurrent SKYLAB-S-191 overpass. This was achieved on August 11, 1973, in SL3 overpass along Track 6--Walker Lake, Nevada, and Mission 248 RB57 flights.

In the aircraft experiment the techniques used involved ratioing the target spectra (+ airmass) to those of a lake (+ airmass), nearby. This method had proved successful in previous geological studies with the same instrumentation at lower altitudes (MX108 Pisgah Crater, California, at 700 m (2000 ft)) (Lyon, 1972).

Scope of the Work

The S-191 experiment was to explore the possibility of securing terrain spectra despite the increased airpath (20 km to 320 km; 65,000 ft to 200 mi) of the SKYLAB vehicle, and thereby including the effects of the ozone layer (9.6 μm absorption band) usually located around 36 km (120,000 ft) altitudes. This would be attempted by using the unique pointing ability of the S-191 system, with astronaut control, to locate and hold a water target (Walker Lake, for example) while tracking from a 45 degree forward view, to local vertical, thereby affecting some degree of atmospheric calibration from the changing airpath during the tracking motion (airmass m = 1.41 to m = 1). In addition SKYLAB would be moving at 34,760 km/hr (6 mi/sec) and the RB57 about 570 km/hr.

Extracted from "Feasibility of Using S-191 Infrared Spectra for Geological Studies from Space", Final Report, Type III, Contract NAS9-13357, December 1976.

Introduction

On several occasions it has been established that rock materials (silicates) in open-terrain surfaces, under ambient (sunlit) conditions, will show mid-infrared spectra by which they can be differentiated, whether the materials be close by, or distant, and whether the spectrometer be stationary, or airborne at low altitudes (Lyon, 1963, 1970, 1972; Lyon and Marshall, 1971; Lyon and Patterson, 1966; Lyon and Green, 1975).

This experiment was aimed at extending the alittudes (air path effects) to those of a high altitude aircraft (RB57, at 20 km) and thence to SKYLAB, in orbit at 320 km, passing over the targets at 34760 km/hr (6 mi/sec) using the pointing abilities of the astronaut-S-191 spectrometer combination.

Two test sites were used--Mono Lake and Walker Lake in western central Nevada, to provide blackbody ($\varepsilon = 0.98$) targets with which to compare the terrain emittance spectra, and hence obtain emissivity spectra. With SKYLAB the astronaut was to acquire the lake at a 45 deg forward view and trace the lake center until it passed by the nadir. This airpath change ($m = 1.41$ to $m = 1$) was to effect some atmospheric corrections. The field of view was then to be moved forward to track-and-hold a geological target until enough spectra could be obtained for calculation of emissivity ($N > 5$).

Discussion of Spectra and Terrain

RB57 Pallet Spectra: Rock and Soil Type Emissivities

Even a preliminary glance at the target spectra of figures 4.3.2 A-D significant differences in the important areas from 8.0 to 10.0μm, which are doubly interesting when the spectral differences are related with the geological map, and with the photographs which show how the alluvials washed into their present locations (Qal) from the surrounding hilly outcrops. In a few cases one can postulate the drainage direction (provenance) for the alluvials from their spectral differences along (see Qal, sites 7, 9, and 12).

Association of spectra with gross mineralogy. The 15 spectra in the other four key figures (figs. 4.3.1.1.1 to 4.3.1.1.4) have been segregated so as to emphasize their similarities and their differences, while relating this to the gross mineralogy of the targets. On each figure the least diagnostic spectrum (Qtm, mafic volcanics) has been included as a dashed line to serve as a reference.

Granitic rocks. In fig. 4.3.1.1.1 the spectra taken over granitic terrain have been compared. Firstly, the two intersections of the Wassuk Range granite (Kgr; Kgr-1, site 88 at 15:29:6 and Kgr-2, site 8a at 16:13:11 GMT) show very similar spectra, considerably depressed in the quartz-region (near 9 m). What is particularly interesting is that the Qoal spectrum (Site 9) taken 13 km to the south near the town of Hawthorne, on an old higher level beach line for Walker Lake, shows almost identical spectra indicative of a granitic soil composition. The fact that along most of the western shore of the lake the Wassuk Range is composed of

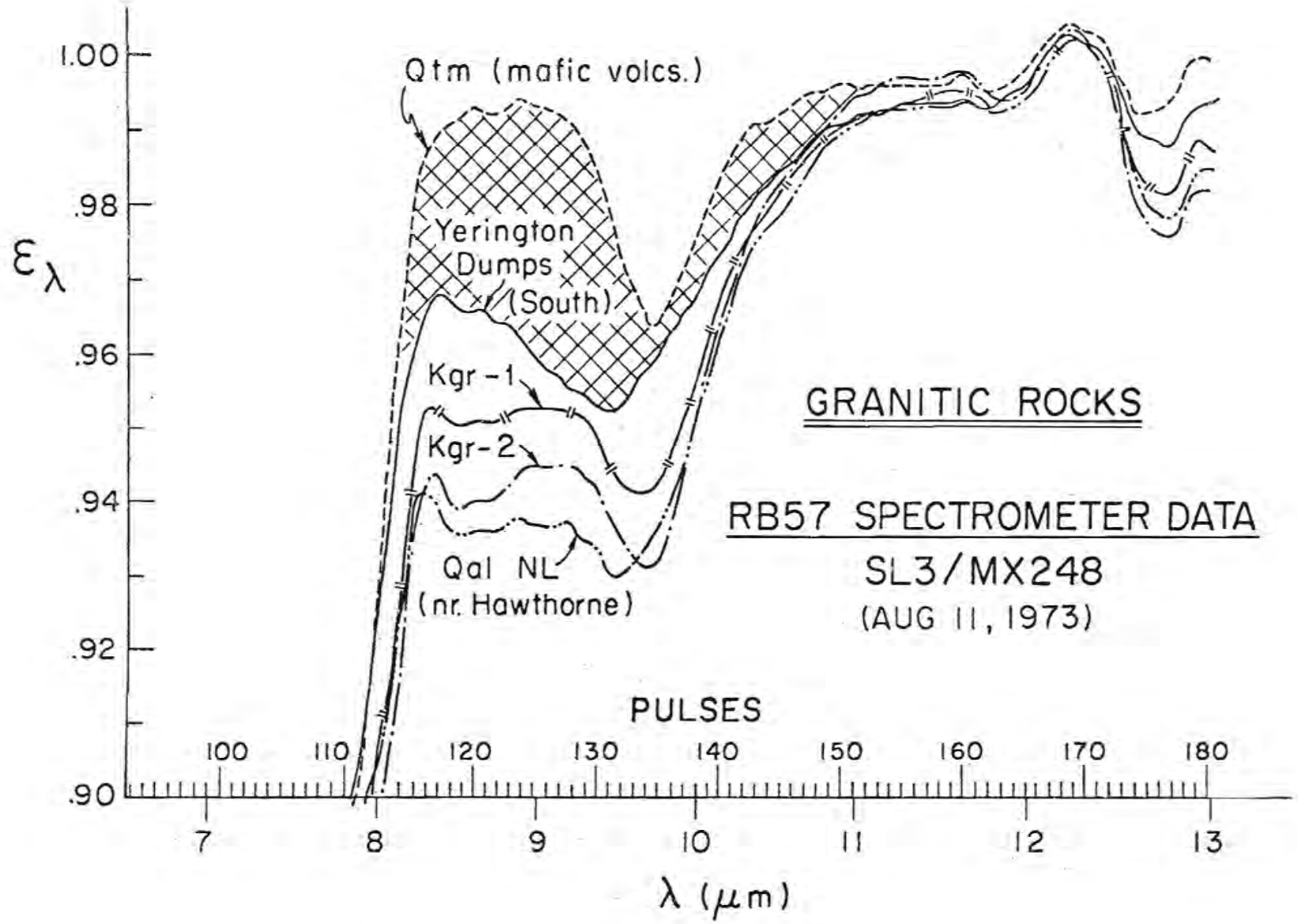

Figure 4.3.1.1.1 Target spectral emissivities (RB57) --granitic rocks

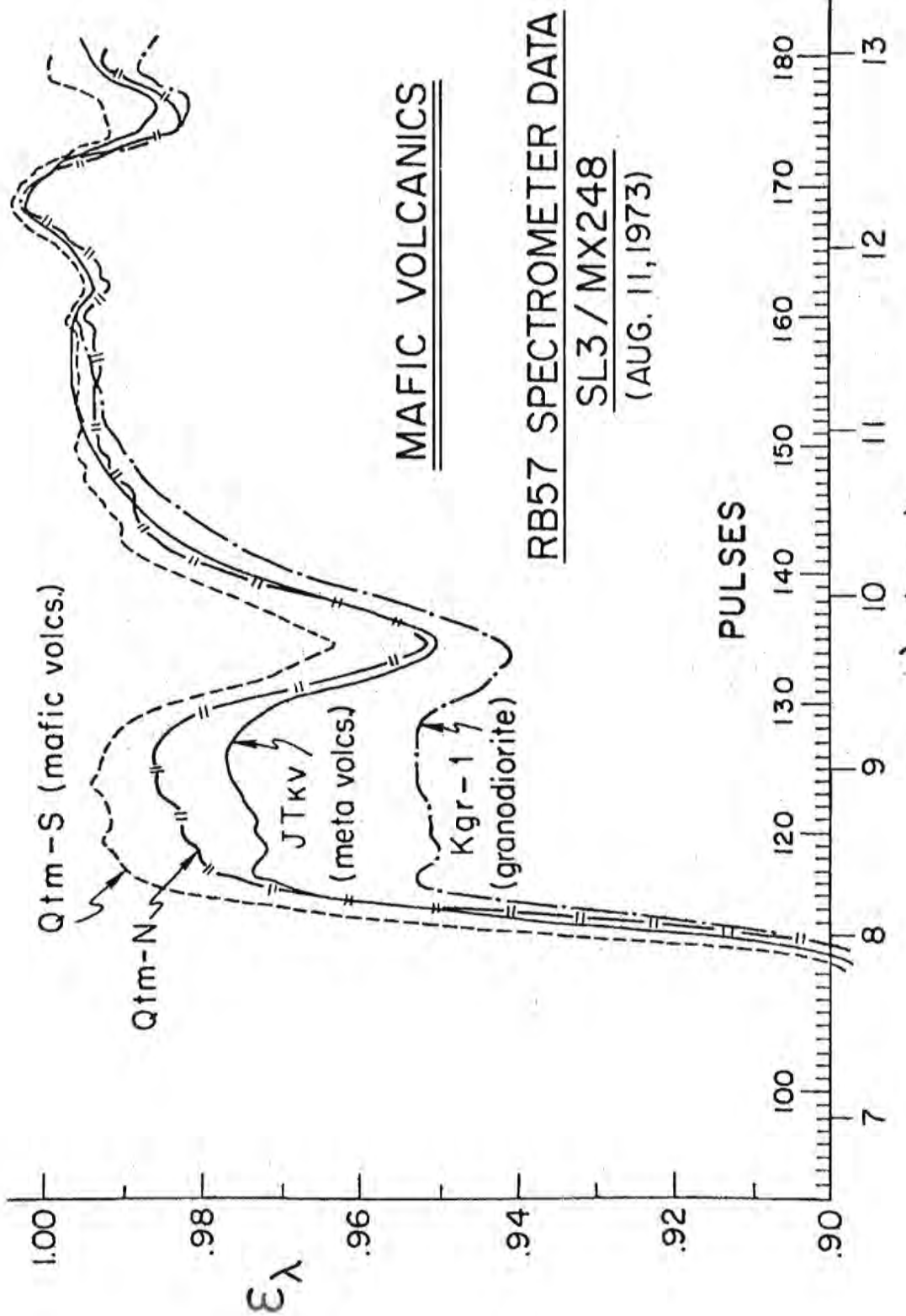

Figure 4.3.1.1.2 Target spectral emissivities (RB57)--mafic volcanics

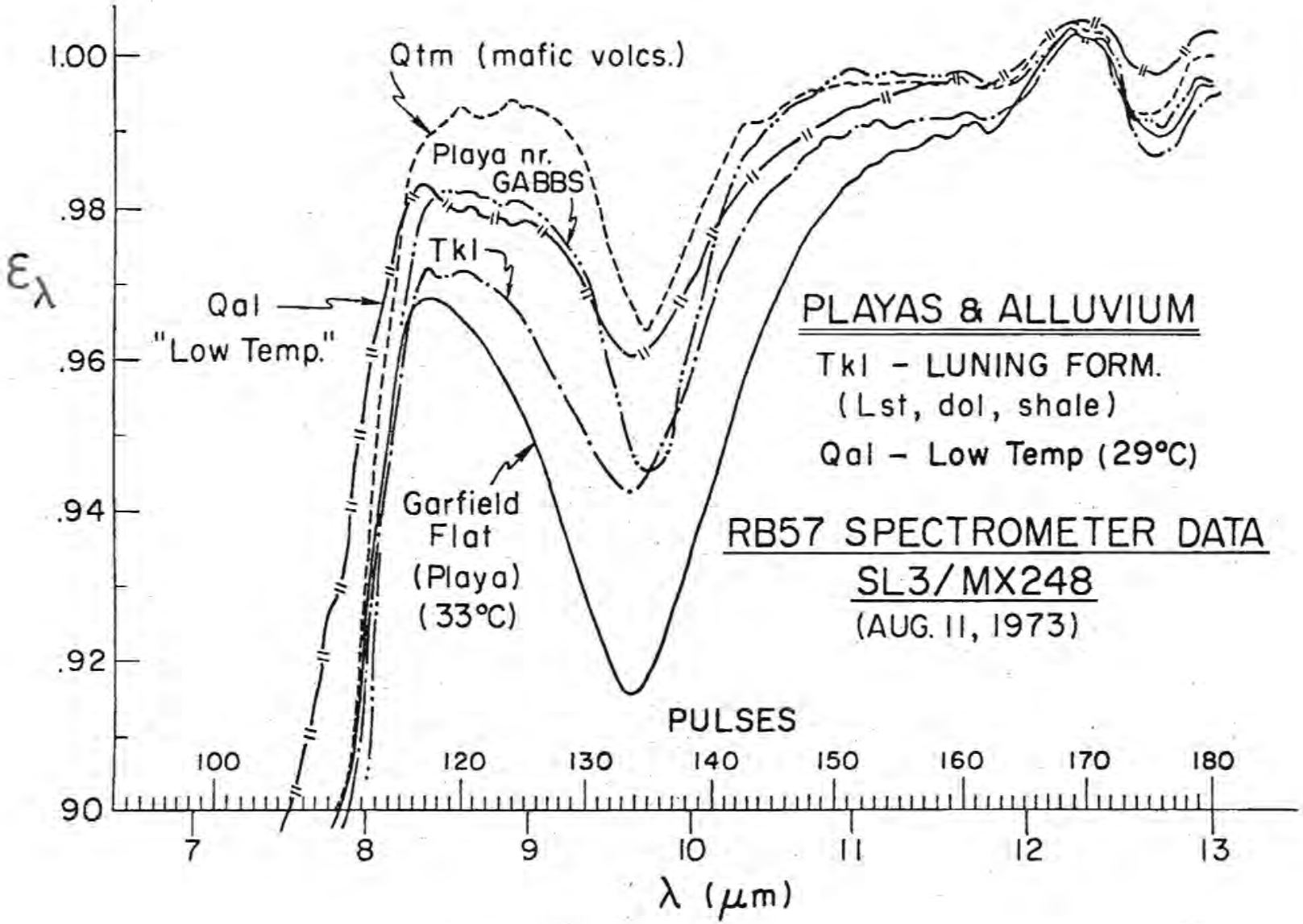

Figure 4.3.1.1.4 Target spectral emissivities (RB57)--playas and alluvium

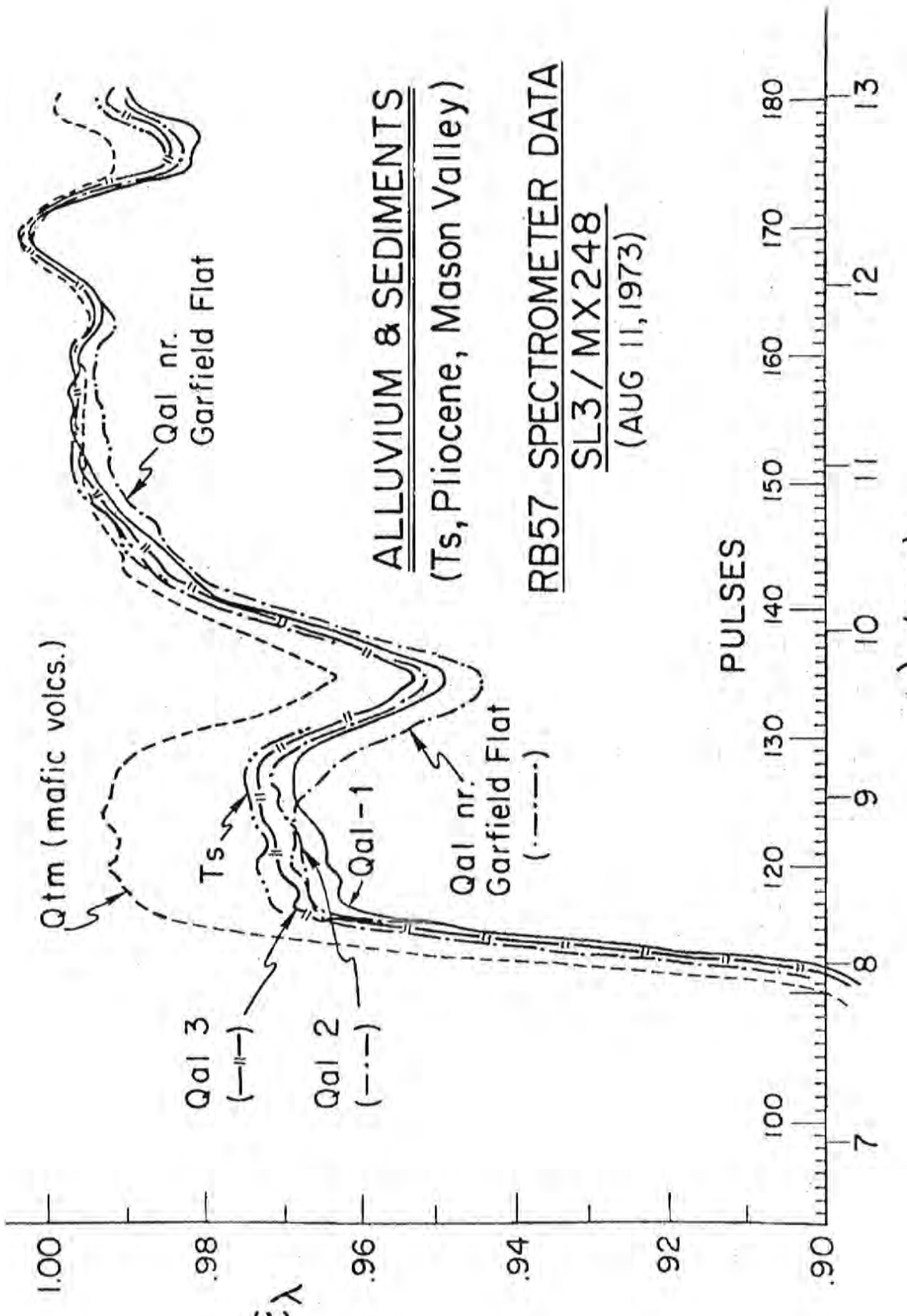

Figure 4.3.1.1.3 Target spectral emissivities (RB57)--alluvium and sediments

granite (Kgr) and prevailing winds (from the NW) would have swept the sands around to site 9 without any hindrance. What is also striking is that the spoil dumps of waste rock (south dumps of the Yerington copper pit--site 1) are somewhat similar, but from their spectra one would infer they contained less quartz but are still feldspar rich. (The south dumps are principally composed of granodiorite and alluvium outwash from the felsic volcanics of the Singatse Range to the west of the copper pit, which would match this analysis.)

Mafic volcanics and metavolcanics. In figure 4.3.1.1.2 the mafic volcanics have been segregated along with some metavolcanics. A spectrum of KGR-1 is included for contrast. The curves are much higher in the quartz area (quartz deficient) but show very little else of significance. This is typical of most emission spectra of basalts (Lyon, 1972, fig. 2). One would rank sites 6, 10, and 11 as mineralogically similar, and to resemble basalts.

Alluvium and sediments. In figure 4.3.2.1.3 several recent alluviums (Qal-1, -2, -3) from sites 2, 3, and 4 near Yerington (southeast of town) are compared with one from site 12 just short of Garfield Flat. Another mapped unit, Ts, a series of sediments has a very similar spectrum to Qal-1, -2, and 03, indicative of a more quartz-feldspathic source than the mafic volcanics of figure 4.3.1.1.2, but the metavolcanics of site 6 could easily be their source provenance, both mineralogically as well as geographically.

Playas and alluvium. A series of playa spectra (Garfield Flat and Gabbs playa) are compared with a sedimentary sequence (Luning Formation, of shales, limes and dolomites) and site 7 alluvium in figure 4.3.1.1.4. The Gabbs playa and site 7 Qal are similar except for the depth of the 9.6 ozone absorption. The carbonates (limes and dolomites) of the Luning Formation should not show reststrahlen features at these wavelengths and only the shale members (clays resembling playa clays) do so. Their spectra are simple, and those of Garfield Flat playa closely resemble the playa sediments of Lavic Lake in southern California overflow previously in Mission 108 (see Lyon, 1972, fig. 2E).

RB57 Pallet Spectra: Geologic Variability

It is additionally instructive to examine the pallet spectra in a geographic sense relating the alluvial outwash soils to some of the exposures of rocks in the surrounding hills. For this purpose one needs to study figures 4.3.2 B, C, and D along with the geological strip map of the RB57 flight line (fig. 2.2).

Figure 4.3.2 A shows the locations of sites 1 through 5, plus their spectra. In these four figures (A-DO the spectral insets are at the same scale, the central cross line being 9μm wavelength, the left border at 8μm, and the right at 10μm. The base line is at 0.94 emittance, the cross line (horizontal) at 0.96 and the top at 1.00. All spectra are traced and scaled directly from figures 4.3.1.1.2 - 4.3.1.1.4 and are exactly correlable. The grid serves to emphasize the relative shapes and strength of the reststrahlen features. All three alluvium Qal-1, -2, and -3

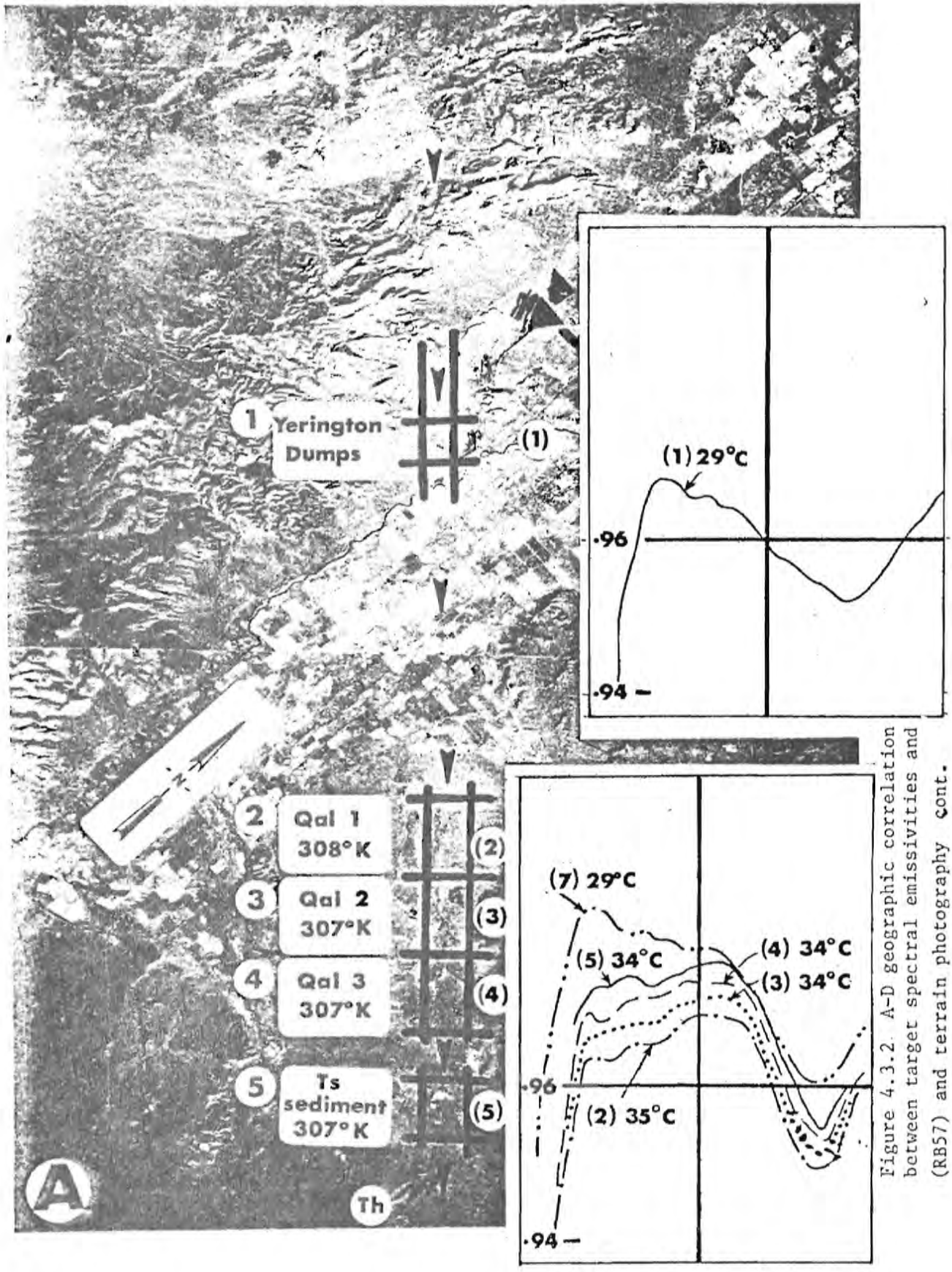

Figure 4.3.2. A-D geographic correlation between target spectral emissivities and (RB57) and terrain photography cont.

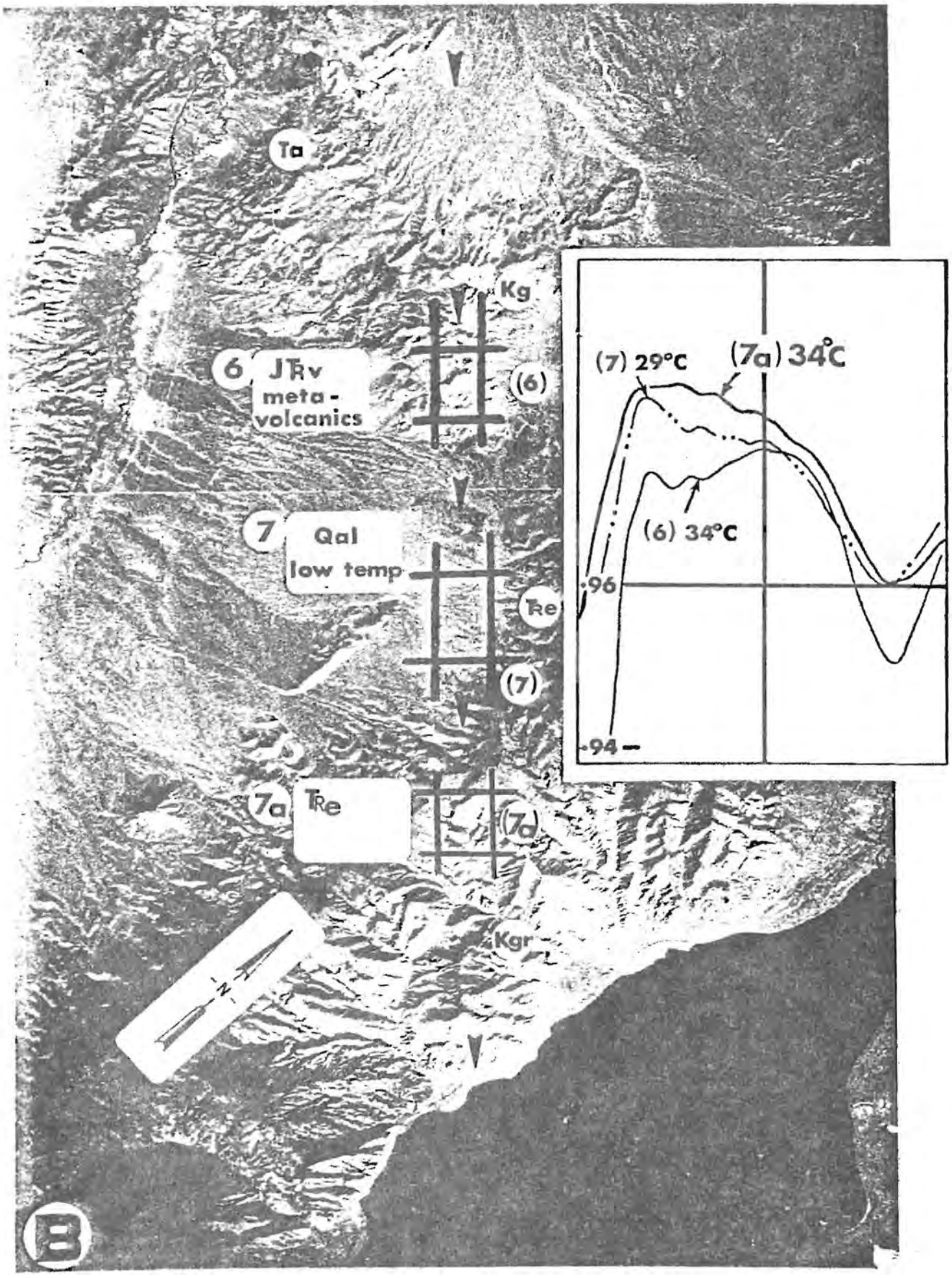
Ta
Kg
6 JTRv meta-volcanics
(6)
7 Qal low temp
Tre
(7)
7a Tre
(7a)
Kgr
N
(7) 29°C
(7a) 34°C
(6) 34°C
96
94
B

are similar coming from closely adjacent patches of the flight line without crossing any mapped geological boundary. The sediment Ts is also similar and geographically close in a slightly closed basin. A spectrum of site 7 alluvium is included to show its spectral differences. The rocks of the Yerington dumps are also clearly different spectrally from either group, but show a shape similar to the site 7 alluvium.

Figure 4.3.2 B shows the site 7 alluvium and the closely adjacent metavolcanics of site 6 which they do not resemble spectrally. Neither does site 7 resemble the granites of sites 8a and 8b further south on the ridge of the Wassuk Range. However, a rock type for which we were not able to obtain spectra, the Excelsior Formation (Tke) of intermediate to felsic volcanics outcrops immediately to the east up the ridge over a strike length of 15 km enclosing the Qal area on all uphill sides. This may have a sufficiently different spectrum so as to produce the Qal spectrum of site 7, particularly if it resembles the mafic volcanics spectrum of sites 10 and 11.

Figure 4.3.2 C shows the two granite (Kgr-1 and -2) and the Qal alluvium probably derived from their weathering, and transport south along the shores of Walker Lake. These spectra have been described in section 4.3.1.1, above.

Figure 4.3.2 D shows in the northern portion two sites (10 and 11) from mafic volcanics which are broadly similar. Site 12 an outwash area to the south could receive sediment from either site 11, or site 13, where the Luning Formation occurs. The site 12 alluvium spectra more closely resemble site 11 of the mafic volcanics, which also ring site 12 in the eastern foothills and also spatially cover about 20 times the area of site 13 Luning Formation. This is another example of using spectra for a clue as to geologic sources for the alluvium.

Site 14, the Garfield Flat playa, does not resemble any other spectra, even that of the playa (site 15) near Gabbs far to the northeast, but is spectrally similar to other playas in southern California (Lavic Lake, see Lyon, 1972, fig. 2E).

Conclusions

1. Time checks between the airborne data sets of the RB57 underflight and the photographic record could be obtained, if the time-of-crossing of shore lines of water bodies are initially correlated. Similar validation was possible with the SKYLAB data sets, although some confusing boresight photography (at high zoom position) often indicated water on the cross hairs, while the S-191 data temperatures indicated warmer land surfaces.

2. The RB57 (vertical viewing) spectrometry can be related meaningfully to ground geology, despite the 20 km of air, if care is taken to use large patches of terrain as targets, and to expect some (small) amount of positional error.

The unrequested summing of spectra from the rapid scanning spectrometer (6 scans/sec; 3 up ramp and 3 down ramp, interleaved) to 1 scan/sec up ramp and 1 scan/sec down ramp tripled the ground-smear per spectrum and destroyed some of the spectral subtelty usually in the data sets. In no way was it possible to directly compare S-191 and RB57 data sets, because of their different mission profiles (azimuths, times of overflight, look angles, etc.) thus the commonality of the 1 sec spectrum was of no assistance.

3. The S-191 was a feasibility test and as such performed well. It is possible to differentiate geological materials from space using the system, but probably not to precisely identify their surface mineralogy. (With the RB57 the rock type mineralogy could be established, albeit in terms broad to a traditional petrographer.)

References

Bellamy, J., 1954. The Infrared Spectra of Complex Molecules. John Wiley & Sons, New York.

Lyon, R. J. P., 1963. Evaluation of infrared spectrophotometers for compositional analysis of lunar and planetary soils, NASA Tech. Note, TN-D-1871, p. 1-118.

Lyon, R. J. P., 1972. Infrared spectral emittance in geological mapping: Airborne spectrometer data from Pisgah Crater, California, Science V. 175, p. 983-986.

Lyon, R. J. P., 1970. Airborne geological mapping using infrared emission spectra: I, Proc. 6th Symp. Rem. Sens. of Environment, Ann Arbor, Mich., April 1970, p. 527-552.

Lyon, R. J. P., and Green, A. A., 1975. "Reflectance and Emittance of Terrain in the Mid-infrared (6-25 m) Region," in Infrared and Raman Spectroscopy of Lunar and Terrestrial Minerals, Academic Press, N. Y., p. 165-195.

Lyon, R. J. P., and Marshall, A. A. 1971. Operational calibration of an airborne infrared spectrometer over geologically significant terrains: I.E.E.E. Trans. Geoscience Electronics, V. GE-9, (3), July 1971, p. 131-138.

Lyon, R. J. P., and Patterson, J., 1966. Infrared spectral signatures--a field geological tool: Proc. 4th Symp. Rem. Sens. Environment, Ann Arbor, Mich., Apr. 1966, p. 215-230.

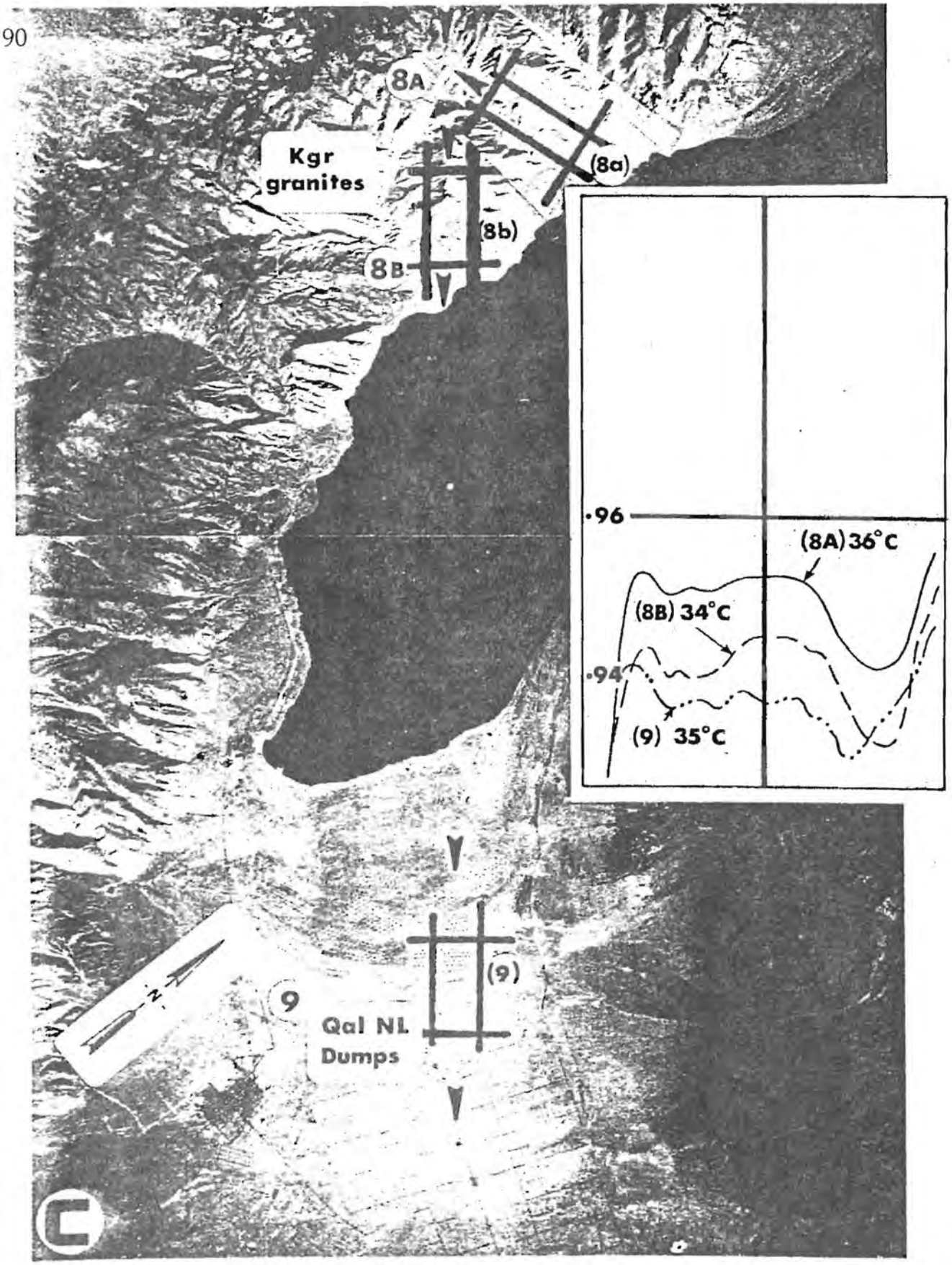
8A
(8a)
Kgr
granites
(8b)
8B
·96
(8A) 36°C
(8B) 34°C
·94
(9) 35°C
(9)
9
Qal NL
Dumps
N

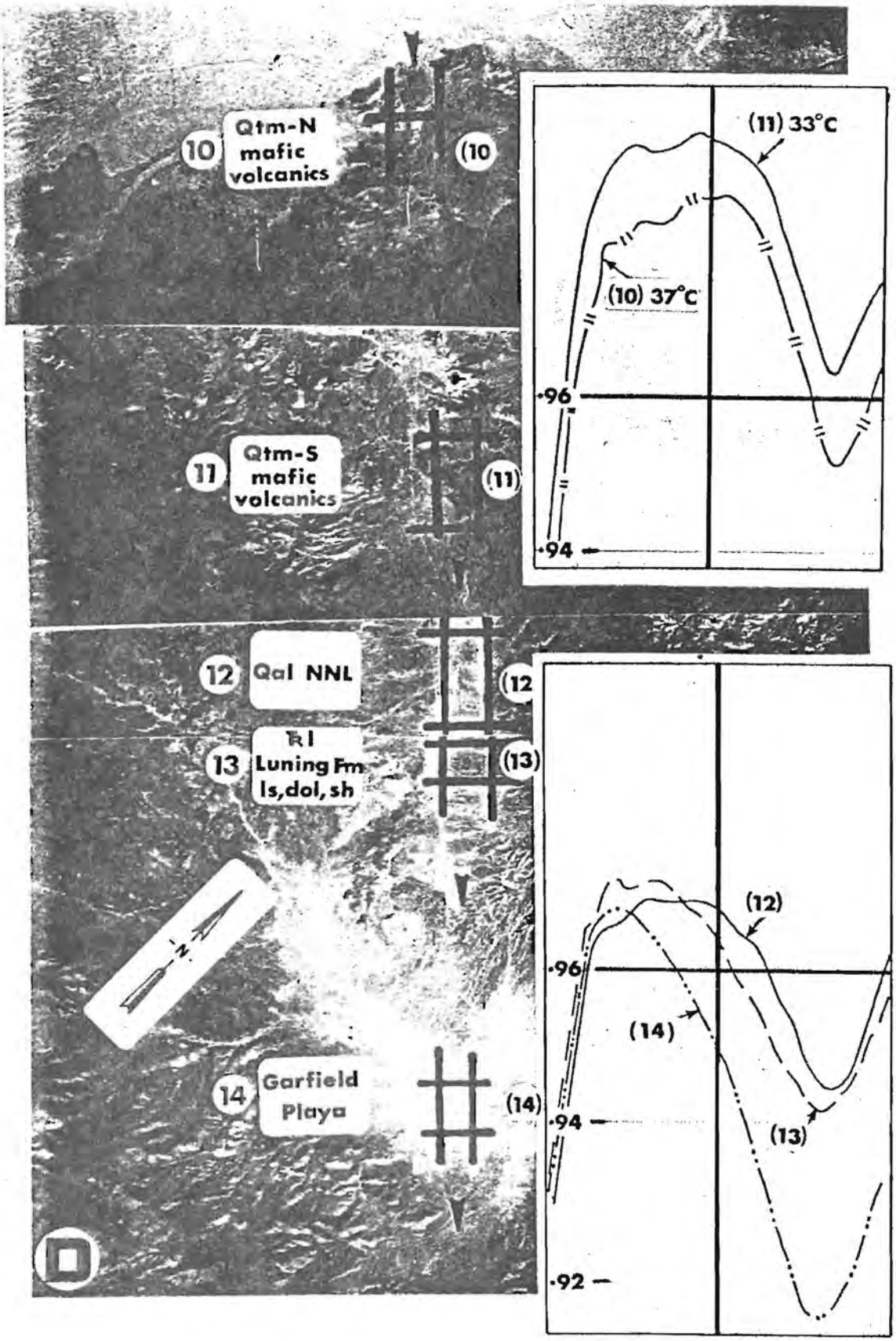
10
Qtm-N
mafic
volcanics
(10)
(11) 33°C
(10) 37°C
·96
·94
11
Qtm-S
mafic
volcanics
(11)
12
Qal NNL
(12)
13
Luning Fm
ls,dol,sh
(13)
N
14
Garfield
Playa
(14)
(12)
·96
(14)
·94
(13)
·92
D

Limb Darkening of Lunar Surface Radiance as Seen from Orbit

W. W. Mendell

NASA Johnson Space Center

The Apollo 17 Command-Service Module carried a thermal infrared scanner to lunar orbit for the purpose of radiometric mapping of the lunar surface [1]. A 45° continuously rotating mirror provided cross-track scanning while the orbital motion of the spacecraft displaced successive scans across the lunar surface. Thermal maps produced from the telemetered data have been utilized to study lunar surface erosional processes and to determine the degradational state (i.e., age) of surface features [2].

The surface thermal regime and the observational constraints at the Moon differ rather dramatically from those associated with remote observations of the Earth. The evacuated, particulate surface has the thermal properties of an excellent insulation material, responding rapidly in temperature to the diurnal variation in solar insolation. At local noon the surface is approximately in radiative equilibrium with the solar input at a temperature of approximately 400 K, while the predawn temperatures dip to 90 K. The absence of a sensible lunar atmosphere permits observation of the surface over any spectral band attainable by the instrumentation.

For the Apollo 17 Infrared Scanning Radiometer (ISR) a silicon-immersed thermistor bolometer was chosen as the system detector because it had a history of reliable performance in space applications and it was free of dependence on cryogens which could constrain the mission lifetime. The effective spectral bandpass ranged from 1.2 μm at the absorption edge of the silicon immersion lens to approximately 70 μm, where the response of the thermistor flake apparently falls off. This unusually wide passband permitted measurement of temperatures as low as 90 K with an NEΔT of 1 K even though the detector temperature was maintained at a constant 311 K. The successful performance of the Apollo 17 ISR implies that similar simple systems could be used in thermal imaging in the outer solar system.

Many findings from the thermal data are discussed in some of the references below [1,2,3]. However, one observation pertinent to the present workshop concerns the directionality of lunar surface emissivity.

Earth-based observers of the Moon have found that the subsolar point appears to have enhanced thermal emission at full Moon and that the brightness temperature distribution across the disk departs from that for a Lambert sphere [4]. The data can be matched by models which predict that 50% of the surface is covered by depressions having a depth to width ratio of approximately unity [5,6]. Such an aspect ratio is not seen in lunar surface structures; and the models were not seriously considered in the design of the orbital mapper.

However, orbital measurements showed subsolar point enhancements in excess of 25 K. Even nighttime scans exhibited limb darkening equivalent to a depression in temperature of approximately 2 K [1]. In retrospect, it is clear that a lower limit for the scale of the "depressions" is fixed by the magnitude of the thermal gradients which can be sustained in the lunar surface layer. That number is of the order of 100 K per millimeter, implying that the "depressions" can be submillimeter in scale. Thus the structures must be thought of as surface roughness rather than topography, and their effects must be incorporated in a model of directional emissivity.

W. W. Mendell

The depth of the surface texture responsible for the directionality probably is best described in terms of particle layers. In that context, there must be a direct connection with the superficial structure responsible for the retroreflective lunar photometric function. The Mercurian surface exhibits a lunar-like photometric function as does the Martian surface, though to a lesser degree. Even terrestrial surfaces are usually non-Lambertian. Interestingly, limb darkening has been observed in thermal data from the Viking orbiters above Mars [7].

The degree of directionality exhibited will depend on the magnitude of the microscale thermal contrasts as well as the aspect ratio of the roughness. The lunar surface surely represents an extreme case. The importance of the phenomenon will be greatest in the determination of thermal inertia by an accurate radiometric measurement. The presence of directional emission in the thermal scene should be considered by the investigator in planning data reduction.

References:

1. Mendell, Wendell W. (1976) Ph.D. Thesis, Rice University, Houston, Texas.
2. Mendell, W. W. (1976) Proc. Lunar Sci. Conf. 7th, p. 2705-2716.
3. Mendell, W. W. and F. J. Low (1975) Proc. Lunar Sci. Conf. 6th, p. 2711-2719.
4. Six, N. F., C. G. Montgomery, J. M. Saari, and R. W. Shorthill (1967) Directional Characteristics of Lunar Thermal Emission in Thermophysics of Spacecraft and Planetary Bodies, ed. G. B. Heller, Academic Press, New York.
5. Buhl, David, William J. Welch, and Donald G. Rea (1968) JGR, 73, 5281-5295.
6. Bastin, J. A. and D. O. Gough (1969) Icarus, 11, 289-319.
7. Kieffer, H. H. (1980) This workshop.

REMOTE SENSING OF LUNAR ROCK COMPOSITION FROM THERMAL INFRARED MEASUREMENTS

A. E. Potter, NASA JSC and T. Morgan, Houston Baptist University

The mid-infrared region, where thermal emission dominates the lunar spectrum, is potentially useful for mineralogical remote sensing, because the molecular vibration spectra in this region (reststrahlen) are directly interpretable in terms of molecular composition. R.J.P. Lyon proposed the use of mid-infrared region for analysis of mineral composition as early as 1963. Since the lunar subsolar point reaches 390°K, ample infrared signal is available.

However, progress in utilization of this spectral region has been slow, relative to progress in reflectance spectroscopy. Atmospheric effects make the observations difficult with ground-based telescopes, and a further difficulty lies in the low spectral contrast of emission features, due to the finely powdered and glassy nature of most of the lunar surface.

We have been able to observe the silicate bands in the 8-14 micron spectra of lunar sites, using a Michelson interferometer with the Wyoming Infrared Observatory 2.3 meter telescope. A spectral resolution of 1 cm^{-1} was used to resolve water absorption lines, so as to permit accurate measures of water vapor effects on the spectra. Water vapor and instrumental effects were minimized by ratioing all the spectra to the Apollo-11 site, for which laboratory spectra are available. The signal-to-noise achieved in the final lunar ratio spectra (after smoothing to 16 cm^{-1} resolution) was in excess of 500. Spectral features with strengths ranging from 1% to 3% were found in the ratio spectra. The spectra of young lunar craters show the strongest spectral contrasts, as expected for the fresh crystalline material exposed at these sites. Absorptions attributable to feldspar and ferromagnesian silicates were found in the spectra. Detection of feldspar is significant, since this mineral has not been observed in the reflective lunar spectrum. Further measurements aimed at collecting data of geological significance are planned.

The Heat Capacity Mapping Mission - System Characteristics, Data Products and Interpretation

John C. Price
Laboratory for Atmospheric Sciences (GLAS)
Goddard Space Flight Center
National Aeronautics and Space Administration

ABSTRACT

A small applications satellite, the Heat Capacity Mapping Mission, has acquired thermal infrared data at a spatial resolution of 500 meters to test the feasibility of useful geologic interpretations of temperature data. The orbital phasing - early morning, early afternoon - was chosen to optimize the measurement of the diurnal range of surface temperature. Through the relationship to the heat flow equation this temperature variation pertains to the near surface property thermal inertia = $(\rho c \lambda)^{1/2}$, where ρc is the volumetric heat capacity and λ is the thermal conductivity.

Image products from the mission illustrate the significant temperature contrast in geologically interesting areas. Day night temperature difference and "apparent thermal inertia" images have been produced in order to enhance the utility of the data. The theoretical relationship between apparent thermal inertia and actual thermal inertia is discussed in terms of a simplified model. In many respects the "apparent thermal inertia" measurement is analogous to a single spectral band measurement, with the difference that it provides information about a finite depth of material (5-10 cm) rather than the very top surface.

MULTISPECTRAL THERMAL IR EXPERIMENTS IN THE EARLY 1970'S, R.K. Vincent, Geospectra Corp. Ann Arbor, Mich. 48104

Thermal infrared scanners with multiple channels in the 8-14 μm wavelength region are important for geological remote sensing because this spectral region contains important compositional information about silicate rocks and minerals that cannot be duplicated by remote sensors operating elsewhere in the electromagnetic spectrum.

A method developed from 1970-1973 was presented whereby compositional differences among igneous silicate rocks were imaged by infrared scanners with two or three channels in the 8 μm to 14 μm wavelength region (R.K. Vincent, 1973 and 1975). The ratio (R1,2) of two infrared scanner channels on the University of Michigan M-7 multispectral scanner was related to chemical and mineralogical parameters for a suite of twenty-six igneous silicate rocks with widely varying compositions. Chemical parameters, consisting of oxide weight percentages, were measured by rapid rock analysis. Mineralogical parameters, consisting of volume percentages of natural minerals, were calculated from a C.I.P.W. computer program, with the oxides as inputs to the program. Forward linear regressions showed that for up to approximately six variables, chemical parameters are better correlated with R1,2 than mineralogical parameters. For more than six variables, the mineralogical parameters are better correlated with R1,2. The best single parameters is $\%SiO_2$, and the best two-parameter combination is $\%SiO_2 + 5.4(\%Fe_2O_3)$, with $\%SiO_2 - \%Al_2O_3$ a close second. The best overall parameter is a mineralogical index (M_{16}), which is based on the volume percentages of sixteen minerals.

The two-channel infrared ratio imaging method was applied to two test areas (R.K. Vincent and F. Thomson, 1971 and 1972). In the Mill Creek, Oklahoma area, quartz sand and sandstone were readily discriminated from other natural materials (including other silicates such as topsoil, as well as non-silicates, such as carbonates and vegetation). In the Pisgah Crater, California area, dacites and basalts were clearly discriminated and were identifiable on the basis of their infrared ratio values. A rhyolitic tuff was discriminated from surrounding alluvium on the basis of the R1,2 infrared ratio, whereas the two could not be separated by color aerial photographs in the visible wavelength region.

The minerals which are most important to traditional rock classification schemes do not have the same relative importance on their control of the R1,2 infrared ratio. Therefore, a continuous index (V_7) was developed which orders the igneous rock samples into categories defined by a traditional rock classification schemes. For a hypothetical scanner with twelve 0.5 μm-wide spectral bands between 8 and 14 μm, looking through 1 km of a dry atmosphere, linear combinations of both single band radiances and ratios of radiances from these twelve bands were sought for estimating V_7. The best result was a linear combination of seventeen ratios, using eleven of the twelve spectral bands, which had a multiple correlation coefficient of 0.99 and estimated V_7 within a standard error of 7.1%. It is likely that an even better estimator of V_7 could be found if different bandwidths and band-

centers, both inside and outside the thermal infrared region were investigated. This theoretical study indicates that future infrared scanners with eight to twelve channels in the 8-14 μm region might be used to produce an image that could be simply level-sliced (divided into discrete gray levels) to map silicate rocks according to traditional rock classification charts.

In 1974 (R. Dillman and R.K. Vincent), a color ratio composite image of three ratio images was made from visible, reflective IR, and thermal IR data collected by the M-7 aircraft multispectral scanner over a region near Halloran Springs, California. This color ratio image made it possible to discriminate granite, gneiss, andesite, quartz monzonite from one another in that area. The mapping accuracy for that experiment was 78% when very sparsely vegetated regions of the color ratio image were compared with a geologic map.

This is a field in which sensor technology appears to be the limiting factor. However, improvements in extrinsic sensor properties, especially an increase in the number of spatially coregistered detector elements in a single dewar, are more important than improvements in intrinsic properties, such as detectivity.

Dillman, R., and R. K. Vincent, Unsupervised Mapping of Geologic Features and Soils in California, Proceedings of the Ninth Symposium on Remote Sensing of Environment, Ann Arbor, Michigan, 1974, pp. 2012-205.

Vincent, R.K., and F. Thomson, Discrimination of Basic Silicate Rocks by Recognition Maps Processed from Aerial Infrared Data, Proceedings of the Seventh International Symposium on Remote Sensing of Environment, pp. 247-252, 1971.

Vincent, R.K., and F. Thomson, Rock Type Discrimination from Ratioed Infrared Scanner Images of Pisgah Crater, California, Science, v. 175, pp. 986-988, 1972.

Vincent, R.K., A Thermal Infrared Ratio Imaging Method for Mapping Compositional Variations Among Silicate Rock Types, Ph.D. Dissertation, Department of Geology and Mineralogy, University of Michigan, Ann Arbor, Michigan, 1973.

Vincent, R.K., The Potential Role of Thermal Infrared Multispectral Scanners in Geological Remote Sensing (Invited Paper), Proceedings of the IEEE, vol. 63, 1975, pp. 137-147.

THE USE OF BROADBAND THERMAL INFRARED IMAGES TO MONITOR AND TO STUDY DYNAMIC GEOLOGICAL PHENOMENA

Richard S. Williams, Jr., U.S. Geological Survey, Reston, Virginia 22092

Introduction

Much of the information in this paper is derived from another review paper, "Terrestrial Remote Sensing: Applications of Thermal Infrared Scanners to the Geological Sciences", which was based on thermal infrared research in geology carried out between 1966 and 1970 by the author when he was assigned to the Air Force Cambridge Research Laboratories (AFCRL) (Williams, 1972a). The 1972 review paper also contains a compilation of references on the use of thermal infrared images in the geological sciences and represents a comprehensive search of the available scientific literature from 1962 through mid-1970. The present paper refers to a few post-1970 thermal infrared studies with which the author is familiar and which are considered to be germane to this Workshop on Geological Applications of Thermal Infrared Remote Sensing Techniques. It should be emphasized, however, that the author's primary research has been directed toward the measurement, from aircraft and satellites, of thermal infrared emission from various types of dynamic geological phenomena in the 3 μm-5.5 μm and 8 μm-14 μm regions of the electromagnetic spectrum. Because of the author's focus on studies of thermal infrared emission from volcanoes and geothermal areas, the 3 μm-5.5 μm broadband was the thermal infrared band most utilized (Friedman and Williams, 1968).

Applications

Airborne thermal infrared images (Williams, 1972b) have been used to monitor five principal dynamic geological phenomena: volcanoes; geothermal areas; ground water discharge into marine, lacustrine, riverine, and estuarine waters; water currents; and water pollution. In all five of these geologic applications, the phenomenon being studied is generally not manifest and hence, cannot be mapped, on aerial photographs or by satellite imaging systems limited to the visible or reflective infrared wavelengths. Although satellite thermal infrared surveys have been made of erupting volcanoes and marine currents and eddies, the inadequate spatial resolution of thermal infrared sensors on civilian satellites has almost precluded their use in studies of other dynamic geological phenomena.

Infrared Surveys of Volcanic Areas.--During the first decade (1960-1970) of the application of airborne thermal infrared imaging techniques to the geological sciences, considerable progress was made in the qualitative study of volcanic thermal processes and geothermal-field convective and conductive heat transfer. Anomalously high infrared emission (in the 3 μm to 5.5 μm and 8 μm to 14 μm wavelength regions), indicating active volcanic processes, was detected by airborne and satellite thermal infrared systems in Hawaii (Fischer and others, 1964; Gawarecki and others, 1965), Alaska, the Cascade volcanoes of the western United States (Moxham and others, 1965), Costa Rica, the Philippines (Moxham and Alcarez, 1966), Italy (Del Bono and others, 1971), Antarctica (Mt. Erebus Volcano), U.S.S.R., Jan Mayen, and Iceland, to name a few of the principal geographic areas. Of all these areas, Surtsey Volcano, Iceland, and other Icelandic volcanoes (for example, Hekla, Askja, Heimaey) have probably received the most comprehensive study by airborne or satellite thermal infrared techniques.

The following generalizations were reached regarding thermal infrared emission from volcanic areas and its detection:

1. Thermal emission from both effusive and explosive-type volcanoes has been recorded successfully by aerial and satellite thermal infrared sensors (Williams and Friedman, 1970).

2. Although all active volcanoes surveyed show some indications of abnormally high infrared emission, thermal anomalies have also been reported for several volcanoes generally regarded as dormant (no historical activity) or inactive (known historical activity). It may be necessary, and prudent, therefore to reclassify some inactive volcanoes as dormant if aerial or field surveys locate any abnormally high infrared emission from either the summit crater or flanks of such volcanoes.

3. The stages of volcanic activity studied by infrared techniques, range from intereruptive through eruptive to late volcanic. Surface thermal anomalies have been documented by infrared surveys, indicating changes in the thermal regime of several volcanic areas in Iceland's neovolcanic median zone: Kverkfjöll, Hekla, and possibly Askja. Such changes in thermal regime, while not necessarily indicative of pre-eruptive activity, did indeed precede the Askja eruption of 1961. Active effusive eruptions were imaged by aerial thermographic methods at Surtsey, Iceland, and Etna, Italy. Active pyroclastic volcanoes imaged by aerial thermographic methods were Irazú Volcano, Costa Rica, and Taal Volcano, the Philippines.

4. The active processes which produce posteruptive and intereruptive thermal anomalies are manifested by radiant emission associated with convective heat transfer from crater or vent areas, convecting fracture and fault systems, porous scoriaceous rocks which emit convective thermal currents, primary and secondary furmaroles and solfateras, and various forms of hydrothermal activity.

5. The most outstanding associated tectonic features are: (a) curvilinear to concentric fractures and fault patterns associated with caldera subsidence or possible resurgence and (b) linear, en echelon fault, and dilation-fissure patterns in planetary rift zones.

6. The main contributions of thermal infrared images (aerial thermographs) have been: (a) the determination of the relative degree of activity or intensity of points of thermal emission; (b) the determination of the geometric relation of thermal anomalies to tectonic patterns; (c) the estimation of the proportion of radiant emission to total heat flow in one effusive eruption, Surtsey in 1966 (Williams and others, 1968); (d) the determination of the threshold of satellite detectability of volcanic processes outside the Earth's atmosphere; (e) the qualified confirmation of the high energy levels involved in effusive, in contrast to explosive, volcanic activity; and (f) the provision of evidence that low spatial-resolution airborne infrared systems with high thermal sensitivity in the 3 μm to 5.5 μm range are suitable for detection from Earth orbit of effusive basalt lava eruptions (Williams and Friedman, 1970).

7. The predictability of volcanic eruptions by means of airborne infrared images probably depends to a large extent on the detection of changes in the pattern of intereruptive convective heat flow by systematic line-scan imaging techniques, preferably using a calibrated system.

Infrared Surveys of Geothermal Areas.--In contrast to the study of volcanoes, where inaccessibility, large areal dimensions, and the often dynamic nature of the thermal regime make the motivation for study usually scientific, the thermal character of many geothermal areas has been intensely studied under the impetus of economic exploitation.

Airborne thermal infrared surveys have been made of geothermal areas in the United States, including several in Yellowstone National Park (McLerran and Morgan, 1964; Miller, 1966; Williams and others, 1976). Surveys also were made in Italy (Del Bono and others, 1971) and Iceland (Friedman and others, 1969), using infrared systems of U.S. manufacture. Again, the high-temperature geothermal areas of Iceland have been the most comprehensively studied. Airborne thermal infrared imaging surveys were made of many of the Iceland areas by the U.S. Air Force (AFCRL) in 1966 and 1968 and by the National Aeronautics and Space Administration (NASA), under an Earth Resources Technology Satellite 1 (ERTS 1) project (Williams and others, 1974, and Williams, 1978a) in 1973. The research in Iceland is now (1980) in its final stages, and a U.S. Geological Survey Professional Paper, "Remote Sensing of High-Temperature Geothermal Areas of Iceland," is in preparation as a cooperative endeavor between the U.S. Geological Survey and the National Energy Authority of Iceland.

The following generalizations governing infrared emission from geothermal areas have been reached:

1. Airborne thermal infrared imaging surveys can be employed to map the surface manifestations (particularly areas of altered ground and anomalously high heat flow) of geothermal activity. It is a most useful technique in remote or poorly known areas - for example, Torfajökull, Iceland (Pálmason and others, 1971). For those areas where the heat flow is higher than normal but below detectability with conventional aerial thermal infrared surveying techniques, it is necessary to resort to sophisticated modelling techniques. Ken Watson in his classic study of anomalously high heat flow in the Raft River area, Idaho, reported on the results of this modelling approach in several papers (Watson, 1971a, 1971b, 1973, 1975; Watson and others, 1971).

2. Under certain conditions, thermal infrared techniques may be used to define the areal extent of a geothermal field. Areal extent is an important parameter when trying to estimate the power potential of a field prior to exploitation. These techniques have been used to yield more accurate estimates of surface geothermal anomalies than were available before (for example, Torfajökull, Iceland).

3. The configuration of thermal anomalies and their relation to tectonic features at the surface, such as faults and fissures, may be determined by infrared surveys. This information may be of value in choosing optimum sites for drillholes in areas to be exploited.

4. Infrared techniques have been used to document changes in the thermal regime of two geothermal areas, Reykjanes and Theistareykir, in Iceland's neovolcanic zone. Successive surveys have shown that changes occur in surface thermal activity with time.

5. A marked increase in surface thermal activity is sometimes found to precede volcanic eruptions; for example, the Askja eruption in north-central Iceland in 1961. Periodic surveys to ascertain changes in surface thermal activity may, therefore, be of value in predicting volcanic eruptions.

6. Airborne thermal infrared imaging techniques can probably be used to follow changes in surface thermal activity caused by exploitation of geothermal areas for power production. The natural surface manifestations of thermal activity normally decrease during exploitation.

7. Although it would be most useful to be able to map areas of geothermal emission from orbital altitudes, the spatial resolution of thermal infrared sensors on civilian satellites is too large. These sensors have a large instantaneous field of view (IFOV), which is 1 km in the National Oceanographic and Atmospheric Administration (NOAA) series of weather satellites and 0.6 km in the Heat Capacity Mapping Mission (HCMM) spacecraft. Landsat multispectral scanner (MSS) images of Iceland, which have a pixel resolution of about 80 m, were used to identify and to grossly map some areas of geothermally altered ground (for example, the Námafjall area, using the variation in spectral reflectance of the altered ground areas (Williams and others, 1974; Williams 1978a). The thermal infrared sensor (MSS band 8) on the Landsat 3 spacecraft had a pixel resolution of 240 m, but the sensor malfunctioned and very little, if any, useable scientific data were acquired. An NEΔT of 1°K and a spatial resolution comparable to the Landsat MSS system ($\sim$80 m) would be required for direct measurement of thermal emission from high-temperature geothermal areas.

Infrared Surveys of Hydrogeologic Phenomena.--The research area of greatest potential application and economic value for airborne thermal infrared surveys using optical-mechanical line-scanner systems is in hydrogeology and related fields. Under certain conditions, airborne scanning radiometers can record ground water discharge into marine (Williams and Fernandopullé, 1972), lacustrine, riverine, and estuarine waters; can depict the flow of water currents (Taylor and Stingelin, 1969); and can often pinpoint the source (outfall) and surface movement of pollutants.

Future Trends

Airborne Applications.--Future trends in applications of aerial thermography in geological studies will likely be directed toward hydrogeologic problems and will emphasize monitoring water pollution in lakes, rivers, estuaries, harbors, and other coastal areas. Research will continue on the use of aerial thermography to measure surface water currents. If hydrological phenomena could be monitored using thermal infrared sensors on orbiting spacecraft, much more data would be made available. Certainly a first step to reaching the objective of operational satellite surveys would be to establish of a solid aerial research program to acquire high altitude ($>$13,000 m) aerial thermography of geothermal, volcanic, and other areas to assess the utility of such data for regional studies.

The number of scientific studies of the dynamic thermal regime of volcanoes will probably increase; the emphasis will be on monitoring thermal changes in volcanoes which pose a threat to human life such as those in the Cascade Range of the northwestern United States. Even the dynamic thermal character of those volcanoes which have observatories (for example, Kilauea, Mt. Vesuvius, and Mt. Etna) is inadequately known. Repetitive surveys of volcanoes may lead to a predictive technique based on the change of surface thermal activity prior to a volcanic eruption. From a purely scientific basis, aerial thermography represents an important tool for the acquisition of data on thermal activity in remote areas such as the Aleutian Islands.

Aerial thermographic surveys of geothermal areas will be increased for scientific reasons and for exploitation of such areas for geothermal power generation and, in colder climes, for hot water distribution for heating and personal and commercial use. The search for geothermal sources of power is being stressed by many countries. Aerial thermography can be used for reconnaissance exploration, assessment of the extent of geothermal areas (particularly at remote sites), and in monitoring changes in the nature of geothermal activity during development and exploitation.

Satellite Applications (Terrestrial).--Geologic applications of orbital thermal infrared scanning radiometers fall into two classes: terrestrial and extraterrestrial. The terrestrial applications discussed previously are still rather few because the spatial and thermal resolution of orbital scanning radiometers is too large. This is particularly true of the spatial resolution. Future improvements in spatial resolution will likely lead to new geologic applications, particularly in marine geology, oceanography, glaciology, and climatology.

Higher resolution satellite thermographic surveys of coastal marine currents will be of particular value in marine geological and oceanographic investigations. Oceanic currents, such as the Gulf Stream, and the discharge of major rivers into coastal marine waters have been recorded by both the NOAA series and the HCMM spacecraft. As can be seen from Figure 1, however, a much improved spatial resolution of thermal sensors on satellites would produce much more useful information. Figure 1 shows large-scale marine eddies off the southwest coast of Iceland imaged on MSS band 4 of Landsat 2 (Williams, 1978b). Whether these eddies can also be delineated thermally is unknown.

Unpublished research by Donald R. Wiesnet (personal commun., 1980) on the Greenland Ice Cap showed that thermal sensors onboard the NOAA series of spacecraft can be used to monitor the thermal regime of glaciers on a seasonal basis. Thermal sensors having a higher spatial resolution would permit such surveys to be conducted seasonally on smaller ice caps, outlet glaciers, and valley glaciers. Of particular interest to glaciologists and climatologists are the varying thermal characteristics of the accumulation and ablation areas of glaciers on a seasonal basis.

As was proven by the studies of the Surtsey Volcano in Iceland and in studies of other volcanoes, it is presently possible to monitor, on a worldwide basis, effusive volcanic activity using orbital thermography (Figure 2). Such research is primarily scientific, however, because it is directed at the monitoring of volcanoes remote from inhabited areas.

Satellite Applications (Extraterrestrial).--Instrumentation similar to that used to acquire terrestrial orbital thermography could be modified and placed in orbit around the planet Mars, the Galilean moon Io, and other planets and moons suspected of being volcanically active. Neither the planet Venus nor Titan, one of Saturn's moons can be thermally imaged,however, because both their surfaces are shrouded by atmospheres. A system similar to the Nimbus II high resolution infrared radiometer (HRIR) could definitely record an effusive volcanic event from either the Ionian or Martian surface at an altitude of 1000 km, if the eruption were of a magnitude not less than the August 1966 effusive eruption on Surtsey, Iceland. An orbiting spacecraft is the only feasible way of monitoring dynamic thermal phenomena on extraterrestrial surfaces because their areas are so huge. In the case of Mars, for example, the area to be monitored is equal to the subaerial (dry-land) area of the Earth's surface.

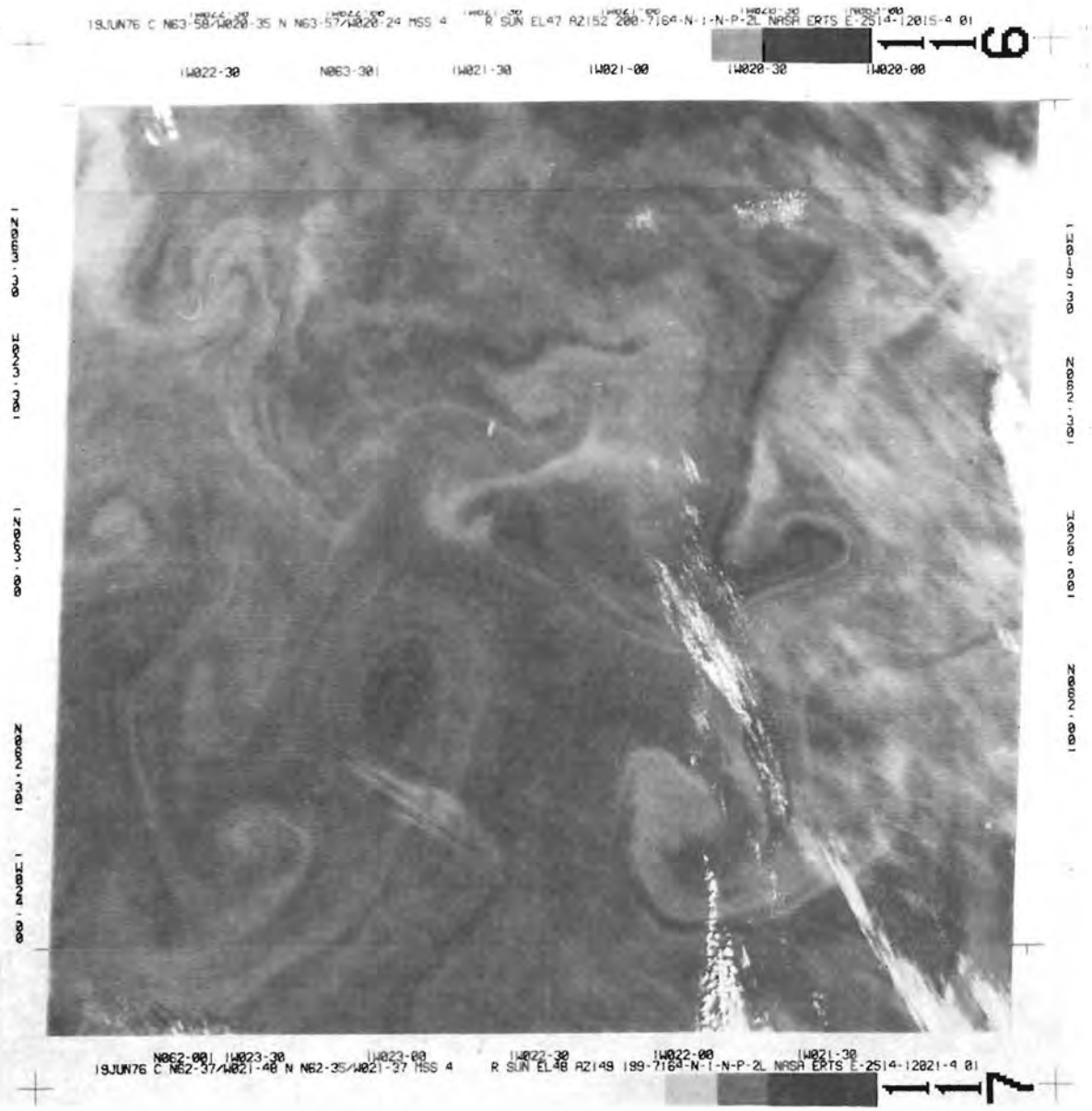

Figure 1.--Landsat 2 MSS band 4 (.5-.6 μm) image of large scale marine eddies off the southwest coast of Iceland on 19 June 1976. An intense bloom of phytoplankton is thought to be the explanation for the tone of the ocean's surface with tonal variations caused by dispersal of the phytoplankton by complex marine currents (Williams, 1978).

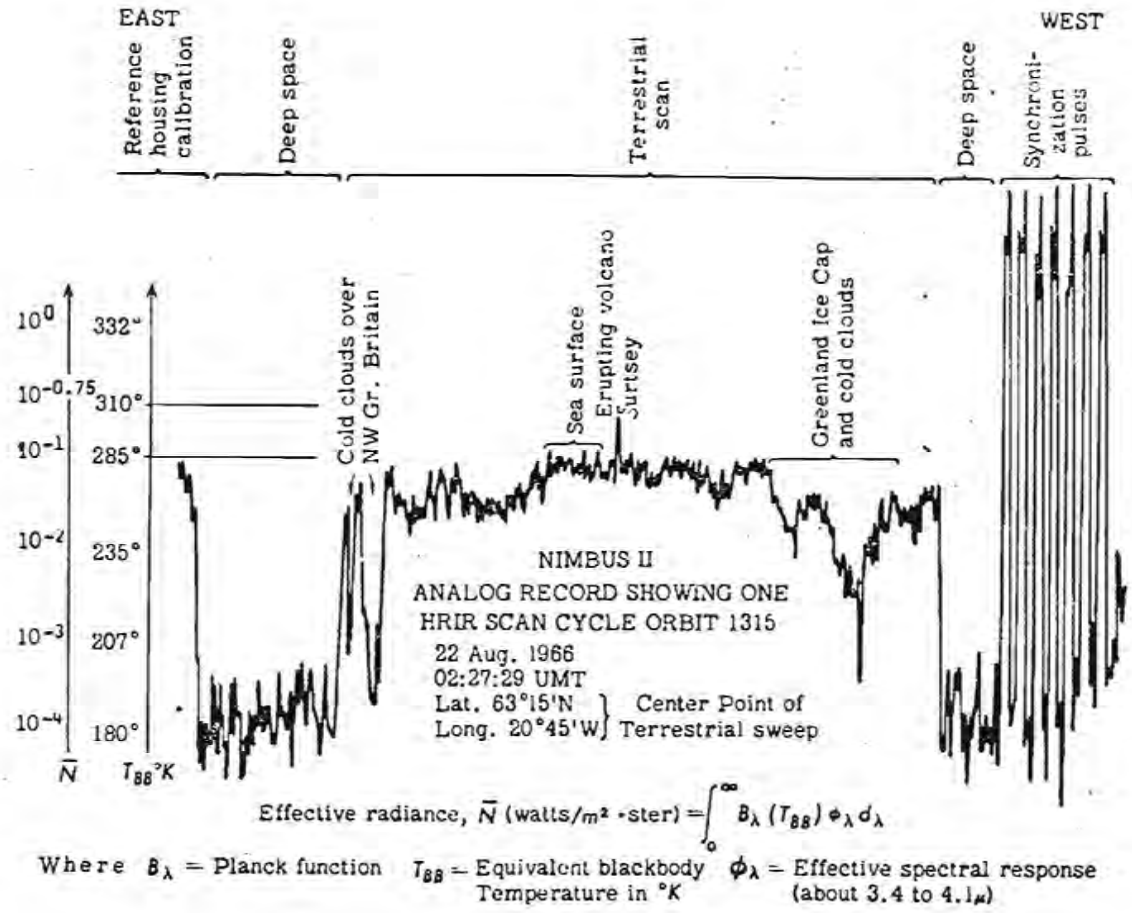

Figure 2 - Effective radiance ($\bar{N}$) from the Earth's surface along a profile from Greenland to Great Britain 02:27:29 UMT, August 22, 1966, recorded at an altitude of 1,114 km by Nimbus 11 HRIR System. This analog oscillograph record of one scan cycle, orbit 1315, was made from the original interrogation of the Nimbus 11 spacecraft. The highest positive spike represents infrared radiation in the 3.4 μm to 4.1 μm wavelength band emitted by lava craters and incandescent flows from Surtsey, integrated with infrared radiation from the surrounding 62-km^2 ocean surface.

References cited

Del Bono, G.L., Williams, R.S., Jr., and Cronin, J.F., 1971, Photogeologic and thermal infrared imagery geologic surveys in Italy in 1966: Bollettino del Servizio Geologico D'Italia, v: XCI (1970), p. 3-44.

Fischer, W.A., Moxham,R.M., Polcyn, Fabian, and Landis, G.H., 1964, Infrared surveys of Hawaiian volcanoes: Science, v. 146, no. 3645, p. 733-742.

Friedman, J.D., and Williams, R.S., Jr., 1968, Infrared sensing of active geologic processes: in Proceedings, Fifth Symposium on Remote Sensing of Environment, University of Michigan, Ann Arbor, Michigan, p. 787-820.

Friedman, J.D.; Williams, R.S., Jr.; Pálmason, Gudmundur; and Miller, C.D., 1969, Infrared surveys in Iceland in 1966: in Geological Survey Research 1969, U.S. Geological Survey Professional Paper 650-C, p. C89-C105.

Gawarecki, S.J., Lyon, R.J.P., and Nordberg, William, 1965, Infrared spectral returns and imagery of the Earth from space and their applications to geologic problems: Scientific Experiments for Manned Orbital Flight, v. 4, Science and Technology Series, American Astronautical Society, p. 13-33.

McLerran, J.H., and Morgan, J.O., 1964, Thermal mapping of Yellowstone National Park: Proceedings, Third Symposium on Remote Sensing of Environment, University of Michigan, Ann Arbor, Michigan, p. 517-530.

Miller, L.D., 1966, Location of anomalously hot Earth with infrared imagery in Yellowstone National Park: Proceedings, Fourth Symposium on Remote Sensing of Environment, University of Michigan, Ann Arbor, Michigan, p. 751-769.

Moxham, R.M., and Alcarez, Arturo, 1966, Infrared surveys at Taal Volcano, Philippines: Proceedings, Fourth Symposium on Remote Sensing of Environment, University of Michigan, Ann Arbor, Michigan, p. 827-843.

Moxham, R.M., Crandell, D.R., and Marlatt, W.E., 1965, Thermal features at Mount Rainier, Washington, as revealed by infrared surveys: Geological Survey Research 1965, U.S. Geological Survey Professional Paper 525-D, p. 93-100.

Pálmason, Gudmundur; Friedman, J.D.; Williams, R.S., Jr.; Jónsson, Jón; and Saemundsson, Kristján, 1971, Aerial infrared surveys of Reykjanes and Torfajökull thermal areas, Iceland, with a section on cost of exploration surveys: in Geothermics (1970), Special Issue 2, U.N. Symposium on the Development and Utilization of Geothermal Resources, Pisa 1970, v. 2, pt. 1, p. 399-412.

Taylor, J.I., and Stingelin, R.W., 1969, Infrared imaging for water resources studies: Journal of the Hydraulics Division, American Society of Civil Engineers, v. 95, no. HY1, Proceedings Paper 6331, January, p. 175-189.

Watson, Kenneth, 1971a, Geophysical aspects of remote sensing: International Workshop on Earth Resources Survey Systems, May 3-14, VII, p. 409-428.

Watson, Kenneth, 1971b, A thermal model for analysis of infrared images: National Aeronautics and Space Administration Third Annual Earth Resources Program Review, Houston, Texas, v. 1, Sec. 13, p. 1-16.

Watson, Kenneth, 1973, Periodic heating of a layer over a semi-infinite solid: Journal of Geophysical Research, v. 78, no. 26, p. 5904-5910.

Watson, Kenneth, 1975, Geologic applications of thermal infrared images: Proceedings, IEEE, v. 63, no. 1, p. 128-137.

Watson, Kenneth, Rowan, L.C., and Offield, T.W., 1971, Application of thermal modeling in the geologic interpretation of IR images: Proceedings, Seventh International Symposium Remote Sensing of Environment, University of Michigan, Ann Arbor, Michigan, v. 3, p. 2017-2041.

Williams, R.S., Jr., 1972a, Terrestrial remote sensing: Applications of thermal infrared scanners to the geological sciences: in Pt. 3, ISA Transducer Compendium, Instrument Society of America, Pittsburgh, Pennsylvania, p. 219-236.

Williams, R.S., Jr., 1972b, Thermography: Photogrammetric Engineering, v. 38, no. 9, p. 881-883.

Williams, R.S., Jr., 1978a, Satellite geological and geophysical remote sensing of Iceland: Type III Progress Rpt. to the National Aeronautics and Space Administration, Goddard Space Flight Center, Greenbelt, Md., Earth Resources Technology Satellite 1 Experiment No. SR 9651; 15 January 1973 - 15 August 1974, 1 January 1978, 66p.

Williams, R.S., Jr., 1978b, Landsat image of dynamic marine phenomena off the southwest coast of Iceland (abs.): EOS (Transactions, American Geophysical Union) v. 59, no. 4, p. 301.

Williams, R.S., Jr., and Friedman, J.D., 1970, Satellite observation of effusive volcanism: British Interplanetary Society Journal, v. 23, No. 6, p. 441-450.

Williams, R.S., Jr., and Fernandopullé, Denis, 1972, Geological analysis of aerial thermography of the Canary Islands, Spain: in Proceedings, Eighth International Symposium on Remote Sensing of Environment, University of Michigan, Ann Arbor, Michigan, p. 1159-1194.

Williams, R.S., Jr.; Friedman, J.D.; Thórarinsson, Sigurdur; Sigurgeirsson, Thorbjörn; and Pálmason, Gudmundur, 1968, Analysis of 1966 infrared survey of Surtsey, Iceland: in Surtsey Research Progress Report, The Surtsey Research Society, Reykjavík, Iceland, v. IV, p. 177-192.

Williams, R.S., Jr.; Bödvarsson, Ágúst; Fridriksson, Sturla; Pálmason, Gudmundur; Rist, Sigurjón; Sigtryggsson, Hlynur; Saemundsson, Kristján; Thorarinsson, Sigurdur; and Thorsteinsson, Ingvi, 1974, Environmental studies of Iceland with ERTS-1 imagery: in Proceedings, Ninth International Symposium on Remote Sensing of Environment, University of Michigan, Ann Arbor, Michigan, v. 1, p. 31-81.

Williams, R.S., Jr., Hasell, P.G., Jr., Sellman, A.N., and Smedes, H.W., 1976, Thermographic mosaic of Yellowstone National Park: Photogrammetric Engineering and Remote Sensing v. 42, no. 10, p. 1315-1324.

DESIGN OF AN AIRCRAFT THERMAL INFRARED MULTISPECTRAL SCANNER (TIMS)

Ford L. Wright, Vice President - Engineering, Daedalus Enterprises, Inc., Ann Arbor, MI 48106

Daedalus has built and delivered about 50 airborne scanner systems in the past decade, including 14 eleven-channel multispectral units which cover 10 bands in the 0.4 - 1.1 μm region and one band in the thermal IR. We believe we are now the only remaining U.S. manufacturer of a standard commercial product line of these type instruments, and we supplied the three most recent NASA multispectral procurements in 1974, 1977 and 1979.

DS-1280 HIGH RESOLUTION MULTISPECTRAL SCANNER.

In September 1978 we undertook development of a 5-channel special purpose multispectral scanner for NASA-NSTL Earth Resources Laboratory under Contract NAS13-98. The resulting instrument, assigned Daedalus Model No. DS-1280, was installed in a Learjet Model 35 aircraft and delivered 15 November 1979. This new scanner has five times better resolution (.54mrad) and six times larger collecting area (7.5-inch dia. optics) than our standard DS-1260 system. Later in this discussion it will be shown how elements from both systems could be combined to create a Thermal Infrared Multispectral System (TIMS) useful for geologic applications.

Since the DS-1280 system shown in Figure 1 is new, it will be useful to describe it briefly, and particularly to contrast it with other more familiar systems such as the DS-1260 or the Bendix M^2S. Specifications of the DS-1260 and the DS-1280 systems are shown in Figure 2. The DS-1280 system was designed exclusively to operate in a jet aircraft at 360±10% knots and 35,000 feet above ground level which is consistent with a 0.54 mrad instantaneous field of view. The 45° rotating-flat 7½" diameter beryllium scan mirror is finished to quarter-wave static flatness and carefully integrated with a computer-designed balancing tube to maintain the necessary dynamic flatness for future upgrade to 0.36 mrad at 54 rps maximum rotation rate. The scan head is mechanically temperature-compensated using low thermal coefficient of expansion nickel alloy steel where necessary to keep the system in focus and alignment over the ±55°C temperature range. The resulting scan head is twice the size and three times the weight of the scan head of the DS-1260 system. At 160 pounds and 38 inches long it is not something one person installs in an RC-10 camera mount!

The DS-1280 system spectrometer design is essentially that of the DS-1260 system, but with 5 channels in the .50 - 1.10 μm region. Two interchangeable detector arrays were supplied, one of which has channel spectral bandwidths about half the other. No thermal IR capability was provided in the DS-1280 system.

The 5-channel digitizer of the DS-1280 system accepts video and encoder clock signals from the scan head and roll and other housekeeping signals from a special Litton LTN-72R Area Navigation System in the aircraft. It outputs 2680 video words and 50 housekeeping/sync words per scan line per channel in NRZ output format to two 14-track Ampex AR-1700 tape recorders

which sequentially encode Miller-squared format at 26,600 bits per inch on the high density digital tape. A digitized output of each channel ratioed by the near IR channel (.94 - 1.1 μm) may also be selected.

The data processing system for use with the DS-1280 was designed and procured by Earth Resources Laboratory and Lockheed Electronics Co. A maximum likelihood classification or simpler clustering schemes are used to identify vegetation of interest. Area and map coordinates of the vegetation of interest are computed and printed. The goal is to operationally process data from about 10,000 square miles of coverage each flight with 3-day turnaround, to reliably classify areas larger than ¼ acre, and to locate by coordinate the areas of interest to within about ¼ mile.

A THERMAL IR MSS ALTERNATIVE.

Usefulness of data from thermal IR bands to geologic investigation appears to be an established fact. In particular, recent analysis of data from the six thermal IR bands of the Bendix 24-channel MSDS instrument has shown high potential value to geologic studies. We believe elements of the DS-1260 and DS-1280 systems can easily be combined with new thermal IR spectrometer developments to give performance parameters in the thermal IR approximately equivalent to those of the 24-channel scanner. A proven operational acquisition instrument with Daedalus customer service and standard spare parts backup would result, rather than a minimally supported one-of-a-kind prototype.

The motor controller and large-optics scan head of the new DS-1280 system would be combined with the operator console and digitizer of the standard 2.5 mrad DS-1260 system to create the proposed TIMS instrument. Motor speeds would change from 27, 32, 36 to 12½, 25, 50 and a 6000 element encoder as used on the 2.5 mrad system would be used instead of the one for .54 mrad. The DEI-116 Scan Head is a classic Newtonian telescope with a field of view which is traversed by a scanning mirror. The scanning mirror is a flat, single facet optical mirror oriented at 45° and centered with respect to its axis of rotation. The mirror is mounted directly on the shaft of a DC motor along with an optical shaft encoder. The 13 inch focal length focusing parabola, a 3-inch diameter secondary mirror and a field stop aperture are thermally compensated to remain in focus throughout the entire operating temperature range. The 7.5 inch diameter optics collect six times as much energy as the 5 inch axe-blade mirror in the DEI-114 scan head of the standard DS-1260 system.

The scan head would be fitted with two field-filling reference sources of new design to match the 7½ inch scan mirror length. One reference source would be operated in a heated-only mode and would be capable of operation to at least 60°C. The other source would be operated in both a cooled and heated mode and would operate from -30 to +50°C. This range of available temperatures would easily allow operation to 8 bit accuracy at the specified temperature sensitivity of the system.

The rack mounted reference source controller would enable the operator to set the temperature of each reference. The reference would be stabilized at the set value using a proportional temperature control circuit. The temperatures of the sources would be displayed on two digital panel meters and would also be recorded on the HDDT through the digitizer unit.

The 6-channel spectrometer would be designed and built specifically for this application. There are a number of trade-offs involving spectral purity, resolution, reliability and cost which would have to be evaluated. However, at this time the most likely design would be to use a grating dispersive element and a catadioptric optical system. However, a possible alternative may be a refractive optical design with germanium element and a sodium chloride dispersing prism.

The digitizer used would be a modified version of the DEI-260 unit, which is standard in the DS-1260 system. The minor modifications would convert the digitizer from a 12-channel visible and IR unit to a 6-channel IR unit. The digitizer provides 8 bit digitization with an accuracy of $\pm$1/2 LSB. The sampling of the data is at a rate of 3000 samples per scan mirror rotation, directly controlled by the motor shaft encoder. Roll correction is provided in the digitizer using the output of the scan head mounted vertical gyro. Sampling accuracy to within $\pm$0.25 mrad of roll stabilized pixel position is achieved.

The digital output format would be the same as the DS-1260's format. The data is coded in Manchester Bi-ϕ-Level form and a packing density of 10,000 bits per inch is maintained on the HDDT for each of the three scan speeds.

The control console would be the same as that currently used with the DS-1260 system. A dual channel monitor oscilloscope in the console provides the monitoring capability. Any two of the six video channels can be monitored prior to digitization, or any two video channels can be monitored after digitization and D/A conversion (either directly or from the reproduce amplifiers of the HDDT).

The mirror scan rate is selected and servo-controlled by the motor control console. The shaft encoder output is compared to an internally generated crystal controlled reference frequency. The servo error voltage controls the duty cycle of a switching-mode regulated DC supply which drives the scan motor.

Specifications for the proposed TIMS are summarized in Figure 3. Specifications for the 24-channel MSDS at some time during its evolution are shown for comparison; there could have been some differences at the time it was completed. Additional TIMS proposed parameters and its operating profile are shown in Figure 4 and 5. The TIMS system could be available within 18 months of a decision to build.

SCANNER DESIGN TRADEOFFS.

It seems to be normal in the scanner business for users not to want quite the parameters that are already designed into an instrument. Thus, it is well to have in mind some of the general engineering, performance, and cost ramifications of certain design tradeoffs. Figure 6 diagrams the parameters most often wanted improved - either all together or one without impacting the others. The universal answer is shown in the triangle, of course, which is to use larger optics to collect more energy.

Some ramifications of requiring larger optics are noted in Figure 7. The scan head size increases in all dimensions, and the field-filling blackbody references increase in size to match the increased scan mirror size. The larger aircraft opening required often has a serious structural impact. Scan motor and controller power and weight are increased to rotate the larger mass. It is more difficult and increasingly costly to maintain required curvature or flatness over a larger optical surface.

Figure 9 shows effects of requiring higher spatial resolution (smaller IFOV) in a scanner system. If a higher scan rate becomes necessary dynamic scan mirror distortion increases considerably, balance and bearings are more critical, and required motor torque due mostly to windage increases as an exponential function of the speed. Since the mirror proposed for TIMS was designed for higher resolution, only the motor power requirement would be a factor.

Finally, although the DS-1260 and DS-1280 systems aren't exactly comparable, it should be pointed out that the latter cost about 2½ times as much and took 14 months to deliver compared to 6 months for standard systems. Initial documentation labor is nearly equal to design labor on a new system; obviously the more "standard" it is the less costly it will be. However, if there are important known reasons to change design parameters, it is usually advisable to do so in the initial design.

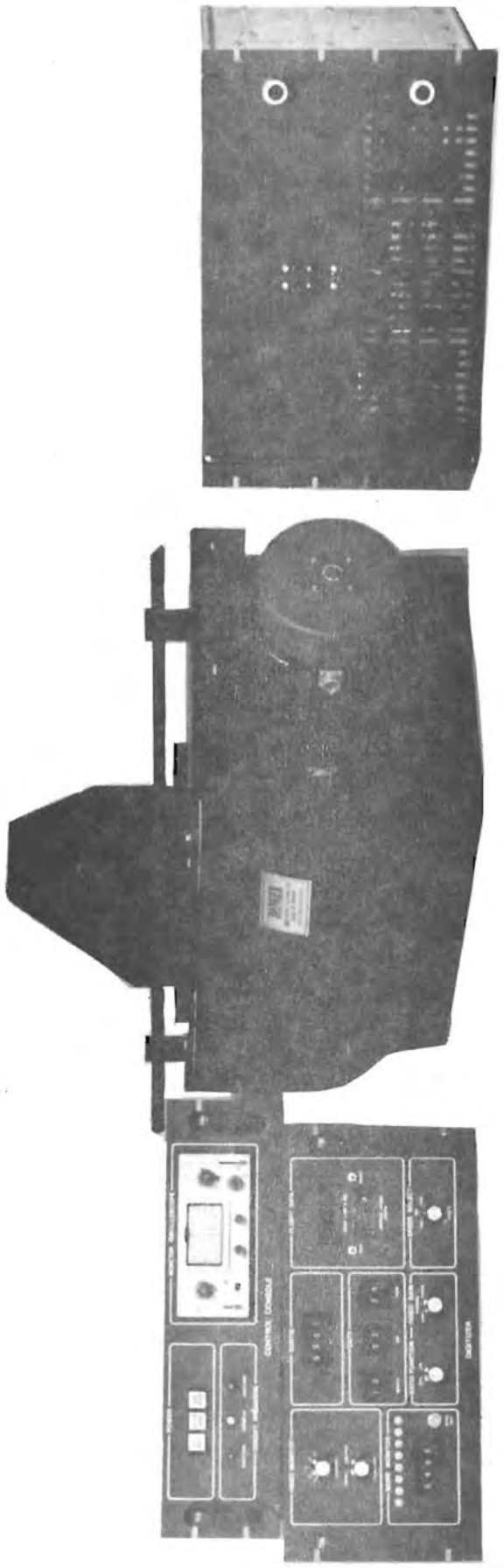

FIGURE 1. DS-1280 MULTISPECTRAL SCANNER SYSTEM

Figure 2

COMPARISON OF DS-1260 AND DS-1280 SPECIFICATIONS

PARAMETER	UNIT	DS-1260	DS-1280
Collecting Diam.	inches	5.0	7.5
Collecting Area	inches^2 (eff.)	6.1	36
Focal Length	inches	6.0	13
Optical Aperture	(effective)	f/2.1	f/1.9
Scan Rate	scans/sec	12½ - 100	27 - 36
Digitized FOV	degrees	86	58.9
IFOV	m rad	2.5	0.54
V/H	radians	.03 - .25	.015 - .02
Words/Scan Line		750	2730
Video Words/Line		716	2680
Digitizer Gains		.5 - 8	.8 - 1.2
Digitization	bits	8	8
Output Bit Rate	K bits/sec	75 - 600	590 - 786
HDDT Packing Density	bits/inch	10,000	26,600
HDDT Encoding		Bi-ϕ-L	Miller^2
Tape Speeds	inches/sec	7½ - 60	22.2 - 29.5
Analog Bandwidth	KHz	16 - 126	209
Roll Correction	degrees	±15	±10
Reference Sources		thermal/VIS	none
Channels		11	5
Head Size (HxWxD)	inches	15x15x15	20x13x38
Head Weight	pounds	50	160
Total Sys. Wgt.	pounds	270	370
Total Sys. Power	AMPS @ 28 VDC	65	60

Shaded areas indicate combination for Thermal IR MSS.

Figure 3
COMPARISON OF TIMS AND MSDS SPECIFICATIONS

PARAMETER	UNIT	TIMS	MSDS
Collecting Diam.	inches	7.5	9.0
Collecting Area	inches^2 (eff.)	36	63
Focal Length	inches	13	17.5
Optical Aperture	(effective)	f/1.9	f/5
Scan Rate	scans/sec	12½ - 50	10 - 100
Digitized FOV	degrees	86	80
IFOV	m rad	2.5	2.0
V/H	radians	.03 - .12	.02 - .2
Words/Scan Line		750	785
Video Words/Line		716	700
Digitizer Gains		.5 - 8	Auto.
Digitization	bits	8	8
Output Bit Rate	K bits/sec	75 - 300	150 - 1500
HDDT Packing Density	bits/inch	10,000	10,000
HDDT Encoding		Bi-ϕ-L	Bi-ϕ-L
Tape Speeds	inches/sec	7½ - 30	12 - 120
Analog Bandwidth	KHz	16 - 63	450
Roll Correction	degrees	$\pm$15	$\pm$8
Reference Sources		thermal	(5)
Channels		6	24
Head Size (HxWxD)	inches	20x13x38	38x54x64
Head Weight	pounds	170	696
Total Sys. Wgt.	pounds	470	3178
Total Sys. Power		110 (D.C.)	11.2 KVA (400Hz) 755 (D.C.)

Wavelength	NEΔT (at 25°C)
8.3 - 8.8 μm	<0.5°C
8.8 - 9.3 μm	<0.5°C
9.3 - 9.8 μm	<0.5°C
10.1 - 11.0 μm	<0.4°C
11.0 - 12.0 μm	<0.4°C
12.0 - 13.0 μm	<0.5°C

Lowest Flight Altitude (at 130 MPH) = 1500 feet

Maximum Ground Resolution (at 1500 ft) = 3.75 feet

Ground Path Coverage (86° FOV) = 1.86 x Altitude

Figure 4. TIMS PARAMETERS

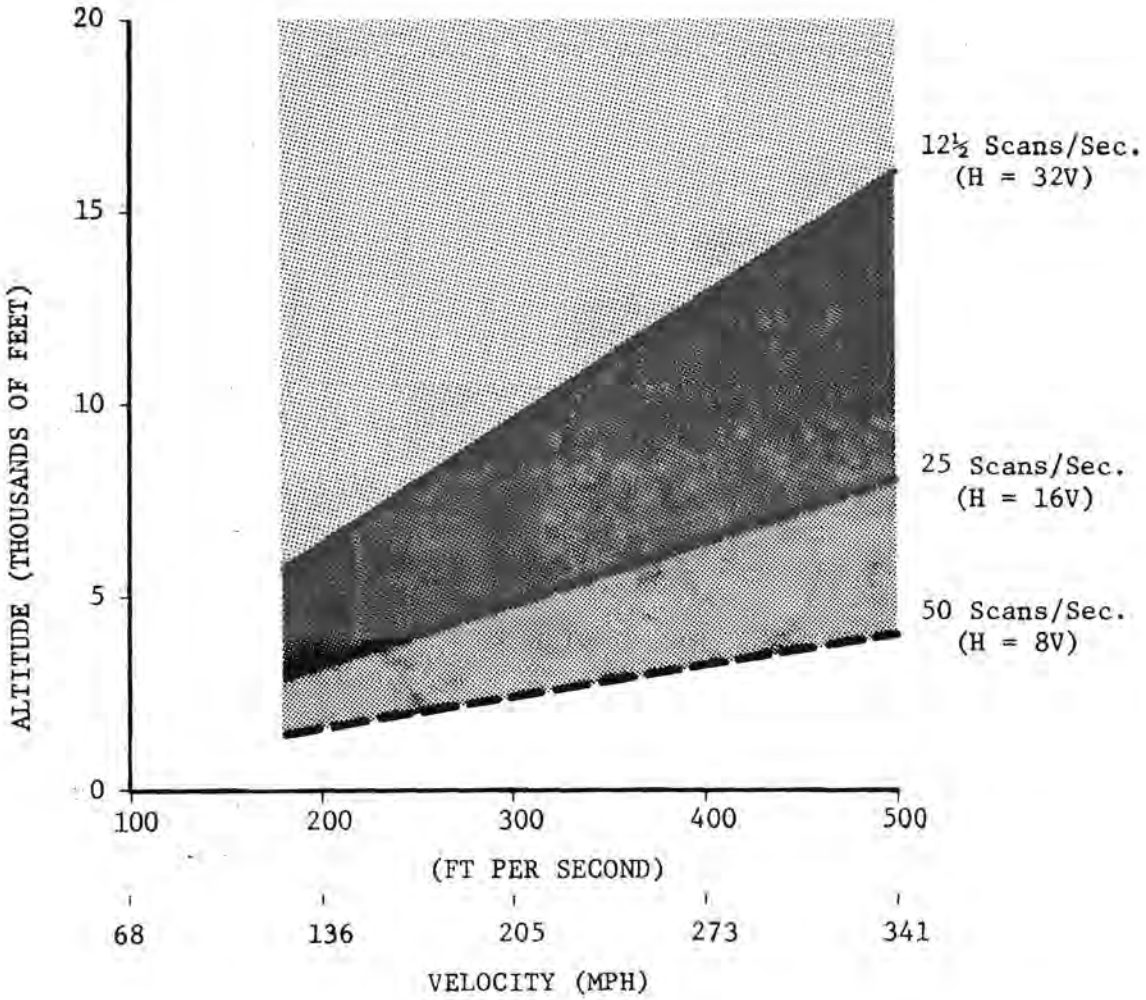

Figure 5. TIMS V-H OPERATING PROFILE

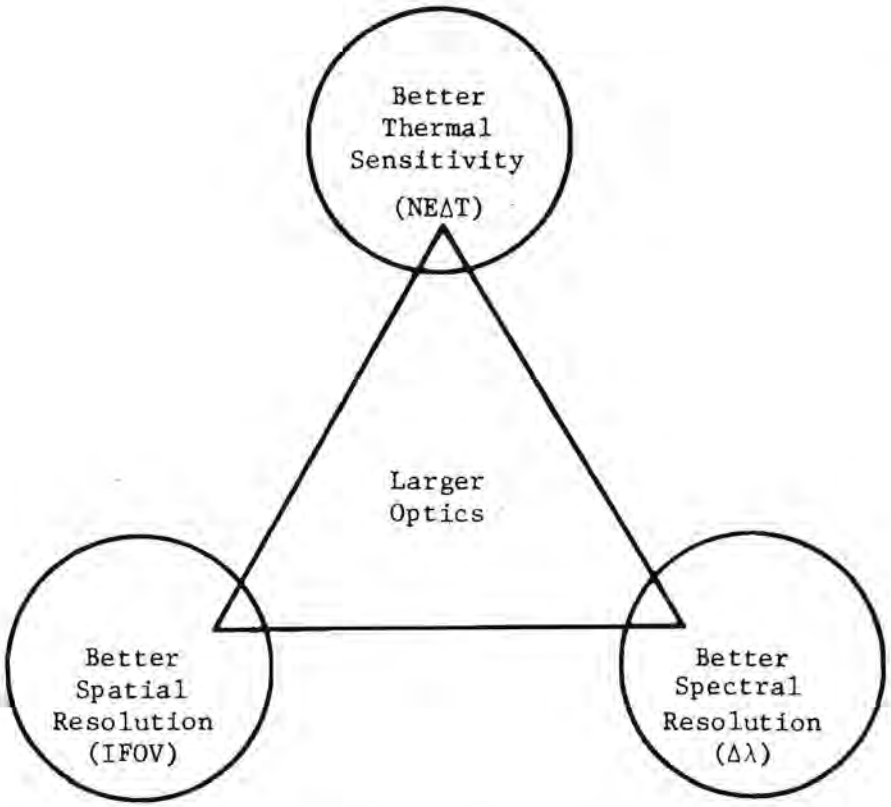

Figure 6. SCANNER DESIGN TRADEOFFS

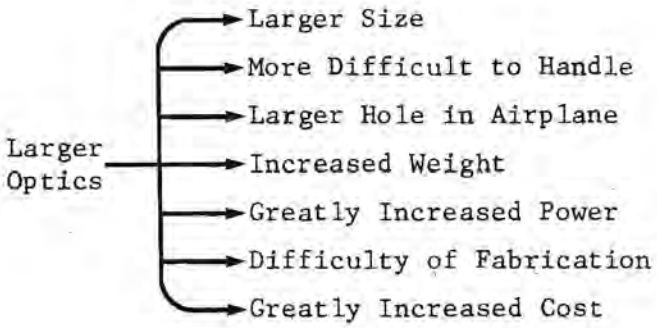

Figure 7. EFFECTS OF LARGER OPTICS

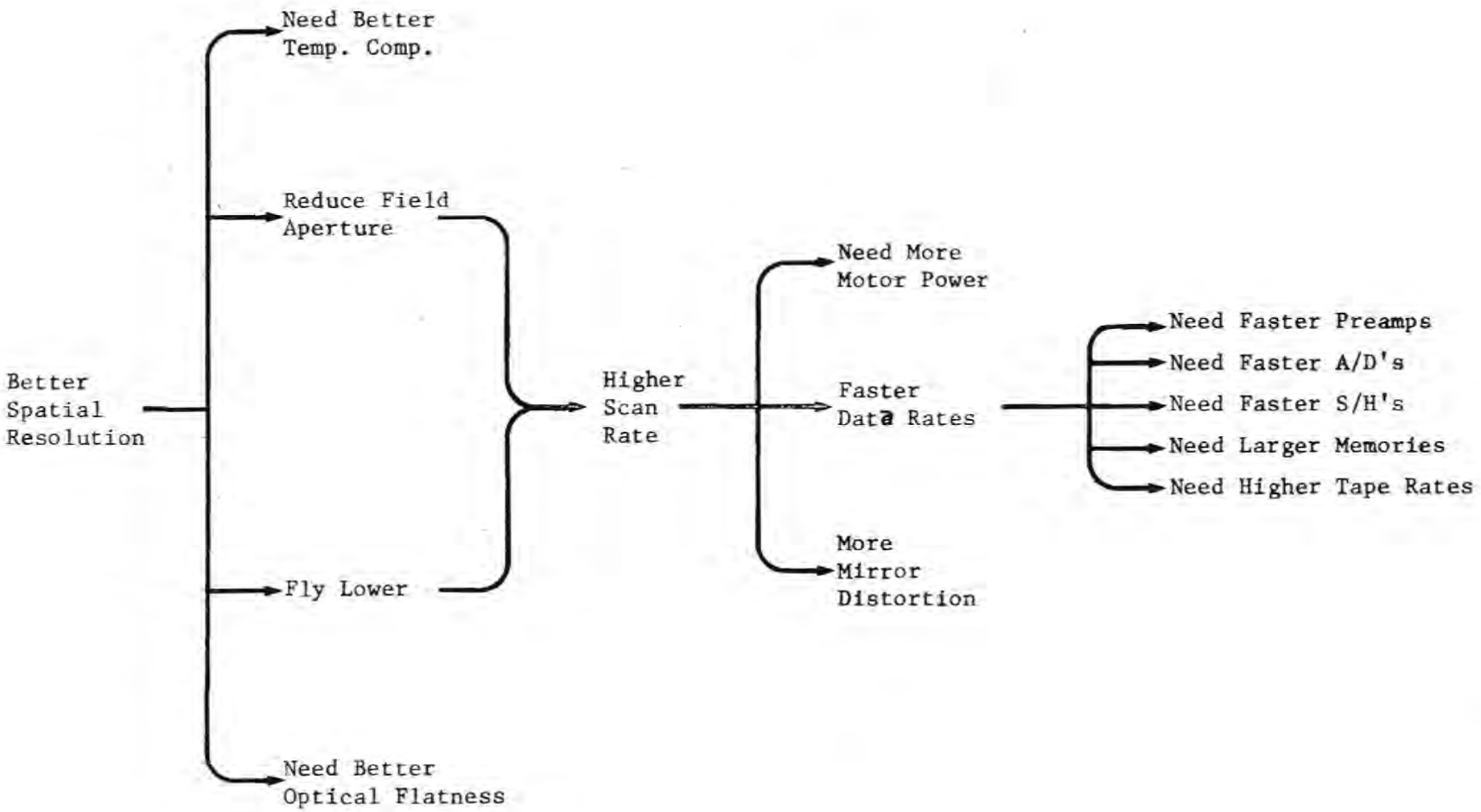

Figure 8. EFFECTS OF REQUIRING BETTER SPATIAL RESOLUTION

Program

Session I, Monday, February 11, 1980

Earth Applications of Thermal IR Techniques
Bob Vincent, Chairman

Introduction: NASA's Interest in the Future Development of Thermal IR Techniques for Geological Applications
J. Taranik

Geological Research in the Thermal IR Region: A Brief Historical Overview
R. Vincent

Use of Broadband Thermal IR Scanners for Geological Remote Sensing
R. Williams

Compilation of Results from Users of the Daedelus Thermal IR Scanner
T. Ory

Multispectral Thermal IR Experiments in the Early 70's
R. Vincent

Recent Multispectral Thermal IR Experiments
A. Kahle

Mathematical Models for Thermal Scene Analysis
E. Link

Session II, Monday, February 11, 1980

Planetary Exploration Applications of Thermal Infrared Techniques
Hugh Kieffer, Chairman

Multispectral Thermal IR Surveys of Mars by the Viking Orbiters
H. Kieffer

Identification of Lunar Rock Types on the Basis of Spectral Infrared Measurements
A. Potter

Spatial Mapping of Spectral Emissivity and Thermal Inertia Variations on the Moon
W. Mendell

Session III, Tuesday, February 12, 1980

Remote Sensing Thermal Infrared Instrumentation: Past, Present, and Future
Alex Goetz, Chairman

The Heat Capacity Mapping Mission: System Characteristics and Data Products
J. Price

The 90 Element Pushbroom Scanner Field Test Instrument
T. Brown

Sensitivity, Resolution, and Atmospheric Considerations in the Design of an Aircraft Thermal Multispectral Scanner
A. Goetz

Design of an Aircraft Multispectral Thermal Infrared Scanner
F. Wright

Session IV, Tuesday, February 12, 1980

Discussion: Future Experimentation Required for the Development of Thermal Infrared Techniques for Geological Applications
Hugh Kieffer, Chairman

Session V, Wednesday, February 13, 1980

Discussion: Technology and Instrumentation Requirements for Future Experimentation in the Thermal IR
Bob Vincent, Chairman

Summary Remarks
R. Vincent
H. Kieffer

Participants

Thomas J. Brown
Honewell Electro-Optics Center
2 Forbes Road
Lexington, Massachusetts 02173

James E. Conel
Code: 183-501
Jet Propulsion Laboratory
4800 Oak Grove Drive
Pasadena, California 91109

Gerald Flanagan
Earth Resources Laboratory
National Space Transportation Laboratories
NSTL Station, Mississippi 39529

Alexander F. H. Goetz
Code: 183-501
Jet Propulsion Laboratory
4800 Oak Grove Drive
Pasadena, California 91109

Anne B. Kahle
Code: 183-501
Jet Propulsion Laboratory
4800 Oak Grove Drive
Pasadena, California 91109

Hugh H. Kieffer
U.S. Geological Survey
2255 North Gemini Drive
Flagstaff, Arizona 86001

Ronald J. Lyon
Department of Applied Earth Sciences
Stanford University
Stanford, California 94305

Wendell W. Mendell
Code: SN6
NASA/Johnson Space Center
Houston, Texas 77058

Stephen M. Nicolais
Superior Oil Company
P.O. Box 1521
Houston, Texas 77001

Thomas Ory
Daedalus Inc.
P.O. Box 1869
Ann Arbor, Michigan 48106

Andrew E. Potter
Code: SN3
NASA/Johnson Space Center
Houston, Texas 77058

John Price
Mail Code 913
Goddard Space Flight Center
Greenbelt, Maryland 20771

Richard R. Richard
Code: ED6
NASA/Johnson Space Center
Houston, Texas 77058

Floyd Sabins
Chevron Oil Field Research Company
P.O. Box 446
La Habra, California 90631

Mark Settle
Code: ERS-2
NASA Headquarters
Washington, D.C. 20546

James V. Taranik
Code: ERS-2
NASA Headquarters
Washington, D.C. 20546

Robert Vincent
Geospectra Corporation
320 N. Main Street, Suite 301
Ann Arbor, Michigan 48104

Michael A. Wiley
Atlantic Richfield Company
P.O. Box 2819 (Exp.)
Dallas, Texas 75221

Richard S. Williams, Jr.
EROS Headquarters
Mail Stop 730
U.S. Geological Survey
Reston, Virginia 22092

Ford Wright
Daedalus Inc.
P.O. Box 1869
Ann Arbor, Michigan 48106

Bibliography

A wide range of references to earlier studies was collected by individual workshop participants and contributed to this report. These references describe various aspects of the development of thermal infrared techniques, the analysis and interpretation of remotely sensed thermal infrared data, and the application of infrared techniques to Earth and planetary studies. The references have been compiled and sorted into the following general categories:

Instrumentation — sensor design; technological capabilities; data acquisition and processing procedures.

Physical Properties — laboratory measurements of the physical properties which govern the infrared characteristics of natural materials, specifically, spectral reflectance, thermal emissivity, thermal conductivity, and heat capacity.

Thermal Surveys/Observations — empirical studies involving the analysis of remotely sensed thermal infrared data for purposes of detecting areal variations in ground temperature; application of thermal infrared surveys to geologic mapping, volcano monitoring, soil moisture studies, etc.

Thermal Surveys/Theory — modeling studies of thermal radiation and energy flux; theoretical investigations which establish a physical basis for the interpretation of thermal surveys.

Thermal Inertia Surveys — theoretical and empirical studies related to the use of multitemporal thermal infrared surveys to detect areal variations in thermal inertia.

Emissivity Surveys — theoretical and empirical studies related to the use of multispectral thermal infrared surveys to detect areal variations in ground emissivity.

Atmospheric Studies — use of infrared techniques to investigate structure and composition of the Earth's atmosphere; analysis of absorption, emission, and scattering phenomena within the atmosphere which affect aerial and orbital remote sensing measurements at thermal infrared wavelengths.

Planetary Studies — use of thermal infrared techniques to investigate the surfaces and atmospheres of other planets, in particular the Moon, Mars, Mercury, Venus, and Saturn.

Instrumentation

Baker L. R. and Scott R. M. (1975) Electro-optical remote sensors with related optical sensors. In *Manual of Remote Sensing* (R. G. Reeves, ed.), p. 325-366. Am. Soc. Photogramm., Falls Church, Va.

Bender M. L., Callaway P. W., Chase S. C., Moore G. F., and Ruiz R. D. (1974) Infrared radiometer for the Pioneer 10 and 11 missions to Jupiter. *Appl. Opt.* **13**, 2623-2628.

Burns E. A. and Lyon R. J. P. (1963) Instrumentation for a mineralogical satellite. *Proc. Int. Astronaut. Cong., 14th* **2**, 237-250.

Chase S. C., Engel J. L., Eyerly H. W., Kieffer H. H., and Palluconi F. D. (1981) Design and performance of the thermal mapper. Submitted to *Appl. Opt.*

Chase S. C., Jr., Engel J. L., Eyerly H. W., Kieffer H. H., Palluconi F. D., and Schofield D. (1978) The Viking Infrared thermal mapper. *Appl. Opt.* **17**, 1243-1251.

Fisher D. F., England G. and Fisher D. S. (1965) *Airborne Infrared Scanning System M1A1*, Univ. of Mich Rpt. No. 6517-1-F, for the Terrestrial Science Laboratory, Air Force Cambridge Research Labs, Bedford Mass., 92p.

Hanel R., Schlachman B., Breihan E., Bywaters R., Chapman F., Rhodes M., Rodgers D., and Vanous D. (1972) Mariner 9 Michelson interferometer. *Appl. Opt.* **11**, 2625-2634.

Hunt G. R. and Logan L. M. (1970) An image selection device for use with a telescope. *Appl. Opt.* **9**, 2786-2787.

Hunt G. R. and Logan L. M. (1971) Convenient technique for calibration of radiometers used for low energy infrared targets. *Appl. Opt.* **10**, 2770.

Hunt G. R. and Vincent R. K. (1968) Modification to the Perkin-Elmer Reflectance Attachment for studying powders. *J. Sci. Instru.* **1**, 470-471.

Kieffer H. H., Neugebauer G., Munch G., Chase S. C., Jr., and Miner E. (1972) Infrared thermal mapping experiment: The Viking Mars orbiter. *Icarus* **16**, 47-56.

Lowe D. S. (1975) Imaging and nonimaging sensors. In *Manual of Remote Sensing* (R. G. Reeves, ed.), p. 367-399. Am. Soc. Photogramm., Falls Church, Va.

Lowe D. S. (1976) Nonphotographic optical sensors. In *Remote Sensing of Environment* (J. Lintz and D. S. Simonette, eds.), p. 155-193. Addison-Wesley, Reading, Mass.

Lyon R. J. P. and Marshall A. A. (1971) Operational calibration of an airborne infrared spectrometer over geologically significant terrains. *IEEE Trans. Geos. Electron.* **GE-9**, 131-138.

Miller C. D. and Roe C. L. (1967) *Tape Recording System for Use with the M1A1 Infrared Scanning System.* Univ. of Mich. Rpt. No. 8435-6-T, for the Terrestrial Sciences Laboratory, Air Force Cambridge Research Laboratories, Bedford, Mass., 31 p.

Morgan J. O. (1962) Infrared technology. In *Proc. First Symp. on Remote Sensing of Environ.*, p. 61-80. U. of Mich. Press, Ann Arbor.

Rehnberg J. D., Yoder J. R., and Hunt G. R. (1967) An earth based infrared Lunar mapper for thermal and compositional studies. *Appl. Opt.* **6**, 1111-1120.

Sabins F. F. (1973) Flight planning and navigation for thermal IR surveys. *Photogramm. Eng.* **39**, 49-58.

Sabins F. F. (1973) Recording and processing thermal IR imagery. *Photogramm. Eng.* **39**, 839-844.

Salisbury J. W. and Hunt G. R. (1969) Orbital infrared experiments. In *Advanced Space Experiments* v. 25, p. 263-278, Adv. Astronaut. Sci. Series, Am. Astronautical Soc.

Strong J. (1958) *Concepts of classical optics*. Freeman, San Francisco, 692p.

Wolfe W. L. (1965) *Handbook of Military Infrared Technology*. Office of Naval Research, Dept. of the Navy, Washington, D. C., 906p.

Physical Properties

Adler H. H. (1968) Infrared spectra of phosphate minerals: splitting and frequency shifts associated with substitution of PO_4 for AsO_4 in mimetite $Pb_5(AsO_4)_3Cl$). *Am. Mineral.* **53**, 1740-1744.

Adler H. H. and Kerr P. F. (1963) Infrared absorption frequency trends for anhydrous normal carbonates. *Amer. Mineral.* **48**, 124-137.

Aronson J. R. and Emslie A. G. (1973) Spectral reflectance and emittance of particulate materials, 2. Application and results. *Appl. Opt.* **12**, 2573-2584.

Aronson J. R., Emslie A. G., Allen R. V., and McLinden H. G. (1967) Studies of the middle and far-infrared spectra of mineral surfaces for application in remote compositional mapping of the moon and planets. *J. Geophys. Res.* **72**, 687-703.

Blevin W. R. and Brown W. J. (1961) Effects of particle separation on the reflectance of semi-infinite diffusers. *J. Opt. Soc. Am.* **51**, 129-134.

Coblentz W. W. (1905) *Investigations of infrared spectra. 1. Infrared absorption spectra. 2. Infrared emission spectra.* Carnegie Inst. Wash. Publ. No. 35.

Coblentz W. W. (1906) *Investigation of infrared spectra. 3. Infrared transmission spectra. 4. Infrared reflection spectra.* Carnegie Inst. Wash. Publ. No. 65.

Coblentz W. W. (1906) Radiometric investigations of infrared absorption and reflection spectra. *U.S. Nat. Bur. Stand. Bull.* **2**, 457-462.

Coblentz W. W. (1908) *Supplementary investigations of infrared spectra. 5. Infrared reflection spectra. 6. Infrared transmission spectra. 7. Infrared emission spectra.* Carnegie Inst. Wash. Publ. No. 97.

Conel J. E. (1965) *Infrared thermal emission from silicates.* JPL Tech. Memo. 33-243.

Conel J. E. (1969) Infrared emissivities of silicates: Experimental results and a cloudy atmosphere model of spectral emission from condensed particulate mediums. *J. Geophys. Res.* **74**, 1614-1634.

Coulson K. L. (1966) Effects of reflection properties of natural surfaces in aerial reconnaissance. *App. Opt.* **5**, 905-917.

Coulson K. L., Bouricius G. M., and Gray E. L. (1965) Optical reflection properties of natural surfaces. *J. Geophys. Res.* **70**, 4601-4611.

Duntley S. Q. (1942) The optical properties of diffusing materials. *J. Opt. Soc. Am.* **32**, 61-70.

Emslie A. G. and Aronson J. R. (1973) Spectral reflectance and emittance of particulate materials. 1: Theory. *Appl. Opt.* **12**, 2563-2572.

Goetz A. F. H. (1967) *Infrared 8-13 μm spectroscopy of the moon and some cold silicate powders.* Ph.D. Thesis, California Inst. Tech.

Griggs M. (1968) Emissivities of natural surfaces in the 8- to 14- micron spectral region. *J. Geophys. Res.* **73**, 7545-7551.

Henry R. L. (1948) The transmission of powder films in the infrared. *J. Opt. Soc. Am.* **38**, 775-789.

Horai K. (1971) Thermal conductivity of rock-forming minerals. *J. Geophys. Res.* **76**, 1278-1308.

Horai K. and Nur A. (1970) Relationship among terrestrial heat flow, thermal conductivity, and geothermal gradient. *J. Geophys. Res.* **75**, 1985-1991.

Hovis W. A., Jr. (1965) Infrared reflectivity of iron oxide minerals. *Icarus* **4**, 425-430.

Hovis W. A., Jr. (1966) Infrared spectral reflectance of some common minerals. *Appl. Opt.* **5**, 245-248.

Hovis W. A., Jr. and Callahan W. R. (1966) Infrared reflectance spectra of igneous rocks, tuffs, and red sandstone from 0.5 to 22 μ. *J. Opt. Soc. Am.* **56**, 639-643.

Hunt G. R. (1976) Infrared spectral behavior of fine particulate solids. *J. Phys. Chem.* **80**, 1195-1198.

Hunt G. R. and Logan L. M. (1972) Variation of single particle mid-infrared emission spectrum with particle size. *Appl. Opt.* **11**, 142-147.

Hunt G. R. and Salisbury J. W. (1974) *Mid-infrared spectral behavior of igneous rocks.* AFCRL-TR-74-0625 Environmental Research Paper 496, 142p.

Hunt G. R. and Salisbury J. W. (1975) *Mid-infrared spectral behavior of sedimentary rocks*. AFCRL-TR-75-0356 Environmental Research Paper 520, 49p.

Hunt G. R. and Salisbury J. W. (1976) *Mid-infrared spectral behavior of metamorphic rocks*. AFCRL-TR-76-003 Environmental Research Paper 543, 67p.

Hunt G. R. and Vincent R. K. (1968) The behavior of spectral features in the infrared emission from particulate surfaces of various grain sizes. *J. Geophys. Res.* **73**, 6039-6046.

Hunt J. M., Wisherd P., and Bonham L. C. (1950) Infrared absorption spectra of minerals and other inorganic compounds. *Anal. Chem.* **22**, 1478-1497.

Idso S. B., Jackson R. D., and Reginato R. J. (1976) Determining emittances for use in infrared thermometry: a simple technique for expanding the utility of existing methods. *J. Appl. Meteorol.* **15**, 16-20.

Knacke R. F. and Thomson R. K. (1973) Infrared extinction cross sections of silicate grains, *Publ. Astron. Soc. Pac.* **85**, 341-347.

Krinov E. L. (1953) *Spectral reflectance properties of natural formations*. NRC Tech. Transl. TT-439, (G. Belkov, Transl.), Aero Methods Laboratory, Academy of Science, USSR, 1947.

Launer P. J. (1952) Regularities in the infrared absorption spectra of silicate minerals. *Am. Mineral.* **37**, 764-784.

Logan L. M. and Hunt G. R. (1970) Emission spectra of particulate silicates under simulated lunar conditions. *J. Geophys. Res.* **75**, 6539-6547.

Logan L. M., Hunt G. R., Balsamo S. R., and Salisbury J. W. (1972) Mid-infrared emission spectrum of Apollo 14 and 15 soils and remote compositional mapping of the Moon. *Geochim. Cosmochim. Acta* **3**, 3069-3076.

Logan L. M., Hunt G. R., and Salisbury J. W. (1972) Infrared emission spectra of Apollo 15 soils. In *The Apollo 15 Soil Samples* (J. W. Chamberlain and C. Watkins, eds.), p. 475-476. Lunar Science Institute, Houston.

Logan L. M., Hunt G. R., Salisbury J. W., and Balsamo S. R. (1972) Mid-infrared emission spectrum of Apollo 14 soil. Significance for compositional remote sensing. In *Lunar Science III* (C. Watkins, ed.), p. 490-492. Lunar Science Institute, Houston.

Logan L. M., Hunt G. R., Salisbury J. W., and Balsamo S. R. (1973) Compositional implications of Christiansen frequency maximums for remote sensing applications. *J. Geophys. Res.* **78**, 4983-5003.

Lyon R. J. P. (1963) *Evaluation of infrared spectrophotometry for compositional analysis of lunar and planetary soils*. NASA Tech. Note TN D-1971, 118p.

Lyon R. J. P. (1964) *Evaluation of infrared spectrophotometry for compositional analysis of lunar and planetary soils. Part II. Rough and powdered surfaces*. NASA Contractor Report CR-100, 172p.

Lyon R. J. P. (1964) Infrared analysis of soil minerals. In *Soil Clay Mineralogy*, p. 170-199, University of North Carolina Press.

Lyon R. J. P. and Burns E. A. (1963) Analysis of rocks and minerals by reflected infrared radiation. *Econ Geol.* **58**, 274-284.

Lyon R. J. P. Tuddenham W. M., and Thompson C. S. (1959) Quantitative mineralogy in 30 minutes. *Econ. Geol.* **54**, 1047-1055.

Pfund A. H. (1945) The identification of gems. *J. Opt. Soc. Am.* **35**, 611-614.

Phinney D. E. and Arp G. K. (1975) *The measurement and interpretation of thermal infrared emissivities*. Tech. Memo. by Life Sciences Application Division of NASA, Feb. 1975.

Robie R. A. and Waldbaum D. R. (1968) *Thermodynamic properties of minerals and related substances at 298.15°K (25.0°C) and one atmosphere (1.0113 bars) pressure and at higher temperatures*. U. S. Geol. Survey Bull. No. 1259, 256p.

Salisbury J. W., Hunt G. R., and Logan L. M. (1974) Infrared spectra of Apollo 16 fines. *Geochim. Cosmochim. Acta* **3**, 3191-3196.

Spitzer W. G. and Kleinman D. A. (1961) Infrared lattice bands of quartz. *Phys. Rev.* **121**, 1324-1335.

Suyawara A. and Yoshizawa Y. (1961) An investigation on the thermal conductivity of porous materials and its application to porous rock. *Aust. Jour. Phys.* **14**, 469-480.

Taylor S. E. (1979) Measured emissivity of soils in the Southwest United States. *Remote Sensing of Environ.* **8**, 359-364.

Van Tassel R. A. and Simon I. (1964) Thermal emission characteristics of mineral dusts. In *The Lunar Surface Layer: Materials and Characteristics* (J. W. Salisbury and P. E. Glaser, eds.), p. 445-468. Academic Press, New York.

Vincent R. K. (1972) Emission polarization study on quartz and clacite. *Appl. Opt.* **11**, 1942-1945.

Vincent R. K. and Hunt G. R. (1968) Infrared reflectance from mat surfaces. *Appl. Opt.* **1**, 53-59.

Vincent R. K., Rowan L. C., Gillespie R. E., and Knapp C. (1975) Thermal-infrared spectra and chemical analyses of twenty-six igneous rock samples. *Remote Sensing of Environ.* **4**, 199-209.

Vincent R. K. and Thomson F. (1972) Spectral compositional imaging of silicate rocks. *J. Geophys. Res.* **77**, 2465-2471.

Watson R. D. (1970) Surface-coating effects in remote sensing measurements. *J. Geophys. Res.* **75**, 480-484.

Weber F. P. (1965) *Exploration of changes in reflected and emitted radiation properties for early remote detection of tree vigor decline.* Master of Science Thesis, Univ. of Mich., 1965.

Wechsler A. E. and Glaser P. E. (1965) Pressure effects on postulated lunar materials. *Icarus* **4**, 335-352.

Thermal Surveys/Observations

Abdel-Hady M. and Matalucci R. V. (1970) *Surface and Subsurface Exploration by Infrared Survey.* Nat. Res. Counc., Highw. Res. Board Spec. Tech. Rep. No. 270,Washington, D. C.

Bell E. E. and Eisner I. C. (1956) Infrared radiation from the White Sands at White Sands National Monument, New Mexico. *J. Opt. Soc. Am.* **46**, 303-304.

Blanchard M. B., Greeley R., and Goettelman R. (1974) Use of visible, near-infrared, and thermal infrared remote sensing to study soil moisture. In *Proceedings of the Ninth Lunar and Planetary Science Conference*, p. 693-700. Pergamon, New York.

Brazel A. and Outcalt S. I. (1973) The observation and simulation of diurnal surface thermal contrast in an Alaskan alpine pass. *Arch. Meteorol. Geoph. Biokl.* **21 (Ser. B)**, 157-174.

Budyko M. I. (1963) *Atlas of the Heat Balance of the Earth*, p. 69. Gidrometeorizdat, Moscow.

Campbell R. W., Jr. (1970) *Detailed Ground Study of 8-13 Micron Infrared Imagery, Corrizo Plains, California.* Stanford Univ. Rep., January 1970, 72p.

Cannon P. J. (1973) The application of radar and infrared imagery to quantitative geomorphic investigations. In *Remote Sensing of Earth Resources, Proceedings of the 2nd Conference on Earth Resources Observation and Information Analysis* (F. Shahrokhi, ed.), p. 503-519. Univ. of Tenn., Tullahoma.

Cassinis R., Lechi G. M., and Tonelli A. M. (1974) Contribution of space platforms to ground and airborne remote-sensing programme over Italian active volcanoes. In *European Earth-Resources Satellite Experiments*, p. 185-197. European Space Research Organization, Neuilly, France.

Cassinis R., Marino C. M., and Tonelli A. M. (1970) Ground and airborne thermal imagery on Italian volcanic areas. In *Proceedings of the U. N. Symposium on the Development and Utilitization of Geothermal Resources, Pisa; Geothermics*, Special Issue 2.

Cassinis R., Marino C. M., and Tonelli A. M. (1971) Evaluation of thermal I. R. imagery on Italian volcanic areas; ground and airborne surveys. In *Proc. Seventh Int. Symp. on Remote Sensing of Environ.*, p. 81-98. U. of Mich. Press, Ann Arbor.

Cassinis R., Marino C. M., and Tonelli A. M. (1974) Remote sensing techniques applied to the study of Italian volcanic areas; the results of the repetition of the airborne I. R. survey compared to the previous data. In *Proc. Ninth Int. Symp. on Remote Sensing of Environ.*, p. 1989-2004. U. of Mich. Press, Ann Arbor.

Chagnon J. Y. and Tanguay M. G. (1972) Thermal infrared imagery at the St-Jean Vianney Landslide. *Proc. 1st Can. Symp. on Remote Sensing*, p. 387-402, Ottawa.

Christiansen R. L. (1968) *A Distinction between Bedrock and Unconsolidated Deposits on 3-5 μm Infrared Imagery of the Yellowstone Rhyolite Plateau.* U. S. Geol. Surv. Tech. Lett., NASA-104, 7 p.

Colwell R. N. (1968) Remote sensing of natural resources. *Sci. Am.* **218**, 54-69.

Cykowski C. B., Frecska S. A., Gillespie R. E., Gliozzi J., Kirch D. L., Manion D. L., Muhm J. R., Neri J., Silver A. N., Stadjuhar S. A., Weissman J. R., and Worman K. E. (1970) *BONANZA, Application of remote sensor data to geologic and economic analysis of the Bonanza Test Site Colorado.* First year summary report prepared for Colorado School of Mines, Golden, Colorado under Letter Contract 9-W-06040, Martin Marietta doc. # MCR-70-80, Denver, CO.

Del Bono G. L., Williams R. S., Jr., and Cronin J. F. (1971) Photogeologic and thermal infrared imagery geologic surveys in Italy in 1966. *Italy Serv. Geol. Boll.* **91**, 3-44.

Dillman R. and Vincent R. K. (1974) Unsupervised mapping of geologic features and soils in California. In *Proc. Ninth Int. Symp. on Remote Sensing of Environ.*, p. 2012-2025. U. of Mich. Press, Ann Arbor.

Elder J. W. (1965) Physical processes in geothermal areas. In *Terrestrial Heat Flow* (W. H. K. Lee, ed.), p. 211-239. Geophys. Monogr. #8, NAS-National Research Council Publication 1288. Am. Geophys. Union.

Fagerlund E., Kleman B., Sellin L., and Svensson H. (1970) Physical studies of nature by thermal mapping. *Earth-Sci. Rev.* **6**, 169-180.

Fischer W. A., Friedman J. D., and Sousa T. M. (1965) *Preliminary Results of Aerial Infrared Surveys at Pisgah Crater, California.* U S. Geol. Surv. Tech. Lett. NASA-5. NASA-CR-62908. 16p.

Fischer W. A., Moxham R. M., Polcyn F., and Landis G. H. (1964) Infrared surveys of Hawaiian volcanoes. *Science* **146**, 733-742.

Friedman J. D. (1970) The airborne infrared scanner as a geophysical research tool. *Opt. Spectra* **4(6)**, 35-44.

Friedman J. D. and Williams R. S. (1968) Infrared sensing of active geologic processes. In *Proc. Fifth Int. Symp. on Remote Sensing of Environ.*, p. 787-815. U. of Mich. Press, Ann Arbor.

Friedman J. D. and Williams R. S., Jr. (1970) Changing patterns of thermal emission from Surtsey, Iceland, between 1966 and 1969. In *Geological Survey Research, 1970*, p. D116-D124. U. S. Geol. Surv. Prof. Pap. 700D.

Friedman J. D. and Williams R. S., Jr. (1970) Comparison of 1968 and 1966 infrared imagery of Surtsey. In *Surtsey Research Progress Report*, v. 5, p. 88-92. The Surtsey Research Society, Reykjavik, Iceland.

Friedman J. D., Williams R. S., Jr., Palmason G., and Miller C. D. (1969) Infrared surveys in Iceland in 1966. In *Geological Survey Research, 1969*, p. C89-C106. U. S. Geol. Surv. Prof. Pap. 650-C.

Friedman J. D., Williams R. S., Jr., and Thorarinsson S. (1970) Thermal emission from Hekla Volcano, Iceland, before eruption of 5 May 1970 (abs.). *Geol. Soc. Am. Abstracts with Programs, 1970 Ann. Mtgs., Milwaukee, Wisc.*, p. 555.

Friedman J. D., Williams R. S., Jr., Thorarinsson S., and Palmason G. (1972) Infrared emission from Kverkfjoell subglacial volcanic and geothermal area, Iceland. *Joekull* **22**, 27-43.

Gawarecki S. J. (1969) Infrared survey of the Pisgah Crater area, San Bernardino County, California: a geologic interpretation. In *Earth Resources Aircraft Program Status Review*, vol. 1, 38 p. NASA-TMX-62564. NASA, Manned Spacecraft Center.

Geiger R. (1965) *The Climate Near the Ground.* Harvard University Press, Cambridge.

Gomez V. R., Friedman J. D., Gawarecki S. J., and Banwell C. J. (1970) Photogeologic and thermal infrared reconnaissance surveys of the Los Negritos-Ixtlan de los Hervores geothermal area, Michoacan, Mexico. In *Proceedings of the U. N. Symp. on Development and Utilization of Geothermal Resources, Pisa, Italy; Geothermics*, Special Issue 2, p. 381-398.

Greene G. W., Moxham R. M., and Harvey A. H. (1969) Aerial infrared surveys and borehole temperature measurements of coal mine fires in Pennsylvania. In *Proc. Sixth Int. Symp. on Remote Sensing of Environ.*, p. 517-525, U. of Mich. Press, Ann Arbor.

Harris D. E. and Woodbridge C. L. (1964) Terrain mapping by use of infrared radiation. *Photogramm. Eng.* **30**, 134-139.

Hase H. (1971) Surface heat flow studies for remote sensing of geothermal resources. In *Proc. Seventh Int. Symp. on Remote Sensing of Environ.*, p. 237-245, U. of Mich. Press, Ann Arbor.

Hochstein M. P. and Dickinson D. J. (1970) Infrared remote sensing of thermal ground in the Taupo region, New Zealand. In *Proceedings of the U.N. Symp. on Development and Utilization of Geothermal Resources, Pisa, Italy; Geothermics*, Special Issue 2, p. 420-423.

Holmes Q. A., Nuesch D. R., and Vincent R. K. (1980) Optimum thermal infrared bands for mapping general rock type and temperature from space. *Remote Sensing Environ.* **9**, 247-263.

Hovis W. A., Jr. (1966) Optimum wavelength intervals for surface temperature radiometry. *Appl. Opt.* **5**, 815-818.

Hunt G. R. (1966) Rapid remote sensing by a spectrum matching technique, 1. Description and discussion of the method. *J. Geophys. Res.* **71**, 2919-2930.

Hunt G. R. (1967) Enhancement of fine detail in the presence of large radiance differences. *Appl. Opt.* **6**, 505-509.

Hunt G. R., Salisbury J. W., and Reed J. W. (1967) Rapid remote sensing by spectrum matching technique. 2. Application in the laboratory and in lunar observations. *J. Geophys. Res.* **72**, 705-719.

Idso S. B., Jackson R. D., and Reginato R. J. (1975) Estimating evaporation: a technique adaptable to remote sensing. *Science* **189**, 991-992.

Idso S. B., Jackson R. D., and Reginato R. J. (1977) Remote-sensing of crop yields. *Science* **196**, 19-25.

Idso S. B., Schmugge T. J., Jackson R. D., and Reginato R. J. (1975) The utility of surface temperature measurements for the remote sensing of surface soil water status. *J. Geophys. Res.* **80**, 3044-3049.

Jackson R. D. and Idso S. B. (1975) Surface albedo and desertification. *Science* **189**, 1012-1013.

Jackson R. D., Reginato R. J. and Idso S. B. (1976) Timing of ground truth acquisition during remote assessment of soil-water content. *Remote Sensing of Environ.* **4**, 249-255.

Kappelmeyer O. and Haenel R. (1974) *Geothermics with Special Reference to Application*. Geoexploration Monographs Series No. 4. Gebruder Borntraeger, Berlin, Germany. 251 p.

Keefer W. R. (1968) *Evaluation of Radar and Infrared Imagery of Sedimentary Rock Terrain, South-Central Yellowstone National Park*. U. S. Geol. Surv. Tech. Lett., NASA-106, 12 p.

Kern C. D. (1963) Desert soil temperatures and infrared radiation received by TIROS III. *J. Atmos. Sci.* **20**, 175-176.

Kern C. D. (1965) *Evaluation of Infrared Emission of Clouds and Ground as Measured by Weather Satellites*. Ph.D. Thesis, Univ. of Washington. 167p.

Knuth W. M. and Fisher W. (1968) Detection and delineation of subsurface coal fires by aerial infrared scanning. *Abstracts for 1967 Meetings* Geol. Soc. Am. Spec. Pap. 115, p. 67-68.

Lange I. M. and Avent J. C. (1973) Ground-based thermal infrared surveys as an aid in predicting volcanic eruptions in the Cascade Range. *Science* **182**, 279-281.

Lattman L. H. (1963) Geological interpretation of airborne infrared imagery. *Photogramm. Eng.* **29**, 83-87.

Lechi G. M., Marino C. M., and Tonelli A. M. (1972) Geological applications of remote sensing surveys in Italy with special reference to their utilization on the volcanic areas. In *Geological Congress Proceedings* **24**, 25-32.

Lechi G. M., Marino C. M., and Tonelli A. M. (1974) Analog techniques of data enhancement applied in the study of geologic and geothermal features of test sites in the Italian region (central Alps and volcanic areas) illustrated by the images from ERTS-I and other remote sensing platforms. In *Proceedings of Symposium on Remote Sensing and Photo Interpretation*, p. 583-596. Can. Inst. Surv., Ottawa.

Lee K. (1969) Infrared exploration for shoreline springs at Mono Lake, California, test site. In *Proc. Sixth Int. Symp. on Remote Sensing of Environ.*, p. 1075-1100. U. of Mich. Press, Ann Arbor.

Lee K. (1976) Ground investigations in support of remote sensing. In *Manual of Remote Sensing*, p. 804-856, (R. G. Reeves, ed.) Am. Soc. Photogramm., Falls Church, Va.

LeSchack L. A., Del Grande N. K., Outcalt S. I., Lewis J., and Tenner C. (1975) *Correlation of Dual-Channel Airborne IR Data with Soil Moisture Measurements, Final Report*. PB-251190/5, NOAA-76021302. Development and Resources Transportation Co., Silver Spring, Maryland. 71p.

Lo Giudice E., Marino C. M., and Tonelli A. M. (1974) Lo studio delle aree vulcaniche con la metodologia remote sensing, rilievi all'infrarosso termico. *Boll. Geofis. Teor. Appl.* **16**, n. 64, 299-321.

Lyon R. J. P. (1974) *Field Mapping Determinations: Ground Support for Airborne Thermal Surveys with Application to Search for Geothermal Resources.* Stanford Remote Sensing Lab. Tech. Rep. 74-8, 50p.

Lyon R. J. P. and Marsh S. E. (1976) *Field Mapping for Heat Capacity Mapping Determinations.* Stanford Remote Sensing Lab. Tech. Rep. 76-3. 94p.

McLerran J. H. and Morgan J. O. (1965) Thermal mapping of Yellowstone National Park. In *Proc. Third Int. Symp. on Remote Sensing of Environ.*, p. 517-530. U. of Mich. Press, Ann Arbor.

Marino C. M. (1975) Applicazione delle teleosservazioni I. R. termico e riprese multispettrali nel campo delle risorse idriche in Italia (Applications of remote sensing / thermal IR and multispectral images / in the field of water resources in Italy). In *Space Exploration: Conversion and Exploration: Conversion and Exploitation of Solar Energy; International Conference on Space, 15th, Proceedings*, p. 91,93-104. Rassegna Internazionale Elettronica Nucleare ed Aerospaziale, Rome.

Marsh S. E. (1975) *The Feasibility of Satellite Thermal Infrared Remote Sensing for Geothermal Resources.* Stanford Remote Sensing Lab. Tech. Rep. 75-12, M. S. Dissertation. Stanford, California. 71p.

Marsh S. E., Lyon R. J. P., and Honey F. H. (1975) Evaluation of NOAA satellite data for geothermal reconnissance studies. In *Proc. Second U. N. Symp. on the Development and Use of Geothermal Resources*, v. 2, p. 1135-1141. Prepared by Lawrence Berkeley Laboratory, University of California for ERDA, NSF, and USGS.

Miller L. D. (1965) Location of anomalously hot earth with infrared imagery in Yellowstone National Park. In *Proc. 4th Int. Symp. Remote Sensing of Environ.*, p. 751-769. U. of Mich. Press, Ann Arbor.

Miller S. H. and Watson K. (1979) The use of thermal data to extend geologic reconnaissance from satellites: Summaries. In *Proc. Thirteenth Int. Symp. on Remote Sensing of Environ.*, p. 108-109. U. of Mich. Press, Ann Arbor.

Moxham R. M. (1967) Changes in surface temperature at Taal Volcano, Philippines 1965-1966. *Bull. Volcanol.* **31**, 215-234.

Moxham R. M. (1969) Aerial infrared surveys at The Geysers geothermal steam field, California. In *Geological Survey Research* 1969, p. C106-C122. U.S. Geol. Surv. Prof. Pap. 650-C.

Moxham R. M. (1970) Thermal features at volcanoes in the Cascade Range, as observed by aerial infrared surveys. *Bull. Volcanol.* **34**, 77-106.

Moxham R. M. (1971) Thermal surveillance of volcanoes. In *The Surveillance and Prediction of Volcanic Activity*, p. 103-124, UNESCO, Paris.

Nordberg W., Bandeen W. R., Conrath B. J., Kunde V., and Persano I. (1962) Preliminary results of radiation measurements from the TIROS III meteorological satellite. *J. Atmos. Sci.* **19**, 20-30.

Nordberg W. and Samuelson R. E. (1965) Terrestrial features observed by the high resolution infrared radiometer. In *Observations from the Nimbus I Meteorological Satellite*, p. 37-46. NASA-SP-89. NASA, Washington.

Offield T. W. (1975) Thermal-infrared images as a basis for structure mapping, Front Range and adjacent plains in Colorado. *Geol. Soc. Am. Bull.* **86**, 495-502.

Offield T. W. (1976) Remote sensing in uranium exploration. *Proc. Symp. Exploration for Uranium Ore Deposits, Vienna*, p. 731-744. (Jointly organized by IAEA and NEA.)

Offield T. W., Rowan L. C., and Watson R. D. (1970) Linear geologic structure and mafic rock discrimination as determined from infrared data. In *Earth Resources Program Review, 3rd*, vol. 1-3, p. 11-1—11-12. NASA Manned Spacecraft Center, Houston.

Outcalt S. I. (1972) A reconnaissance experiment in mapping and modeling the effect of land use on urban thermal regimes. *J. Appl. Meteorol.* **11**, 1369-1373.

Palmeson G., Friedman J. D., Williams R. S., Jr., Jonsson J., and Saemundsson K. (1970) Aerial infrared surveys of Reykjanes and Torfajokull thermal areas, Iceland, with a section on the cost of exploration surveys. In *U. N. Symposium on Development and Utilization of Geothermal Resources, Pisa, Italy; Geothermics*, Special Issue 2, p. 399-412.

Peel R. F. (1974) Insolation weathering: some measurements of diurnal temperature changes in exposed rocks in the Tibesti region, central Sahara. *Zeit. Geomorph.* **21**, 19-28.

Perry W. J. and Crick I. H. (1976) Aerial thermal infrared survey, Rabaul area, Papua, New Guinea, 1973. In *Volcanism in Australasia*, p. 211-219. Elsevier, New York.

Pierce K. L. (1968) *Evaluation of Infrared Imagery Applications to Studies of Surficial Geology — Yellowstone Park*. U. S. Geol. Sur. Tech. Lett. NASA-93, 35 p.

Pinter P. J., Jr., Stanghellini M. E., Reginato R. J., Idso S. B., Jenkins A. D., and Jackson R. D. (1979) Remote detection of biological stresses in plants with infrared thermometry. *Science* **205**, 585-587.

Pohn H. A., Offield T. W., and Watson K. (1972) Geologic material discrimination from Nimbus satellite data. In *U. S. Geological Survey Programs, Annual Earth Resources Program Review No. 4*, v. 3, p. (59)1-4.

Poley J. Ph. and Steveninck J. V. (1970) Delineation of shallow salt domes and surface faults by temperature measurements at a depth of approximately 2 metres. *Geoph. Prosp.* **18 Suppl.**, 666-700.

Quiel F. (1974) *Some Limitations in the Interpretation of Thermal IR Imagery in Geology*. LARS Information Note O 62874, Purdue University.

Rosema A., Bijleveld J. H., Reiniger P., Tassone G., Blyth K., and Gurney R. J. (1978) "TELL-US" A combined surface temperature, soil moisture and evaporation mapping approach. In *Proc. Twelfth Int. Symp. on Remote Sensing of Environ.*, p. 2267-2276. U. of Mich. Press, Ann Arbor.

Rowan L. C., Offield T. W., Watson K., Cannon P. J., and Watson R. D. (1970) Thermal infrared investigations, Arbuckle Mountains, Oklahoma. *Geol. Soc. Am. Bull.* **81**, 3549-3562.

Rowan L. C., Offield T. W., Watson K., Watson R. D., and Cannon P. J. (1969) Thermal infrared investigations, Mill Creek Area, Oklahoma. In *NASA Second Annual Earth Resources Aircraft Program Status Review*, v. 1, 25p. NASA-TM-X-66913. Houston, Texas.

Sabins F. F. (1967) Infrared imagery and geologic aspects. *Photogramm. Eng.* **29**, 83-87.

Sabins F. F. (1969) Thermal infrared imagery and its application to structural mapping in southern California. *Geol. Soc. Am. Bull.* **80**, 397-404.

Sabins F. F. (1978) Thermal infrared imagery. In *Remote Sensing—Principles and Interpretation*, p. 119-175. Freeman, San Francisco.

Schneider S. R., McGinnis D. F., Jr., and Pritchard J. A. (1979) Use of satellite infrared data for geomorphology studies. *Remote Sensing of Environ.* **8**, 313-330.

Sellin L. and Svensson H. (1970) Airborne thermography. *Geoforum* **2**, 49-60.

Simonett D. S. (1968) Land evaluation studies with remote sensors in the infrared and radar regions. In *Land Evaluation* (G. A. Stewart, ed.), p. 349-366, CSIRO Symp.

Smedes H. W. (1968) *Geological Evaluation of Infrared Imagery, Eastern Part of Yellowstone National Park, Wyoming and Montana*. U. S. Geol. Surv. Tech. Lett., NASA-83, 46 p.

Staff of Spectral Africa (1977) Better mapping through remote sensing. *Coal, Gold, and Base Minerals South Africa* **25(9)**.

Staff of Spectral Africa (1978) Some practical applications of thermal infrared linescanning. *Mining Magazine*, 398-413.

Stingelin R. W. (1968) An application of infrared remote sensing to ecological studies: Bear Meadows Bog, Pennsylvania. In *Proc. Fifth Int. Symp. on Remote Sensing of Environ.*, p. 435-440. U. of Mich. Press, Ann Arbor.

Stingelin R. W. (1969) Operational airborne thermal imaging surveys. *Geophysics* **34**, 760-771.

Strangway D. W. and Holmer R. C. (1966) The search for ore deposits using thermal radiation. *Geophysics* **31**, 229-242.

Thomas J., Pedeux J. P., and Arnaud C. (1975) Thermal infrared technique applied to modern investigation. *Geophys. Prospect.* **23**, 513-525.

Tonelli A. M. (1975) Contribution of ERTS-1 and Skylab missions to regional studies in Italy. *Proc. Br. Interplanetary Soc. J.* **28**, 647-652.

Tonelli A. M., Carli L., Ferretti O., and Nicolli C. (1974) *Applicazione del "Remote Sensing" in alcune zone agricole del Trentino-Alto Adige*. Economia Trentina, N. I., Trento, Italy.

Valentine K. W. G., Lord T. M., Watt W., and Bedwany A. L. (1971) Soil mapping accuracy from black and white, color, and infrared aerial photography. *Can. J. Soil Sci.* **51**, 461-469.

Vickers R. S. and Lyon R. J. P. (1967) Infrared sensing from spacecraft: a geological interpretation. *Thermophys. Spacecraft and Planet. Bodies* **20**, 585-607.

Vincent R. K. (1975) The potential role of thermal infrared multispectral scanners in geological remote sensing. *Proc. IEEE* **64**, 137-147.

Vinogradov B. V., Grigoryev A. A., Lipatov V. B., and Chernenko A. P. (1972) Thermal structure of the sand desert from the data of IR aerophotography. In *Proc. Eighth Int. Symp. on Remote Sensing of Environ.*, p. 729-737. U. of Mich. Press, Ann Arbor.

Wagner T., Vincent R. K., Drake B., Mitchell R., and Jackson P. (1972) *Tunnel-site Selection by Remote Sensing Techniques*. Univ. Mich. Tech. Rep. 10018-13-F, AD-748663. 101p.

Waldrop H. A. (1969) *Detection of Thick Surficial Deposits on 8-14μm Infrared Imagery of the Madison Plateau, Yellowstone National Park*. U. S. Geol. Surv. Interagency Rep., NASA-166, 8p.

Wallace R. E. and Moxham R. M. (1967) Use of infrared imagery in study of the San Andreas fault system, California. In *Geological Survey Research, 1967*, p. D147-D156. U. S. Geol. Surv. Prof. Pap. 575-D.

Warwick D., Hartopp P. G., and Viljoen R. P. (1979) Application of the thermal infrared linescanning technique to engineering geological mapping in South Africa. *J. Eng. Geol.* **12**, 159-179.

Watson K. (1971) Geophysical aspects of remote sensing. In *Int. Workshop on Earth Resources Survey Systems, VII*, p. 408-428. NASA-TM-X-68912. NASA, Washington.

Watson K. (1974) Geothermal reconnaissance from quantitative analysis of thermal infrared images. In *Proc. Ninth Int. Symp. Remote Sensing of Environ.*, p. 1919-1932. U. of Mich. Press, Ann Arbor.

Watson K. (1975) Geologic applications of thermal infrared images. *Proc. IEEE* **63**, 128-137.

West T. R. (1972) Engineering soils mapping in Indiana by computer from remote sensing data. *Proc. Indiana Acad. Sci.* **81**, 210-216.

White D. E., Fournier R. O., Muffler L. J. P., and Truesdale L. H. (1968) *Geothermal Studies of Yellowstone National Park (Test Site 11) Wyoming*. U. S. Geol. Surv. Tech. Lett. NASA-109, 11p.

White D. E. and Miller L. D. (1969) Geothermal infrared anomalies of low intensity, Yellowstone National Park. In *Earth Resources Aircraft Program Status Review*, v.1, p. 16-1—16-4. NASA-TM-X-62564. NASA, Manned Spacecraft Center.

Williams R., Jr. (1972) Terrestrial remote sensing, applications of thermal infrared scanners to the geological sciences. In *ISA Transducer Compendium*, pt. 3, p. 219-236. Instrument Society of America, Pittsburgh.

Williams R. S., Jr. (1972) Thermography. *Photogramm. Eng.* **38**, 881-883.

Williams R. S., Jr. and Fernandopulle D. (1972) Geological analysis of aerial thermography of the Canary Islands, Spain. In *Proc. Eighth Int. Symp. on Remote Sensing of Environ.*, p. 1159-1194. U. of Mich. Press, Ann Arbor.

Williams R. S., Jr. and Ory T. R. (1967) Infrared imagery mosaics for geological investigations. *Photogramm. Eng.* **33**, 1377-1380.

Wolfe E. W. (1971) Thermal IR for geology. *Photogramm. Eng.* **37**, 43-52.

Thermal Surveys/Theory

Bhumralkar C. M. (1974) *Numerical Experiments on the Computation of Ground Surface Temperature in an Atmospheric Circulation Model*. R-1511-ARPA, AD-783922. Rand Corporation, Santa Monica, California.

Budyko M. I. (1956) *The Heat Balance of the Earth*. (English Trans.: Stepanova, N. A., 1958, Office of Technical Services, U.S. Dept. of Commerce, Washington, D. C.) Leningrad.

Carslaw H. S. and Jaeger J. E. (1959) *Conduction of Heat in Solids*. Oxford at the Clarendon Press, Sec. ed., 510p.

Carson J. E. and Moses H. (1963) The annual and diurnal heat-exchange cycles in upper layers of soil. *J. Appl. Meteorol.* **2**, 397-406.

Chandrasekhar S. (1960) *Radiative Transfer*. Dover, New York. 393p.

Crank J. and Nicholson P. (1947) A practical method for numerical evaluation of solutions of partial differential equations of the heat-conduction type. *Proc. Can. Phil. Soc.* **43**, 50-67.

Deardorff J. W. (1978) Efficient prediction of ground surface temperature and moisture, with inclusion of a layer of vegetation. *J. Geophys. Res.* **83**, 1889-1903.

Ellis J. S., Haar T. H. vonder, Levitus S., and Oort A. H. (1978) The annual variation in the global heat balance of the Earth. *J. Geophys. Res.* **83**, 1958-1962.

Hunt G. R. (1980) Electromagnetic radiation: The communication link in remote sensing. In *Remote Sensing in Geology* (B. S. Siegel and A. R. Gillespie, eds.), p. 5-45. Wiley, New York.

Irvine W. M. (1965) Light scattering by spherical particles: radiation pressure, asymmetry factor on extinction cross section. *J. Opt. Soc. Am.* **55**, 16-21.

Jaeger J. C. (1953) Pulsed surface heating of semi-infinite solid. *Q. J. Appl. Math.* **11**, 132-137.

Jaeger J. C. and Johnson C. H. (1953) Note on diurnal temperature variation. *Geofis. Pura Appl.* **24**, 104-106.

Janza F. J. (1975) Interaction mechanisms. In *Manual of Remote Sensing*, (R. G. Reeves, ed.) ch. 4, p. 75-179. Am. Soc. Photogramm., Falls Church, Va.

Kahle A. B. (1977) A simple thermal model of the earth's surface for geologic mapping by remote sensing. *J. Geophys. Res.* **82**, 1673-1680.

Kimball B. A., Jackson R. D., Nakayama F. S., Idso S. B., and Reginato R. J. (1976) Soil-heat flux determination: temperature gradient method with computed thermal conductivities. *Soil Sci. Soc. Am. J.* **40**, 25.

Kimball B. A., Jackson R. D., Reginato R. J., Nakayama F. S., and Idso S. B. (1976) Comparison of field-measured and calculated soil-heat fluxes. *Soil Sci. Soc. Am. J.* **40**, 18.

Lettau H. (1951) Theory of surface-temperature and heat-transfer oscillations near a level ground surface. *Trans. Am. Geophys. Union* **32**, 189-200.

Lettau H. (1954) Improved models of thermal diffusion in the soil. *Trans. Am. Geophys. Union* **35**, 121-132.

Lettau H. H. (1957) Computation of heat budget constituents of the earth/air interface. In *Exploring the Atmosphere's First Mile*, (Lettau and Davidson, eds.), v. 1, p. 305-327. Pergamon, New York.

Monteith J. L. (1973) *Principles of Environmental Physics*. American Elsevier, New York. 240p.

Outcalt S. I. (1972) The development and application of a simple digital surface-climate simulation. *J. Appl. Meteorol.* **11**, 629-636.

Outcalt S. I. (1972) The simulation of subsurface effects on the diurnal surface thermal regime in cold regions. *Artic* **25**, 305-307.

Outcalt S. I. (1975) The analysis of the near-surface energy transfer environment from thermal infrared imagery. *J. Glaciol.* **15(73)**, 267-276.

Philip J. R. (1957) Evaporation and moisture and heat field in the soil. *J. Meteorol.* **14**, 354-366.

Philip J. R. and deVries D. A. (1957) Moisture movement in porous materials under temperature gradients. *Trans. Am. Geophys. Union* **38**, 222-232.

Rosema A. (1975) *A Mathematical Model for Simulation of the Thermal Behavior of Bare Soils Based on Heat and Moisture Transfer*. NIWARS-Publ.-11. Netherlands Interdepartmental Working Group on the Application of Remote Sensing, Delft, Netherlands.

Rosema A. (1975) Simulation of the thermal behavior of bare soils for remote sensing purposes. In *Heat and Mass Transfer in the Biosphere* (D. A. de Vries and N. H. Afgan, eds.) Scripta Book Co., Washington, D. C.

Saltzman B. and Pollack J. A. (1977) Sensitivity of diurnal temperature range to changes in physical parameters. *J. Appl. Meteorol.* **16**, 614-619.

Schieldge J. P. (1980) On estimating the sensible heat flux over land. *Agric. Meteorol.*, in press.

Stearns C. R. (1969) Application of Lettau's theoretical model of thermal diffusion to soil profiles of temperature and heat flux. *J. Geophys. Res.* **74**, 532-541.

Suits G. H., Vincent R. K., Horwitz H. M., and Erickson J. D. (1973) *Optical Modeling of Agricultural Fields and Rough-textured Rock and Mineral Surfaces*. ERIM 31650-78-T, NASA CR-134243. Environmental Research Institute of Michigan, Ann Arbor. 46p.

Thornthwaite C. W. and Holzman B. (1939) The determination of evaporation from land and water surfaces. *U. S. Monthly Weather Rev.* Jan., 1939, p. 4-11.

Watson K. (1970) A thermal model for analysis of infrared images. In *NASA Third Annual Earth Resources Program Review*, v. 1, Sec. 13, p. 1-16. NASA. Manned Spacecraft Center, Houston.

Watson K. (1971) *A Computer Program of Thermal Modeling for Interpretation of Infrared Images*. PB-203578, USGS-GD-71-023. 33p.

Watson K. (1973) Periodic heating of a layer over a semi-infinite solid. *J. Geophys. Res.* **78**, 5904-5910.

Watson K. (1978) Thermal phenomena and energy exchange in the environment. In *Mathematical and Physical Principles of Remote Sensing*, p. 109-174. Centre National d'Etudes Spatiales, Strossbourg, France.

Watson K., Rowan L. C., and Offield T. W. (1971) Application of thermal modeling in the geologic interpretation of IR images. In *Proc. Seventh Int. Symp. on Remote Sensing of Environ.*, p. 2017-2041. U. of Mich. Press, Ann Arbor.

Zdunkowski W. G. and Trask D. C. (1971) Application of a radiative-conductive model to the simulation of nocturnal temperature changes over different soil types. *J. Appl. Meteorol.* **10**, 937-948.

Thermal Inertia Surveys

Dejace J., Megier J., Kohl M., Maracci M., Reiniger P., Tassone G., and Huygen J. (1979) Mapping thermal inertia, soil moisture and evaporation from aircraft day and night thermal data. In *Proc. Thirteenth Int. Symp. on Remote Sensing of Environ.*, p. 1015-1024. U. of Mich. Press, Ann Arbor.

Gillespie A. R. and Kahle A. B. (1977) Construction and interpretation of a digital thermal inertia image. *Photogramm. Eng.* **43**, 983-1000.

Kahle A. B., Gillespie A. R., and Goetz A. F. H. (1976) Thermal inertia imaging — a new geologic mapping tool. *Geophys. Res. Lett.* **3**, 26-28.

Kahle A. B., Gillespie A. R., Goetz A. F. H., and Addington J. D. (1975) Thermal inertia mapping. In *Proc. Tenth Int. Symp. on Remote Sensing of Environ.*, p. 985-990. U. of Mich Press, Ann Arbor.

Kline R. J. (1977) *Discrimination of Geologic Materials by Thermal-Inertia Mapping within the Raft River Test Site*. M. S. thesis, Colorado School of Mines, 165p.

Miller S. H. and Watson K. (1977) Evaluation of algorithms for geological thermal-inertia mapping. In *Proc. Eleventh Int. Symp. Remote Sensing of Environ.*, p. 1147-1160. U. of Mich Press, Ann Arbor.

Pohn H. A. (1976) A comparison of Landsat images and Nimbus thermal-inertia mapping of Oman. *U. S. Geol. Surv. J. of Res.* **4**, 661-665.

Pohn H. A., Offield T. W., and Watson K. (1974) Thermal inertia mapping from satellite — discrimination of geologic units in Oman. *U. S. Geol. Surv. J. of Res.* **2**, 147-158.

Pratt D. A. and Ellyett C. D. (1978) Image registration for thermal inertia mapping, and its potential use for mapping of soil moisture and geology in Australia. In *Proc. Twelfth Int. Symp. on Remote Sensing of Environ.*, p. 1207-1217. U. of Mich. Press, Ann Arbor.

Pratt D. A. and Ellyett C. D. (1979) The thermal inertia approach to mapping soil moisture and geology. *Remote Sensing of Environ.* **8**, 151-168.

Price J. C. (1977) Thermal inertia mapping: a new view of the Earth. *J. Geophys. Res.* **82**, 2582-2590.

Sawatzky D. L., Kline R. J., and Watson K. (1975) Application of the thermal inertia mapping technique to aircraft and satellite data (abstract). *Soc. Explor. Geophys. Annu. Int. Meet., Abstr.* **45**, 67.

Watson K. (1979) Regional thermal inertia mapping to discriminate geologic materials. In *Proc. Thirteenth Int. Symp. Remote Sensing of Environ.*, p. 777-778. U. of Mich. Press, Ann Arbor.

Watson K., Pohn H. A., and Offield T. W. (1972) Thermal inertia mapping from Nimbus Satellite data. In *Proc. Eighth Int. Symp. on Remote Sensing of Environ.*, p. 1237. U. of Mich. Press, Ann Arbor.

Emissivity Surveys

Aronson J. R. and Emslie A. G. (1972) The prospects for mineral analysis by remote infrared spectroscopy. *The Moon* **5**, 3-15.

Buettner K. J. K. and Kern C. D. (1965) Determination of infrared emissivities of terrestrial surfaces. *J. Geophys. Res.* **70**, 1329-1337.

Hovis W. A., Jr., Baline L. R., and Callahan W. R. (1968) Infrared aircraft spectra over desert terrain 8.5μm to 16μm. *Appl. Opt.* **7**, 1137-1140.

Hovis W. A. and Tobin M. (1967) Spectral measurements from 1.6μ to 5.4μ of natural surfaces and clouds. *Appl. Opt.* **6**, 1399-1402.

Kahle A. B., Madura D. P., and Soha J. M. (1979) *Processing of multispectral thermal IR data for geological applications*. JPL Publ. 79-89. NASA-CR-162682. 43p.

Kahle A. B., Madura D. P., and Soha J. M. (1980) Middle infrared multispectral aircraft scanner data: analysis for geological applications. *Appl. Opt.* **19**, 2279-2290.

Kahle A. B. and Rowan L. C. (1980) Evaluation of multispectral middle infrared aircraft images for lithologic mapping in the East Tintic Mountains, Utah. *Geology* **8**, 234-239.

Lyon R. J. P. (1971) Comparison of airborne infrared spectral emittance and radar scatterometer data from Pisgah Crater Lava Flows. In *Proc. Seventh Int. Symp. on Remote Sensing of Environ.*, p. 1449. U. of Mich. Press, Ann Arbor.

Lyon R. J. P. (1972) Infrared spectral emittance in geologic mapping, airborne spectrometer data from Pisgah Crater, California. *Science* **175**, 983-986.

Lyon R. J. P. and Green A. A. (1973) *Field Studies in Support of Nimbus-E Surface Composition Mapping Radiometer*. Stanford Remote Sens. Lab. Tech. Rep. 73-1, 99p.

Lyon R. J. P. and Patterson J. W. (1966) Infrared spectral signatures—a field geological tool. In *Proc. Fourth Int. Symp. on Remote Sensing of Environ*, p. 215-230. U. of Mich. Press, Ann Arbor.

Lyon R. J. P. and Patterson J. W. (1969) Airborne geological mapping using infrared emission spectra. In *Proc. Sixth Int. Symp. on Remote Sensing of Environ.*, p. 527-552. U. of Mich., Ann Arbor.

Prabhakara C. and Dalu G. (1976) Remote sensing of the surface emissivity at 9μm over the globe. *J. Geophys. Res.* **81**, 3719-3724.

Quade J. G., Chapman P. E., Brennan P. A., and Blinn J. C. III (1970) *Multispectral Remote Sensing of an Exposed Volcanic Province*. JPL Tech. Memo. 33-453, NASA-CR-113826, 43p.

Rowan L. C. and Watson K. (1971) Multispectral analysis of limestone, dolomite, and granite, Mill Creek, Oklahoma. In *NASA Earth Resources Program Review 3rd*, v. 1-3, p. 12-1-12-14. Houston, Texas.

Vincent R. K. (1972) *Rock-type Discrimination from Ratio Images of Pisgah Crater, California*. Tech. Rep. 31650-77-T, Willow Run Lab., Ann Arbor.

Vincent R. K. (1973) *A Thermal Infrared Ratio Imaging Method for Mapping Compositional Variations among Silicate Rock Types*. Ph.D. Dissertation, Dept. of Geology and Mineralogy, Univ. of Mich., Ann Arbor.

Vincent R. K. (1977) Geochemical mapping by spectral ratioing methods. In *Remote-Sensing Applications for Mineral Exploration*, p. 251-278. (W. L. Smith, ed.) Dowden, Hutchinson and Ross, Stroudsburg, Pa.

Vincent R. K. and Thomson F. (1971) Discrimination of basic silicate rocks by recognition maps processed from aerial infrared data. In *Proc. Seventh Int. Symp. on Remote Sensing of Environ.*, p. 247-251, U. of Mich. Press, Ann Arbor.

Vincent R. K. and Thomson F. (1972) Rock type discrimination from ratioed infrared scanner images of Pisgah Crater, California. *Science* **175**, 986-988.

Vincent R. K. and Thomson F. (1972) Spectral compositional imaging of silicate rocks. *J. Geophys. Res.* **77**, 2465-2471.

Vincent R. K., Thomson F., and Watson K. (1972) Recognition of exposed quartz sand and sandstone by two-channel infrared imagery. *J. Geophys. Res.* **77**, 2473-2477.

Atmospheric Studies

Burke C. J. (1945) Transformation of polar continental air to polar maritime air. *Meteorology* **2**, 94-112.

Businger J. A., Wyngaard J., Izumi Y., and Bradley E. (1971) Flux profile relationships in the atmospheric surface layer. *J. Atmos. Sci.* **28**, 181-189.

Conel J. E. (1969) Infrared emissivities of silicates: Experimental results and a cloudy atmosphere model of spectral emission from condensed particulate mediums. *J. Geophys. Res.* **74**, 1614-1634.

Deirmendjian D. (1964) Scattering and polarization properties of water clouds and hazes in the visible and infrared. *Appl. Opt.* **3**, 187-196.

Duntley S. Q. (1973) Measuring earth-to-space contrast transmittance from ground stations. *Appl. Opt.* **12**, 1317-1324.

Duntley S. Q., Gordon J. I., Taylor J. H., White C. T., Boileau A. R., Tyler J. E., Austin R. W., and Harris J. L. (1964) Visibility. *Appl. Opt.* **3**, 549-598.

Emslie A. G. (1966) Theory of diffuse spectral reflectance of a thick layer of absorbing and scattering particles. In *Thermophysics and Temperature Control of Spacecraft and Entry Vehicles* (G. B. Heller, ed.), Prog. Astronaut. Aeronaut., v. 18, p. 281-289. Academic, New York.

Goody R. M. (1964) *Atmospheric Radiation*. Clarendon Press, Oxford.

Hovis W. A. and Tobin M. (1967) Spectral measurements from 1.6μ to 5.4μ of natural surfaces and clouds. *Appl. Opt.* **6**, 1399-1402.

Hulst H. C. van de (1957) *Light Scattering by Small Particles*. Wiley, New York. 470p.

Jaeger J. C. (1953) Conduction of heat in a solid with periodic boundary conditions, with an application to the surface temperature of the Moon. *Proc. Cambridge Philos. Soc.* **49**, 355-359.

Kern C. D. (1965) *Evaluation of Infrared Emission of Clouds and Ground as Measured by Weather Satellites*. Ph.D. Thesis, Univ. of Washington. 167p.

Kondratyev K. Ya. (1969) *Radiation in the Atmosphere*. Academic Press, New York.

Kuo H. L. (1968) The thermal interaction between the atmosphere and the earth and propagation of diurnal temperature waves. *J. Atmos. Sci.* **25**, 682-706.

Lettau H. H. (1957) Computation of heat budget constituents of the earth/air interface. In *Exploring the Atmosphere's First Mile* (Lettau and Davidson, eds.), v. 1, p. 305-327. Pergamon, New York.

Lettau H. (1969) Note on aerodynamic roughness-parameter estimation on the basis of roughness-element description. *J. Appl. Meteorol.* **8**, 828-832.

Lyon R. J. P., Honey F. R., and Ballew G. I. (1975) A comparison of observed and model-predicted atmospheric perturbations on target radiances measured by ERTS: Part I - observed data and analysis. In *Conference on Decision and Control, 6th, and Symposium on Adaptive Processes, 14th, Houston, Texas, Dec. 10-12, 1975, Proceedings*, p. 244-249. IEEE, New York.

Plass G. N. and Kattawar G. W. (1968) Calculations of reflected and transmitted radiance for Earth's atmosphere. *Appl. Opt.* **7**, 1129-1148.

Robinson G. D. (1970) Meteorological aspects of radiation. *Adv. Geophys.* **14**, 285-306.

Samuelson R. E. (1965) *Radiative Transfer in a Cloudy Atmosphere*. NASA-TR-215. 91p.

Sasamori T. (1968) The radiation cooling calculation for application to general circluation experiments. *J. Appl. Meteorol.* **7**, 721-729.

Schuster A. (1905) Radiation through a foggy atmosphere. *Astrophys. J.* **21**, 1-22.
Schwerdtfeger P. (1976) *Physical Principles of Micro-meteorological Measurements*. Elsevier, New York. 113p.
Selby J. E. A., Kneizys F. X., Chetwynd J. H., Jr., and McClatchey, R. A. (1978) *Atmospheric Transmittance/ Radiance: Computer Code LOWTRAN 4*. Air Force Geophysics Lab., Rep. # AFGL-TR-78-0053. Hanscom AFB, Mass. 100p.
Sellers W. D. (1965) *Physical Climatology*. University of Chicago Press, Chicago, Ill. 272p.

Planetary Studies

Allen C. W. (1963) *Astrophysical quantities*. Univ. of London, Athlone Press, 2nd Ed., 291p.
Aumann H. H. and Kieffer H. H. (1973) Determination of particle sizes in Saturn's Rings from their eclipse cooling and heating curves. *Astrophys. J.* **186**, 305-311.
Becklin E. E., Hansen O., Kieffer H., and Neugebauer G. (1973) Stellar flux calibration at 10 and 20 μm using Mariner 6, 7, and 9 results. *Astron. J.* **78**, 1063-1066.
Buhl D. (1967) *Radiation anomalies on the lunar surface*. Univ. of Calif., Berkley, Space Sci. Lab. Ser. 8, Issue # 1, NASA-CR-84017, 173p.
Buhl D. (1971) Lunar rocks and thermal anomalies. *J. Geophys. Res.* **76**, 3384-3390.
Buhl D., Welch J., and Rea D. G. (1968) Radiation and thermal emission from illuminated craters on the lunar surface. *J. Geophys. Res.* **73**, 5281-5295.
Burns E. A. and Lyon R. J. P. (1964) Feasibility of remote compositional mapping of the lunar surface: effects of surface roughness. In *The Lunar Surface Layer* (J. Salisbury and P. Glaser, eds.), p. 469-481. Academic, New York.
Chase S. C., Jr., Hatzeneler H., Kieffer H. H., Miner E., Munch G., and Neugebauer G. (1971) Infrared Radiometry experiment on Mariner 9. *Science* **175**, 308-309.
Chase S. C., Miner E. D., Morrison D., Munch G., Neugebauer G., and Schroder M. (1975) Preliminary infrared radiometry of the night side of Mercury from Mariner 10. *Science* **185**, 142-144.
Chase S. C., Miner E. D., Morrison D., Munch G., and Neugebauer G. (1976) Mariner 10 infrared radiometer results: Temperatures and thermal properties of the surface of Mercury. *Icarus* **28**, 565-578.
Christensen P. R. and Kieffer H. H. (1979) Moderate resolution thermal mapping of Mars: the channel terrain around the Chryse Basin. *J. Geophys. Res.* **84**, 8233-8238.
Coblentz W. W. (1922) Further measurements of stellar temperatures and planetary radiation. *Proc. Nat. Acad. Sci. U. S.* **8**, 330-333.
Coblentz W. W. and Lampland C. O. (1927) Further radiometric measurements and temperature estimates of the planet of Mars, 1926. *Sci. Pap. Bur. Stand.* **22**, 237-276.
Conrath B. J. (1975) Thermal structure of the martian atmosphere during the dissipation of the dust storm of 1971. *Icarus* **24**, 36-46.
Gifford F., Jr. (1956) The surface-temperature climate of Mars. *Astrophys. J.* **123**, 154-161.
Goetz A. F. H. (1967) *Infrared 8-13 μm spectroscopy of the moon and some cold silicate powders*. Ph.D. Thesis, California Inst. Tech., Pasadena.
Goetz A. F. H. (1968) Differential infrared lunar emission spectroscopy. *J. Geophys. Res.* **73**, 1455-1466.
Hanel R., Conrath B., Hovis W., Kunde V., Lowman P., Maguire W., Pearl J., Pirraglia J., Prabhakara C., Schlachman B., Levin G., Straat P., and Burke T. (1972) Investigation of the martian environment by infrared spectroscopy on Mariner 9. *Icarus* **17**, 423-442.
Hanel R. A., Conrath B. J., Hovis W. A., Kunde V. G., Lowman P. D., Pearl J. C., Prabhakara C., Schlachman B., and Levin G. V. (1972) Infrared spectroscopy experiment on the Mariner 9 mission: preliminary results. *Science* **175**, 305-308.
Hulst H. C. van de and Irvine W. M. (1962) General report on radiation transfer in planets: scattering in model planetary atmospheres. In *La Physique des Planetes, 11th Liege International Astrophysical Symposium*, p. 78-98. Siege de la Societe Universite, Liege, Belgium.

Hunt G. R. (1965) Infrared spectral emission and its application to the detection of organic matter on Mars. *J. Geophys. Res.* **70**, 2351-2357.

Hunt G. R. (1979) Thermal infrared properties of the martian atmosphere. 4. Predictions of the presence of dust and ice clouds from Viking IRTM spectral measurements. *J. Geophys. Res.* **84**, 2865-2874.

Hunt G. R., Logan L. M. and Salisbury J. W. (1973) Mars: components of infrared spectra and the composition of the dust cloud. *Icarus* **18**, 459-469.

Hunt G. R. and Salisbury J. W. (1964) Determination of compositional differences on the lunar surface using ground based infrared spectroscopy. In *Working Group on Extraterrestrial Resources, Report of Third Annual Meeting*, p. 31-46. J. F. Kennedy Space Center.

Hunt G. R. and Salisbury J. W. (1964) Lunar surface features: mid-infrared spectral observations. *Science* **146**, 641-642.

Hunt G. R. and Salisbury J. W. (1969) Mid-infrared spectroscopic observations of the moon. *Philos. Trans. R. Soc. London* **264A**, 109-139.

Hunt G. R., Salisbury J. W., and Vincent R. K. (1968) Infrared images on the eclisped moon. *Sky and Telescope* **36**, 223-225.

Hunt G. R., Salisbury J. W., and Vincent R. K. (1968) Lunar eclipse: infrared images and an anomaly of possible internal origin. *Science* **162**, 252-254.

Hunt G. R., Salisbury J. W., and Vincent R. K. (1969) Comments on "Lunar Thermal Anomalies and Internal Heating" by J. M. Saari. *Astrophys. Space Sci.* **4**, 370-372.

Kieffer H. (1976) Infrared radiometry in *A Geological Basis For Exploration of the Planets*, (R. Greeley and M. H. Carr, ed.), p. 55-56. NASA SP-417.

Kieffer H. H. (1976) Soil and surface temperatures at the Viking landing sites. *Science* **194**, 1344-1346.

Kieffer H. H. (1979) Mars South Polar spring and summer temperatures: a residual CO_2 frost. *J. Geophys. Res.* **84**, 8263-8288.

Kieffer H. H., Chase S. C., Jr., Martin T. Z., Miner E. D., and Palluconi F. D. (1976) Martian north pole summer temperatures: dirty water ice. *Science* **194**, 1341-1344.

Kieffer H. H., Chase S. C., Jr., Miner E., Munch G., and Neugebauer G. (1973) Preliminary report on infrared radiometric measurements from the Mariner 9 spacecraft. *J. Geophys. Res.* **78**, 4291-4312.

Kieffer H. H., Chase S. C., Jr., Miner E. D., Palluconi F. D., Munch G., Neugebauer G., and Martin T. (1976) Infrared thermal mapping of the martian surface and atmosphere: first results. *Science* **193**, 780-786.

Kieffer, H. H., Christensen P. R., Martin T. Z., Miner E. D., and Palluconi F. D. (1976) Temperatures of the martian surface and atmosphere: Viking observation of diurnal and geometric variations. *Science* **194**, 1346-1351.

Kieffer H. H., Martin T. Z., Peterfreund A. R., Jakosky B. M., Miner E. D., and Palluconi F. D. (1977) Thermal and albedo mapping of Mars during the Viking primary mission. *J. Geophys. Res.* **82**, 4249-4291.

Ksanfomaliti L. V., and Moroz V. I. (1975) Infrared radiometry on board Mars-5. *Cosmic Res.* **13**, 65-67.

Logan L. M., Balsamo S. R., and Hunt G. R. (1973) Absolute measurements and computed values for martian irradiance between 10.5 and 12.5μm. *Icarus* **18**, 451-458.

Logan L. M. and Hunt G. R. (1970) Emission spectra of particulate silicates under simulated lunar conditions. *J. Geophys. Res.* **75**, 6539-6547.

Logan L. M. and Hunt G. R. (1970) Infrared emission spectra, enhancement of diagnostic features by the lunar environment. *Science* **169**, 865-866.

Logan L. M., Hunt G. R., Balsamo S. R., and Salisbury J. W. (1972) Mid-infrared emission spectrum of Apollo 14 and 15 soils and remote compositional mapping of the Moon. *Geochim. Cosmochim. Acta* **3**, 3069-3076.

Logan L. M., Hunt G. R., and Salisbury J. W. (1972) Infrared emission spectra of Apolla 15 soils. In *The Apollo l5 Soil Samples* (J. W. Chamberlain and C. Watkins, eds.), p. 475-476. Lunar Science Institute, Houston.

Logan L. M., Hunt G. R., and Salisbury J. W. (1975) The use of mid-infrared spectroscopy in remote sensing of space targets. In *Infrared and Raman Spectroscopy of Lunar and Terrestrial Mineral* (C. Karr, ed.), Chapter 5, p. 117-142. Academic Press, New York.

Logan L. M., Hunt G. R., Salisbury J. W., and Balsamo S. R. (1972) Mid-infrared emission spectrum of Apollo 14 soil. Significance for compositional remote sensing. In *Lunar Science III* (C. Watkins, ed.), p. 490-492. Lunar Science Institute, Houston.

Lyon R. J. P. (1963) *Evaluation of infrared spectrophotometry for compositional analysis of lunar and planetary soils.* NASA Tech. Note TN D-1971, 118p.

Lyon R. J. P. (1964) *Evaluation of infrared spectrophotometry for compositional analysis of lunar and planetary soils. Part II. Rough and powdered surfaces.* NASA Contractor Report CR-100, 172p.

Lyon R. J. P. and Burns E. A. (1962) Infrared spectral analysis of the lunar surface from an orbiting spacecraft. In *Proc. Second Int. Symp. on Remote Sensing of Environ.*, p. 309-327. U. of Mich. Press, Ann Arbor.

Martin T. Z. and Kieffer H. H. (1979) Global thermal behavior of Mars in dusty conditions. 2. 15-μm band measurements. *J. Geophys. Res.* **84**, 2843-2852.

Martin T. Z., Kieffer H. H., and Miner E. D. (1978) Mars atmospheric behavior from Viking Infrared Thermal Mapper measurements. In *The Mars Reference Atmosphere; Proceedings of the Twenty-first Plenary Meeting, Innsbruck, Austria, May 29-June 10, 1978* (A. Kliore, ed.), p. 81-90. JPL, Pasadena, California.

Martin T. Z., Peterfreund A. R., Miner E. D., Kieffer H. H. and Hunt G. E. (1979) *Thermal Infrared properties of the martian atmosphere. 1. Global behavior at 7, 9, 11, and 20 μm.* *J. Geophys. Res.* **84**, 2830-2342.

Moroz V. I. and Ksanfomaliti L. V. (1972) Preliminary results of astrophysical observations of Mars from Mars-3. *Icarus* **17**, 408-422.

Moroz V. I., Ksanfomaliti L. V., Krasovskii G. N., Davydov V. D., Parfent'ev N. A., Zhenulev V. S., and Filippov G. S. (1976) Infrared temperatures and thermal properties of the martian surface measured by the Mars-3 orbiter. *Cosmic Res.* **13**, 346-358.

Morrison D., Sagan C., and Pollack J. B. (1969) Martian temperatures and thermal properties. *Icarus* **11**, 36-45.

Murcray F. H., Murcray D. G., and Williams W. J. (1970) Infrared emissivity of lunar surface features. *J. Geophys. Res.* **75**, 2662-2669.

Murray B. C. and Wildey R. L. (1964) Surface temperature variations during the lunar nighttime. *Astrophys. J.* **139**, 734-750.

Neugebauer G., Munch G., Chase S. C., Jr., Hatzenbeler H., Miner E., and Schofield D. (1969) Mariner 1969: preliminary results of the infrared radiometer experiment. *Science* **166**, 98-99.

Neugebauer G., Munch G., Kieffer H. H., Chase S. C., Jr., and Miner E. (1971) Mariner 1969 infrared radiometer results: temperatures and thermal properties of the martian surface. *Astron. J.* **76**, 719-728.

Peterfreund A. R., and Kieffer H. H. (1979) Thermal infrared properties of the martian atmosphere. 3. Local dust clouds. *J. Geophys. Res.* **84**, 2853-2863.

Peterfreund A. R., Kieffer H. H., and Palluconi F. D. (1977) Thermal inertia of the Elysium region of Mars. In *Lunar Science VIII*, pp. 765-767. Lunar Science Institute, Houston.

Pettit E. and Nicholson S. B. (1930) Lunar radiation and temperature. *Astrophys. J.* **71**, 102-135.

Roelof E. C. (1968) Thermal behavior of rocks on the lunar surface. *Icarus* **8**, 138-159.

Saari J. M. and Shorthill R. W. (1963) Isotherms of crater regions on the illuminated and eclipsed moon. *Icarus* **2**, 115-136.

Sagan C. and Pollack J. B. (1967) Anisotropic nonconservative scattering and the clouds of Venus. *J. Geophys. Res.* **72**, 469-477.

Salisbury J. W. and Hunt G. R. (1967) Infrared images: implication for the lunar surface. *Icarus* **7**, 47-58.

Salisbury J. W. and Hunt G. R. (1967) Infrared images of Tycho on the dark moon. *Science* **155**, 1098-1100.

Salisbury J. W. and Hunt G. R. (1968) Martian surface materials: effect of particle size on spectral behavior. *Science* **161**, 365-366.

Salisbury J. W. and Hunt G. R. (1969) Compositional implications of the spectral behavior of the Martian surface. *Nature* **222**, 132-136.

Salisbury J. W., Hunt G. R., and Logan L. M. (1974) Infrared spectra of Apollo 16 fines. *Geochim. Cosmochim. Acta* **3**, 3191-3196.

Salisbury J. W., Vincent R. K., Logan L. M., and Hunt G. R. (1970) Infrared emissivity of Lunar surface features. 2. Interpretation. *J. Geophys. Res.* **75**, 2671-2682.

Shorthill R. W. and Saari J. M. (1965) Nonuniform cooling of the eclipsed Moon: a listing of thirty prominent anomalies. *Science* **150**, 210-212.

Sinton W. M. (1962) Temperatures on the lunar surface. In *Physics and Astronomy of the Moon* (Z. Kopal, ed.), p. 407-428. Academic Press, New York.

Sinton W. and Strong J. (1960) Radiometric observations of Mars. *Astrophys. J.* **131**, 459-469.

Wechsler A. E. and Glaser P. E. (1965) Pressure effects on postulated lunar materials. *Icarus* **4**, 335-352.

Wesselink A. F. (1948) Heat conductivity and nature of the lunar surface material. *Bull. Astron. Inst. Neth.* **10**, 351-363.

Winter D. F. and Saari J. M. (1969) A particulate thermophysical model of the lunar soil. *Astrophys. J.* **156**, 1135-1151.

Zimbelman J. R. and Kieffer H. H. (1979) Thermal mapping of the northern equatorial and temperate latitudes of Mars. *J. Geophys. Res.* **84**, 8230-8251.

☆ U.S. GOVERNMENT PRINTING OFFICE: 1982—569-011/2815